Aalto University
School of Engineering

Sai Suryavenkatesh Villa

A Numerical Methodology and Analysis of Borehole Thermal Energy Storage Performance

Master Thesis submitted for examination for the degree of Master of Science in Technology.
Espoo, 28 Sept 2020
Thesis supervisor: Prof. Annukka Santasalo-Aarnio
Thesis advisor: M.Sc. Timo Sivula

Aalto University
School of Engineering

Aalto University, P.O. BOX 11000, 00076
AALTO
www.aalto.fi

Abstract of the master's thesis

Author Sai Suryavenkatesh Villa

Title of thesis A Numerical Methodology and Analysis of Borehole Thermal Energy Storage Performance

Master programme Sustainable Energy Conversion Processes **Code** ENG3069

Thesis supervisor Santasalo-Aarnio Annukka

Thesis advisor(s) Timo Sivula

Date 28.09.2020 **Number of pages** 91+6 **Language** English

Abstract

The heating and cooling industry occupies major energy demand across the European Union in the form of the residential, commercial, and industrial sectors. The share of renewable energy has grown from 11.7% in 2004 to 21.1% in 2018 (Eurostatistics, 2020) creating fluctuation for heat production. Underground thermal energy storage balances the mismatch between the availability and demand of heat by storing heat underground. Borehole Thermal Energy Storage (BTES) is the promising underground large-scale energy storage option due to its ease of construction, eco-friendly and cost-effective materials. BTES has a major edge on the integration of various renewable heat sources to conserve heat energy for longer periods. However, they are certain optimizing aspects that need to be resolved for each BTES system such as the design of geometry, heat extraction losses, geographical and hydrological conditions, optimal temperature drop between discharge and charge periods, storage surface area to depth ratio, optimal borehole spacing, and overall efficiency.

This work presents the numerical modeling and analysis of the BTES using monitoring data as the input in finite element analysis-based software COMSOL *Multiphysics* ®. In this 3D modeling, we are doing the numerical analysis of the hexagonal geometry of the seasonal BTES system for 5 years to analyze the effect of the operational parameters on the system. The cases of High-Temperature BTES system of 126 boreholes tested with varying geometrical and thermal properties to analyze their effect on heat losses.

The main objective is to reduce the heat losses by studying and evaluating the operational parameters and thereby providing the optimal efficiency without dropping the minimum temperatures in BTES. Results show that the BHE arrangement, mass flow rate, thermal conductivities of the soil, and rock, top insulation material are major factors in reducing the heat losses which can be optimized to improve efficiency. This work is carried out in collaboration with Heliostorage Oy, providing part of the initial parameters from existing pilot BTES projects in Finland.

Keywords Borehole Thermal Energy Storage, hexagonal geometry, geographical, borehole spacing, COMSOL

Preface

This Master thesis is collaborative research work for Heliostorage Oy with Aalto University. Heliostorage Oy is the Finnish high tech startup founded in 2016 that works on replacing current fossil heating solutions with sustainable, emission-free solar alternatives.

First and foremost, I would like to thank my Prof. Annukka Santasalo-Aarnio for her immense support from the beginning of the thesis work. This thesis would not have been unfolded if she had not accorded me this opportunity to be a part of this challenging research. I would like to thank M.Sc. Sampson Tetteh for his assistance in writing the thesis and his fruitful advice on other aspects of the work. I would like to especially thank my thesis advisor Timo Sivula and Fabian Sander from Heliostorage for providing various materials, showing equal interest and encouragement from the beginning till the end which motivated me to research further.

I would like to extend my gratitude to Petri Hakala at the Geological Survey of Finland for providing valuable data and suggestions to this work and without his suggestions, I couldn't create this model within this time frame.

Lastly but they are first in my life, my parents who always stood by me and with my decisions especially on my wish to study in this wonderful university. Thank you to my friends, and loved ones who happened to be my side.

Espoo,
Sai Suryavenkatesh Villa

Table of Contents

Abstract 2
Preface 2
Abbreviations 8
Nomenclature 9
1. Introduction 13
2. Background of TES 16
2.1 Aquifer Thermal Energy Storage (ATES) 17
2.2 Cavern Thermal Energy Storage (CTES) 18
2.3 Tank Thermal Energy Storage (TTES) 19
2.4 Pit Thermal Energy Storage (PTES) 19
2.5 Borehole Thermal Energy Storage (BTES) 20
2.5.1 Principle of BTES 21
2.5.2 Preliminary investigation of the site 22
2.5.3 Construction 22
2.5.4 Finnish Ground Conditions 23
2.5.5 Design Considerations 25
2.5.6 Piping Materials 29
2.5.7 Insulation 32
2.5.8 Grout materials for borehole heat exchangers 35
3. BTES Methodology in COMSOL 37
3.1 Numerical simulation of the in-situ design 37
3.2 Geometry 39
3.3 Variables and Selections 42
3.4 Physics 46
3.4.1 Case of charging: 48
3.4.2 Case of discharging: 49
3.5 Multiphysics 54
3.5.1 Case of Charging 54
3.5.2 Case of Discharging 58
3.6 Mesh 60
3.6.1 Meshing sequence order 60
3.6.2 Element type 61
3.6.3 Element size and distribution 61
3.6.4 Element order and mesh quality 63

4. Results 66
4.1 Period 1 Analysis 66
4.2 Period 5 Analysis 71
4.3 Thermal conductivities of the rock analysis 76
4.4 Thermal conductivities of the soil analysis 77
4.5 Thickness of the finnfoam analysis 78
4.6 Economical Value 79
4.7 Exergy Analysis 80
5. Discussion 81
6. Conclusion 84
7. References 86
8. Appendix 92
8.1 Simulation Results 92
8.1.1 Period 2 92
8.1.2 Period 3 94
8.1.3 Period 4 96

Table of Figures

Figure 1. BTES during summer in the charging phase from buildings (Underground Energy, 2020) ...21
Figure 2. BTES system during winter during discharging phase to buildings (Underground Energy, 2020) ...21
Figure 3. Buildings constructed on the surface of the BTES system where boreholes are drilled at the depth 100-200m beneath the surface (Nordell, Grein, & Kharseh , 2007)...23
Figure 4. Circular BTES (M.Rad, S.Fung, & A.Rosen, 2017) ...26
Figure 5. Hexagonal BTES in Aerial View (Kallesøe & Pedersen, 2019) ...28
Figure 6. BTES series connection of boreholes followed in DSLC project, Canada (Kallesøe & Pedersen, 2019)...29
Figure 7. Parallel and Series connection of one of the Heliostorage BTES projects at Kokkola, ...29
Figure 8. Range of price, wall thickness, and external diameter for commercially available pipe materials (Mendrinos, Katsantonis, & Karytsas, 2016) ...31
Figure 9. Expected service life (indicative) versus delivered geothermal energy costs by a coaxial BHE using an external pipe made of different market available materials (Mendrinos, Katsantonis, & Karytsas, 2016) ...32
Figure 10. Thermal conductivity of various insulation materials (Villasmil, Fischer, & Worlitschek, 2019) ...33
Figure 11. Price of the types of Insulation Materials, according to the thickness (Villasmil, Fischer, & Worlitschek, 2019)...34
Figure 12. Top view of Hexagonal geometry designed in different component of the COMSOL.....39
Figure 13. 3D view of BTES geometry in blocks divided into work planes according to the heat characteristics in COMSOL ...40
Figure 14. Selection of 2nd work plane in BTES geometry of COMSOL that representing soil height 41
Figure 15. Side view of work planes in COMSOL model without finnfoam material on top of the boreholes...41
Figure 16. Insulation foam material in work plane 3 on top of boreholes in BTES to prevent the heat losses ...42
Figure 17. BHEs are selected from the component selections to 3D geometry of the COMSOL simulation. Once selected can be utilised in various physics and Multiphysics stages. ...42
Figure 18. Boundaries of the ring 1 are selected from the component selections so that ring 1 can have various physics and Multiphysics and can even mesh separately if needed. ...43
Figure 19. Edges of the Ring 1 are selected to find an average value of the borehole edges in ring 1 ...44
Figure 20. Edges of the Ring 6 are selected to find the average value of borehole edges in ring 6 44
Figure 21. Edges of all the rings are selected in the selections to find an average value of the borehole edges...45
Figure 22. Boundaries of the BTES field selected to find the average value of the surrounding boundaries...45
Figure 23. Lower insulation layer was selected in COMSOL to find the average heat characteristics and give separate meshing...46
Figure 24. A partial differential equation in coefficient form...49
Figure 25. 3D geometry of BTES subsystem without insulation layer on top surface assigned with different physics and multiphysics ...55
Figure 26. Inward Heat Flux in the ground represents the geothermal flux and its gradient around.....57
Figure 27. Soil Insulation Layer of tope of the BTES which is usually at the depth of 1-1.5m beneath the ground...57
Figure 28. Element size window for providing meshing size ...62
Figure 29. Tetrahedral mesh on the surface to accommodate edge mesh in the borehole and borehole edge was unselected for different meshing since the tetrahedral mesh on the larger areas of the model. ...62
Figure 30. Top view of the tetrahedral mesh on the ground surface to accommodate all the borehole edges and ...63
Figure 31. Tetrahedral mesh selection finer on the top surface, normal on the bottom, and swept mesh in the middle ...63

Figure 32. Swept mesh inside each of the borehole and tetrahedral mesh accumulated towards the edges of the borehole....64
Figure 33. Mesh statistics of a 3D subsystem of BTES model that defines the type, number and quality of elements....65
Figure 34. Power injection (charging) in the first six months for the first year. Ring 1 shows the least power consumption and the remaining rings combined with ring 6 show the highest power consumption....67
Figure 35. Temperature injection(charging) in the first six months for the first year. Ring 1 received the highest temperature from injection and the last outer Ring 6 receives the least temperature. 68
Figure 36. Power extraction (discharging) in the last six months for the first year. Ring 6 supplies the least power and the remaining rings combined with Ring 1 produce the highest power. 70
Figure 37. Extraction temperatures(discharging) in the last six months for the first year. Temperatures from the ring 6 supply the least temperature whereas Ring 1 supplies the highest core temperature. 71
Figure 38. Power injection(charging) in the first six months for the fifth year. Ring 1 shows the least power consumption and the remaining rings combined with Ring 6 show the highest power consumption....72
Figure 39. Injection Temperatures(charging) in the first six months for the fifth year. Ring 1 received the highest temperature from injection and the last outer Ring 6 receives the least temperature. .73
Figure 40. Power extraction(discharging) in the last six months for the fifth year. Ring 6 supplies the least power and the remaining rings combined with Ring 1 produce the highest power. 75
Figure 41. Extraction temperatures(discharging) in the last six months for the fifth year. Ring 6 supply the least temperature and Ring 1 supply highest temperature. 76
Figure 42. Analysis of various thermal conductivity values of the rock from k_rock =1-4 W/mK 77
Figure 43. Analysis of various thermal conductivity values of the soil ranging from k_soil=1-4 W/mK 78
Figure 44. Analysis of various thickness sizes of insulation foam ranging from a thickness of 10cm to 30cm....79
Figure 45. Cost curve of 3 types of sensible heat storages: TTES, BTES, and PTES excluding the VAT and subsidies (Mauthner & Herkel, 2016) 79
Figure 46. Power injection(charging) in the first six months for the second year....92
Figure 47. Injection temperatures(charging) in the first six months for the second year....92
Figure 48. Power extraction(discharging) in the last six months for the second year....93
Figure 49. Extraction temperatures(discharging) in the last six months for the second year....93
Figure 50. Power injection(charging) in the first six months for the third year....94
Figure 51. Injection temperatures(charging) in the first six months for the third year....94
Figure 52. Power extraction(discharging) in the last six months for the third year 95
Figure 53. Extraction temperatures(discharging) in the last six months for the third year 95
Figure 54. Power injection(charging) in the first six months for the fourth year....96
Figure 55. Injection temperatures(charging) in the first six months for the fourth year....96
Figure 56. Power extraction(discharging) in the last six months for the fourth year 97
Figure 57. Extraction temperatures(discharging) in the last six months for the fourth year....97

Abbreviations

ATES	Aquifer Thermal Energy Storage
BHE	Borehole Heat Exchanger
BTES	Borehole Thermal Energy Storage
CTES	Cavern Thermal Energy Storage
TTES	Tank Thermal Energy Storage
STES	Seasonal Thermal Energy Storage
BAR	BHE field Aspect Ratio
CAR	Cavern Aspect Ratio
GSHP	Ground Source Heat Pump
HDPE	High-Density Polymer Polyethylene
HTR	Heat Transfer Rate
PEX	Cross-Linked Polyethylene
PP	Polypropylene
PTES	Pit Thermal Energy Storage
PUR-PIR	Polyurethane-Polyisocyanurate
PVC	Polyvinylchloride
RES	Renewable Energy System
STC	Solar Thermal Collectors
TES	Thermal Energy Storage
TRT	Thermal Response Test
TTES	Tank Thermal Energy Storage
VIP	Vacuum Insulation Panels
XPS	Extruded Polystyrene

Nomenclature

Parameters shortcuts	Explanation	Unit
r_borehole	Borehole radius	m
H_borehole	Borehole length	m
r_inner	Collector pipe inner radius	m
r_outer	Collector pipe outer radius	m
k_fluid	Thermal conductivity of working fluid	$\mathrm{Wm^{-1}K^{-1}}$
Cp_fluid	Specific Heat capacity of working fluid	$\mathrm{Jkg^{-1}K^{-1}}$
rho_fluid	Density of working fluid	$\mathrm{kgm^{-3}}$
k_rock	Bedrock thermal conductivity, avg. value from 2 TRTs	$\mathrm{Wm^{-1}K^{-1}}$
Cp_rock	Specific Heat capacity of bedrock	$\mathrm{Jkg^{-1}K^{-1}}$
D/H	Ratio of a diameter of BTES to the height of the borehole	no units
d_borehole	Distance between the 2 boreholes	m
finnfoam	Finnfoam thickness layer	m
k_finnfoam	Thermal conductivity of insulation	$\mathrm{Wm^{-1}K^{-1}}$
rho_finnfoam	Density of insulation layer	$\mathrm{kgm^{-3}}$
Cp_finnfoam	Specific Heat capacity of insulation material	$\mathrm{Jkg^{-1}K^{-1}}$
rho_rock	Bedrock density	$\mathrm{kgm^{-3}}$

rho_soil	Soil density	$\mathrm{kgm^{-3}}$
Cp_soil	Specific heat capacity of soil	$\mathrm{Jkg^{-1}K^{-1}}$
k_soil	Soil thermal conductivity	$\mathrm{Wm^{-1}K^{-1}}$
k_grout	Thermal conductivity of BHE filling	$\mathrm{Wm^{-1}K^{-1}}$
Cp_grout	Specific heat capacity of BHE filling	$\mathrm{Jkg^{-1}K^{-1}}$
rho_grout	Density of BHE filling	$\mathrm{kgm^{-3}}$
T_init	Initial temperature of bedrock	$℃, \mathrm{K}$
Q_fluid	Flow rate of collector fluid during charging	$\mathrm{Lmin^{-1}}$
Q_fluid_purku	Volumetric flow rate during heat discharging	$\mathrm{Lmin^{-1}}$
k_pipe	Pipe thermal conductivity	$\mathrm{Wm^{-1}K^{-1}}$
dz	Infinitesimal length parameter	m
v_fluid	Fluid velocity in collector during charging	$\mathrm{m/s}$
dS_pipe	Area of pipe outer surface	$\mathrm{m^2}$
dV_pipe	Volume of pipe inner surface	$\mathrm{m^3}$
dV_pipe_outer	Volume of pipe outer surface	$\mathrm{m^3}$
dS_grout	Grout Area	$\mathrm{m^2}$
dV_grout	Volume of BHE filling material	$\mathrm{m^3}$

mu_fluid	Dynamic Viscosity of water	Pa.s
Re_fluid	Reynolds number	no units
Pr_fluid	Prandtl number	no units
Nu_fluid	Nusselt number	no units
h_fluid	Convective heat transfer coefficient	$\mathrm{Wm^{-2}K^{-1}}$
R_fluid	Convective thermal resistance	$\mathrm{s^3.K.kg^{-1}.m^{-1}}$
R_pipe	Pipe thermal resistance	$\mathrm{s^3.K.kg^{-1}.m^{-1}}$
R_fp	Thermal resistance between fluid and pipe outer surface	$\mathrm{s^3.K.kg^{-1}.m^{-1}}$
Shank_spacing	Distance between collector shanks	m
b_fluid_to_grout	Heat transfer coefficient on the pipe outer surface	$\mathrm{Wm^{-2}K^{-1}}$
R_multipole	Borehole thermal resistance during charging (Multipole method)	$\mathrm{s^3.K.kg^{-1}.m^{-1}}$
R_grout	Thermal resistance of water inside BHE	$\mathrm{s^3.K.kg^{-1}.m^{-1}}$
b_grout_to_soil	Heat transfer coefficient on the borehole wall	$\mathrm{Wm^{-2}K^{-1}}$
v_fluid_purku	Flow velocity during discharging	$\mathrm{ms^{-1}}$
q_geothermal	Geothermal heat flux	$\mathrm{Wm^{-2}}$
Re_fluid_purku	Reynolds number during discharging	no units
Nu_fluid_purku	Nusselt number during discharging	no units

h_fluid_purku	Convective thermal resistance during discharge	$\mathrm{Wm^{-2}K^{-1}}$
R_fluid_purku	Convective thermal resistance during discharge	$\mathrm{s^3.K.kg^{-1}.m^{-1}}$
b_fluid_to_grout_purku	Heat transfer coefficient from fluid to grout	$\mathrm{Wm^{-2}K^{-1}}$
R_multipole_purku	Borehole thermal resistance during discharging	$\mathrm{s^3.K.kg^{-1}.m^{-1}}$
R_grout_purku	Thermal resistance of water inside BHE during discharging	$\mathrm{s^3.K.kg^{-1}.m^{-1}}$
b_grout_to_soil_purku	Heat transfer coefficient from the grout to soil	$\mathrm{Wm^{-2}K^{-1}}$

1. Introduction

Climate change has been the major issue around the globe, where every nation needs to make collective efforts in tackling greenhouse gas emissions. There has been a mounting pressure to reduce use the of fossil fuels to decrease greenhouse house emissions which emits CO_2 and other toxic pollutants. So, there is an essential transition needed towards the adaptation of renewable resources from the conventional ones. Intermittent renewables like solar energy, wind energy occupy the major arena in this transition from fossil fuels but lack the flexibility due to mismatch in demand and supply of heat in seasons.

According to the (Eurostatistics, 2020), heating and cooling represent almost 40% of the European Union's (EU)s energy consumption. So, the increasing consumption of heating and cooling produces larger amounts of CO_2 emissions which could be reduced by various Thermal energy storage (TES) systems. (Reuss, 2015). The renewable energy share of Finland is 41.2% in 2018 and out of which the heating cooling sector occupies 55% of gross energy consumption (Eurostatistics, 2020). Intermittent renewable sources like solar energy, wind energy, and wave energy are facing issues with inconsistent supply and demand (Dinker, Agarwal, & Agarwal, 2017). Hence the energy storage systems come in place to address these significant barriers (Xu, Wang, & Li, 2014). Among the intermittent renewable sources, solar energy is the most affordable, eco-friendly, and widely used application around the world. Heat received from solar irradiation in summer can be stored through thermal energy storage for later use in the winter season. With the integration of the TES system, we can solve the misalignment between supply and demand which enables not only in space heating and cooling but also in domestic water supply throughout the year (Xu, Wang, & Li, 2014). TES systems also have the advantage of utilizing excess heat until it is consumed, which indirectly increases the energy conservation (Alva, Lin, & Fang, 2018). There is a strong need to store energy in various forms of TES solutions from sensible energy storage to thermochemical storage (Honkonen, 2016). So, huge amounts of energy will be stored in suitable thermal energy storage technologies while heat demand is lower and will utilize later while heat demand is higher which is otherwise called Seasonal thermal energy storage or long-term heat storage (Fisch, Guigas, & Dalenback, 1998). To store large amounts of thermal energy, high volume storage units. Hence, large

storage materials should possess the capable thermal-physical properties like high latent heat, high specific heat, and high thermal thermal conductivity to withhold the high thermal energy and also material must be cost-effective, availability, reliability, thermal and chemical stability (Reuss, 2015) (Alva, Lin, & Fang, 2018). (Fisch, Guigas, & Dalenback, 1998) performed two kinds of large scale solar systems: short-term or diurnal and long-term heat storage or seasonal heat storage and concluded that seasonal heat storage could reach 50-70% annual demand and whereas short-term heat storage reaches 10-20% for space heating and domestic water heating. Seasonal thermal storage has great potential in replacing conventional fossil fuels, enable in the reduction of CO_2 emissions, and cost-effective to short-term storages but it has challenges with greater volumes of storage, greater heat losses (Xu, Wang, & Li, 2014).

Various seasonal storage systems are compared under the competent ground conditions, and (Janiszewski, et al., 2016) proposed that Borehole Thermal Energy Storage (BTES) is the ideal long term heat storage for cost-effective, longevity and easier integration with Renewable Energy sources (RES) compared to other sensible heat storages whereas integrated with rock pit thermal energy is favored for short term thermal energy storage in Finland. They are some problems with the BTES efficiency due to the increasing heat losses among other Underground Thermal Energy Storage (UTES) systems that provide the space to explore this issue (Xu, Wang, & Li, 2014) (Vallin, 2019).

In this thesis, we are going to study the Numerical modeling and analysis of the BTES system to examine the operation parameters effect on BTES performance. BTES modeling is needed to study the in-depth analysis ranging from subsystem design to whole community/building simulations and tool selection to analyze the simulations depends upon the requirement of the objective of analysis (Lanahan & Tabares-Velasco, 2017). Some studies studied the impact of hydrological measures on the BTES performance, but they are other geological parameters that show the effect on the efficiency of BTES, where it needs to be explored in depth. Analysis tools such as TRNSYS and EnergyPlus are used for studying the whole building/system analysis whereas Multiphysics tools such as COMSOL are used for modeling and analysis of heat transfer and fluid characteristics but either of those tools cannot be connected with other objectives (Lanahan & Tabares-Velasco, 2017). These analyses forecast the

thermodynamic performance and payback period that assist in the investment process (Vallin, 2019). A three-dimensional Numerical Modelling has become a good and efficient method to analyze and simulate the thermal energy storage heat characteristics in the subsystem. In this work, finite element method-based software COMSOL *Multiphysics* ® is used for 126 borehole BTES simulation to analyze the effect of the operational parameters on BTES efficiency.

One of the major drawbacks in sensible heat storage systems is the storage of thermal energy at high temperatures which subscribes to inevitable heat losses (Honkonen, 2016). A protracted period of sensible heat storage systems means seasonal sensible storage releases a significant amount of heat losses. The main objective of the thesis is to study the major factors that are contributing to increasing heat losses and thereby decreasing the efficiency of BTES over prolonged periods. The utilization and potential of BTES system integrated with solar collectors and waste heat sources are investigated in terms of the major contribution behind its heat losses and how it varies every year over the parametric changes. This work is done in collaboration with Heliostorage Oy, providing part of the initial parameters from existing pilot BTES projects in Finland.

Numerical modeling of simulation and analysis is carried out from the in-situ optimal parameters on the seasonal BTES system with eight hours charging phase for six months followed by sixteen hours discharging phase for the next six months. This comprehensive analysis is executed for five years to study how the model is developing an inadequate period. This research analysis did not study the characterization of heat losses due to the groundwater table since the influence of the groundwater table is not the scope of this research. This research explicitly states how the heat losses are developed in a seasonal BTES system over five years. This methodology from the 3-D finite element analysis provides the idea of major contributions to the seasonal BTES heat losses and provides few recommendations on geometric design based on numerical modeling and analysis.

The main research objectives of this master's thesis are :

1. To find how much we lose from the extraction during the discharging phase of BTES and what is the feasible borehole diameter-to-depth ratio?
2. To investigate what are the major contributors to heat losses per year, and how can we control the heat losses to increase the efficiency?

2. Background of TES

Thermal energy storage (TES) works on the principle of changing internal energy, and it is the kind of sustainable technology that stores the massive heating/cooling energy as the storage to utilize it for lateral use to meet the energy demand (Honkonen, 2016). The concept of passive energy storage existed since the time of early humans where they used the underground to keep warm themselves during winter and vice-versa in summer. When the solar heat up the ground surface in summer it takes significant time to reach the underground which varies with the depth. This shows the significant temperature difference between the ambient temperatures and underground temperatures. In summer, underground temperatures much lower than the ambient temperature whereas in the winter, the underground temperatures are much higher than ambient temperatures. In winter, the underground temperatures become much warmer due to the increase in geothermal gradient with depth. TES systems significantly cost lower than electric storage systems and provide nearly 100% round efficiency compared to 80% in the case of batteries (Lanahan & Tabares-Velasco, 2017). Thermal energy is stored in the form of heat in the materials based on different methods: Sensible heat storage, latent heat storage, and thermochemical heat (Dinker, Agarwal, & Agarwal, 2017). Sensible heat storage technologies are the most cost-effective among the latent heat storage and thermochemical methods as they use natural materials as the underground storage medium (Honkonen, 2016) (Reuss, 2015). Sensible heat storage technologies need larger volumes of storage capacity for short(diurnal) and long-term energy storage(seasonal) (Fisch, Guigas, & Dalenback, 1998). Here the short period of storage lasts for days and weeks whereas the long-term periods last for months and years of loading and unloading the thermal temperatures (Bakema, Snijders, & Nordell, 1995).

In the beginning days of seasonal storage systems are mainly designed to meet heat energy demand in winter, but today there is also increasing demand for the cooling energy demand in summer as well due to increasing temperatures every year (Bakema, Snijders, & Nordell, 1995). Solar heat energy as the intermittent renewable energy system (RES) for the sensible heat storage gets collected during the summer for charging the cold fluid in different natural storage medium and store in the form of thermal/heat energy. Similarly, industrial waste heat or sewage waste heat acts as a

great source of heat for the sensible heat storage systems along with the solar systems (Fisch, Guigas, & Dalenback, 1998). Although we have the intermittent Renewable Energy Systems (RES) with the sensible heat storage system to meet the mismatch between the energy supply and demand but the economic value over the fossil fuels is the major value proposition that is needed for the companies over the adaptation of environmentally friendly thermal storage systems. (Nordell B. , Large Scale Thermal Energy Storage, 2000) (Janiszewski, et al., 2016) summarised that underground thermal energy systems (UTES) have the tapping potential on the economic viewpoint since the storage medium as the soil, or hard rock or unconsolidated rock materials are already present in nature. There is always an economic variance during the injection and extraction of thermal energy which could be balanced by reducing the heat losses and increasing efficiencies along with fulfilling the building and energy demand. Some feasible sensible energy storage technologies are depending upon the various geographical, hydrogeological conditions.

There are various sensible heat storage technologies namely the Aquifer Thermal Energy Storage (ATES), Cavern Thermal Energy Storage (CTES), Tank Thermal Energy Storage (TTES), Pit Storage Energy System (PTES), Borehole Thermal Energy Storage (BTES) (Nordell B. , Large Scale Thermal Energy Storage, 2000). BTES has the most flexibility of loading and unloading thermal energies with the feasibility of small-scale and large-scale applications over the other UTES system (Janiszewski, et al., 2016) (Honkonen, 2016). But the BTES has a lower efficiency rate due to high losses with the achievable building demand, which lacks comprehensive research on it (Vallin, 2019).

2.1 Aquifer Thermal Energy Storage (ATES)

An aquifer is the water and mineral layer that is trapped between the solids of the underground. ATES systems use the aquifer as the storage media to store heat extracting from the solar energy and one or more pair of wells are drilled into the aquifer to inject and extract the heat from the groundwater (Nordell B. , Large Scale Thermal Energy Storage, 2000). The general functioning of the charging ATES systems is by heating the cold water that is pumped from the cold well during summer to the heat exchanger, where it heats the circulating water and sends it to the hot well to utilize in the winter. In winter, the discharging of the ATES system takes place by cooling down

the aquifer when the hot water is pumped from the hot well and circulated in the heat exchanger, where it cools down the hot water and sends back to the cold well. ATES systems can be used for short and long-term periods. One of the added advantages is the addition of heat recovery from the building will be sent to the hot well during the charging phase in summer. Hydrogeological site conditions are one of the limitations of the ATES system. Proper planning is crucial in ATES systems to make sure the short-circuiting does not take place. Short-circuiting in the context means the interference between the water of the cold well and hot well.

2.2 Cavern Thermal Energy Storage (CTES)

Cavern thermal energy storage (CTES) needs large caverns underground to store large amounts of thermal energy in the form of water. To build a new cavern, we need to excavate large storage amounts of underground volume where the initial budget would be higher. One of the ways to greatly reduce the initial budget would be to use the existing caverns. These existing caverns were shunned caverns and oil storages which can be reformed into water reservoirs for CTES. Usually, caverns are placed very deep so that they are less likely to be affected by ambient temperatures due to seasonal changes. The major advantage of CTES is higher injection and extraction rates that result in an incapability to produce higher power (Nordell B. , 2000). One of the safety measures of the CTES construction is to prevent groundwater leakage from entering the caverns that lead to heat losses. In CTES, heat losses happen by the convection of heat through the cavern walls because the storage walls are not insulated, and water is in direct contact with those rock masses. This temperature differentiation of storage water and rock mass leads to heat losses in the initial 1-2 years and get leveled up later (Honkonen, 2016). Since the volume of the caverns is massive, thermal stratification of the water helps to reduce the heat losses during the charging phase. Thermal stratification develops due to the difference in the density of the two water layers as a result of the different temperatures. This difference in temperature puts lighter and warmer water on the top while denser and colder water at the bottom. Thermal stratification in CTES can be improved with the increase in aspect CAR (Honkonen, 2016). Here CAR is the ratio between the depth of the cavern to the width of the cavern. A higher aspect ratio would provide better results in thermal stratification but lacks in

mechanical stability. So, we should have an optimal aspect ratio for mechanical stability without compromising thermal stratification.

2.3 Tank Thermal Energy Storage (TTES)

TTES is made by artificial built huge water reservoirs to store energy. These huge water tanks can be situated above the ground surface or underground but preferably underground considering environmental conditions. The tanks are made of precast or in-situ concrete or steel wall with built-in elements like stainless steel liner to ensure water and steam tightly sealed off (Honkonen, 2016). Usually, precast concrete is popular for underground storage because it occupies less space and time but it is preferable when integrates with current buildings. Due to the stainless steel liner in the concrete or steel wall, the tank becomes lighter in weight but brings the corrosion problems (ARANER, 2020). The piping system is situated in the center of the TTES to inject or extract water from various levels of height under the seasonal temperatures. This arrangement enables the thermal stratification is not getting affected while charging and discharging thermal energy from the TTES. The design of the tank shapes influences the efficiency of the TTES system that indirectly leads to heat losses. So the optimal design of the shape of TTES depends on the ratio of surface to the volume which has to be minimal. Barrel and sphere-shaped tanks are the optimal design that has the lowest surface area to volume ratio to increase heat efficiency. Heat losses are caused by two major factors in the TTES system namely by the blending of the hot and cold water, and by convection of heat to the surroundings. Ground conditions for the TTES must be stable to reduce the price of the groundwork for foundations. Apart from the price of the tank, there are no such limitations in geographical locations, unlike the other sensible TES systems (Honkonen, 2016).

2.4 Pit Thermal Energy Storage (PTES)

The process of PTES is like CTES in terms of excavating but in the form of the pit with larger diameters and fill it with water. This larger pit excavated to soil, or rock mass acts as a water reservoir to store the heat. The inclination of the storage walls could be around 1:2 for lining fittings around. We can increase pit volume by excavating at the bottom side locks. PTES should be designed with water resistance to prevent water leakage in the storage volume as well as the energy of the losing water in the storage volume (Honkonen, 2016). Usually, the bottom and sides of the storage are made with

bentonite liners, polymer liners, elastomers, and metal liners and sometimes also with the concrete to prevent the water leakage. Since the PTES is not deep like CTES, charging and discharge are faster (Kallesøe & Pedersen, 2019) and it can store the temperatures up to 90℃ due to the large volume of water in the pit. In the PTES system, floating cover is the most expensive part that insulates on top and they are different kinds like floating insulation, stiff insulation elements, and expanded clay or glass insulation depending upon the position of the installation and its purpose (Honkonen, 2016). Usually, PTES occupies large areas which makes it difficult to construct in urban areas so the top of the insulation can be reformed as the park, parking, or any recreational area .

2.5 Borehole Thermal Energy Storage (BTES)

BTES is the most popular and flexible UTES system due to its financial advantage and ease of construction (Honkonen, 2016). Unlike other UTES systems, BTES doesn't need any large excavations. From fig.1, it is visible that the BTES system stores heat in the ground by circulating water in underground vertical pipes acting as a heat exchanger. Considering the kind of soil properties, hydrogeological and economic conditions at high latitudes in among all the seasonal thermal energy storage (STES) systems, (Janiszewski, et al., 2016) proposed that Borehole Thermal Energy Storage (BTES) is the feasible seasonal thermal energy storage (STES) system in Finland. BTES uses natural bedrock or soil as the storage medium to store the heat energy. During the summer season, the hot water coming from the STC or any heat source like industrial waste heat is pumped to the middle of the BTES field from where the hot water starts flowing towards the edge of the area through the BHEs placed in the drilled boreholes and connected in parallel or series among each other. During this process, the heat is transferred from the water to the rock via heat conduction. During the charging phase in the summer heat is concentrated in the center of BTES and colder temperatures are gradually in the outer edge of BTES as shown in *Figure 1*. On the other hand, as shown in *Figure 2*, when we need to discharge it, cold water is sent to the edges of (Energy, 2020)he BTES field and extracted warmer from the center of the BTES mechanism. To minimize thermal losses BTES is built in a cylindrical shape to maximize the volume-to-surface ratio. Moreover, considerable design of a borehole TES creates certain temperature distribution in the rocks, with the high temperatures

concentrated at the core in the center of BTES and gradually decreasing towards the edges, which helps to reduce the thermal losses. The charging and discharging power of a BTES is relatively low due to slow energy transfer in the borehole medium. BTES are typically not insulated due to cost reasons; however, their geometry can be altered to reduce losses through their surfaces.

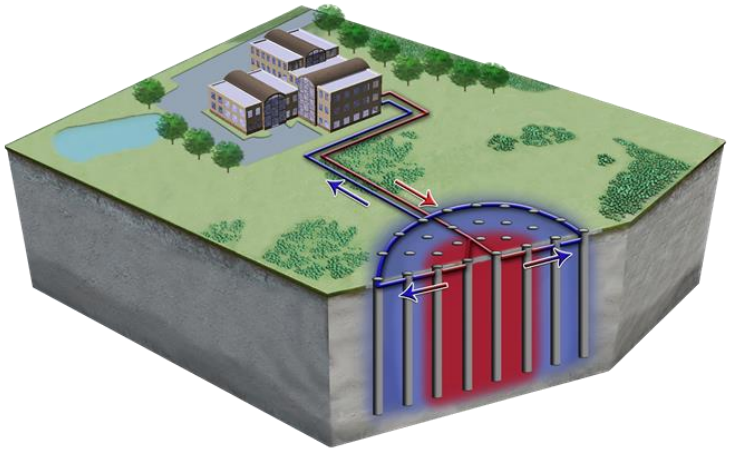

Figure 1. BTES during summer in the charging phase from buildings (Underground Energy, 2020)

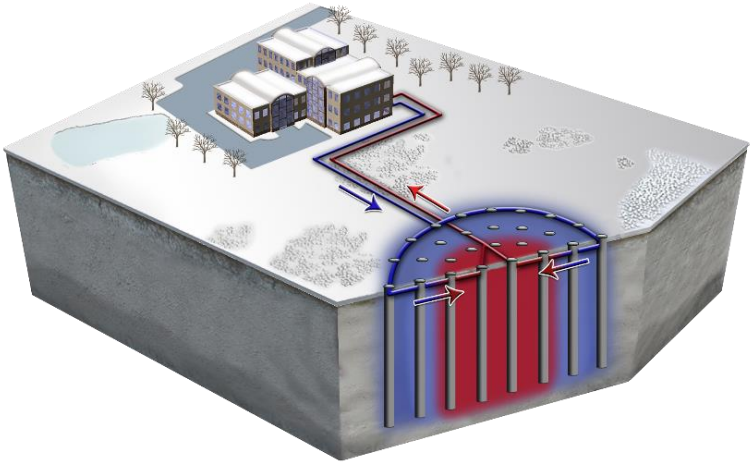

Figure 2. BTES system during winter during the discharging phase to buildings (Underground Energy, 2020)

2.5.1 Principle of BTES

Usually, any sensible heat storage requires a high amount of heat capacity. BTES uses the underground soil or unconsolidated rock as the storage medium to store the heat from the intermittent or waste heat sources. BTES uses the principle of heating the subsurface in the center of any geometrical design and gently cools down the

temperatures by circulating through the closed-loop systems in the borehole (Kallesøe & Pedersen, 2019). In the case of Scandinavian regions, an open-filled borehole system is used in the hard rock due to great heat exchange performance which is not similar in the rest of Europe due to unconsolidated rock conditions (Reuss, 2015). The distance between these boreholes typically ranges 2.5m-5m depends upon the area of the site, the volume of the storage, and thermal properties (Gehlin, 2016). The borehole's heat exchangers (BHEs) in the boreholes are responsible for carrying the heat transfer during the charging phase in the summer and discharging phase in winter. BTES can store up to the temperatures of 90℃ and is the ideal sensible storage system to integrate with other renewable heat sources, storage systems as well as the heat pumps (Kallesøe & Pedersen, 2019). Heat losses depend upon the several factors of thermal properties and hydraulic properties, insulation materials, the geometry of the BTES, and groundwater flow. Usually, heat losses are associated with conductive heat transfers between the storage volume and bedrock. Injection temperatures into the storage area based on heat demand and the temperature difference are affected by unseasonal fluctuations in temperatures. The charging and discharging speed of heat transfer in BTES is relatively slow due to the low HTR in the pipes. In such case integration of tanks would speed up the heat transfer process.

2.5.2 Preliminary investigation of the site

A preliminary investigation of the site includes the seismic testing of the area, existing or new infrastructure, core drilling, building heat demand, the power capacity of BTES, etc. There will be a screening process to check the hydrogeological conditions to make sure that there will be adequate depth to the groundwater table from the boreholes. The screening process also examines the thermal properties of the soil or unconsolidated rock and grout material. All the energy systems, including the BTES, need to have a detailed study on the heat source, building issues, environmental aspects, and other risk analysis (Kallesøe & Pedersen, 2019).

2.5.3 Construction

Based on the preliminary screening process, we will get the regulative framework idea on the geological, drilling, and hydrological conditions of the site, and thermal properties of the soil or rock. The preferable condition of the BTES is a drillable area with high heat capacity, and while drilling the area, the soft residue is more exigent and longstanding than hard rock. So, the normal direct rotary mud drilling technique is

preferred for the soft residues, and as per the (Kallesøe & Pedersen, 2019) guidelines, it is suggested to use casing while drilling the soft residues to avoid the cavities, surplus amount of grout, and from boreholes crash. The distance between the BHEs and borehole must be sealed to preserve the groundwater resources from in contact and to provide a considerable amount of high thermal conductivity between the BHE and borehole in unsaturated conditions. Grouting takes place in the closed-loop systems of BHEs from the bottom of the borehole in an upward direction. The ground surface of BTES can be reformed to use it as a parking lot, park, and also can construct the building as shown in *Figure 3*.

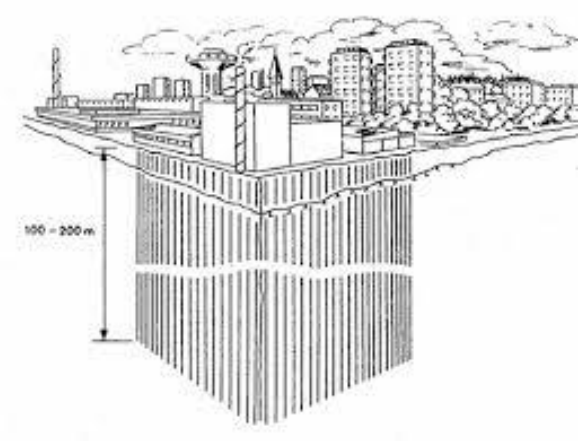

Figure 3. Buildings constructed on the surface of the BTES system where boreholes are drilled at the depth 100-200m beneath the surface (Nordell, Grein, & Kharseh , 2007)

2.5.4 Finnish Ground Conditions

Thermal properties are an important factor for consideration when selecting thermal energy storage sites. Finland's geology is comprised primarily of crystalline Precambrian bedrock which is thermally stable and hence suitable for storing underground energy. Finland lies on the Baltic or Fennoscandian shield, where most of the bedrocks have thermal conductivity between $2 - 4\ \mathrm{Wm^{-1}K^{-1}}$, and volumetric heat capacities close to 2.2MJ/m^{3}K (Honkonen, 2016). There are various kinds of bedrocks in Southern Finland as shown in *Table 1* whose thermal conductivity typically ranges between $3.5 - 4\ \mathrm{Wm^{-1}K^{-1}}$. Thermal conductivity of the rock plays a major role in the performance of thermal distribution between boreholes and bedrock volume but at the same time heat losses occur with increasing thermal conductivity. The higher the volumetric heat capacity in *Table 1* i.e Migmatitic granite, provides better storage

efficiency and higher the thermal conductivity provides the higher extraction rates indeed the thermal losses.

Table 1. Thermal conductivity and volumetric heat capacity of the rocks that occupy the major area of Finland

Rock type	Thermal conductivity (W/mK)	Volumetric heat capacity ($MJ/m^{-3}K$)
Granodiorite	3.50	1.85
Migmatitic Granite	3.90	2.34
Felsic Gneiss	3.47	2.08
Mica Gneiss	3.75	2.08

As per (Nordell B., 1994), crystalline bedrock can be influenced by groundwater in unfavorable conditions like fractures in the roughness of the bedrocks. Groundwater water can have a significant influence on the heat losses from the borehole when the groundwater has a considerable flowrate (Honkonen, 2016). Although groundwater movement can increase the volumetric heat capacity of the storage system, groundwater movement within and through the storage volume can interfere with the desired temperature zones and increase losses. (Penttinen, 2000) mentioned that the groundwater table will have no influence on the flow rate from the borehole when the depth of the ground table is placed thrice more than the depth of the borehole.

Table 2. Thermal Properties of soils and rocks across higher latitudes

Type of Storage medium	Density [kg m-3]	Thermal Conductivity [W m-1 K-1]	Heat Capacity [kJ kg-1 K-1]	Volumetric Heat capacity [kWh m-3 K-1]
Granite	2700	2.9-4.2	830	0.62
Pegmatite	2700	2.9-4.2	860	0.62
Syenite	2650	2.2-3.3	850	0.65
Diorite	2800	2.2-3.3	850	0.66
Gabbro	3000	2.2-3.3	860	0.72
Diabase	3000	2.2-3.3	860	0.72
Sandstone	2700	3.0-5.0	730	0.55
Clayshale	2800	1.7-3.5	850	0.66
Limestone	2700	1.7-3.0	840	0.63
Quarzite	2650	5.0-7.0	790	0.58
Gneiss	2700	2.5-4.7	830	0.62
Leptite	2700	2.5-4.5	830	0.62
Marble	2700	2.5-3.5	770	0.58
Water	1000	0.62	4180	1.18

The thermal properties of the soils (separate from rock) depend upon the porous structure, saturated, unsaturated, and permeability factor. Various rocks and soils with geological compositions and thermal properties namely density, thermal conductivity, heat capacity, and volumetric heat capacity across higher latitudes depicted in *Table 2*. The average value of soil thickness in Finland can range from 8.5 meters to 100 meters which also an important consideration for selecting the right geological location to appropriate TES method (Honkonen, 2016).

2.5.5 Design Considerations

BTES is the volume or rock or soil sediment approached with the volume of BHE array (Skarphagen, Banks, Frengstad, & Gether, 2019). BTES utilizes the higher volumetric capacity of rock or soil sediments to charge the large quantities of water in pipes to store the heat during the summer season and utilize it in the winter season. The design of the BTES system is the strategic step in the process of reducing heat losses economically. Borehole storage design depends upon the in-situ parameters, thermal properties of the storage medium, and heat demand of the residential building or industry. The thermal performance of BHEs is influenced by the parameters like depth of BHE, operation time, shank spacing between the pipes in BHE, the temperature of the fluid, and its flow rate apart from the thermal properties of grout and surrounding rock (Gultekin, Aydin, & Sisman, 2019). Several geometries for the BTES had been evolved since the 1990s from the linear geometry to square-shaped geometry to circular shaped geometry to hexagonal geometry. The strategical design changes in BTES geometry had evolved to achieve the lower surface area/volume(D/H) ratio in a cost-effective way to abate the heat losses. A higher lower surface area/volume ratio leads to conductive heat losses. An optimal cost-effective value is to have an equal surface diameter to the length of the borehole ratio in an array shape. (Ying & Seth, 2016) confirmed that the geometrical array of rectangular-shaped (2×8) provided better thermal performance compared to the square-shaped (4×4) because the larger perimeter gave better heat dissipation around the surrounding soil/rock. Cylinder and Hexagonal geometrical arrays are the best possible means to have the maximum internal volume with the minimum surface area. *Figure 4* represents a cylindrical BTES model with a borehole field radius of 27m representing the connection of 90 boreholes in series.

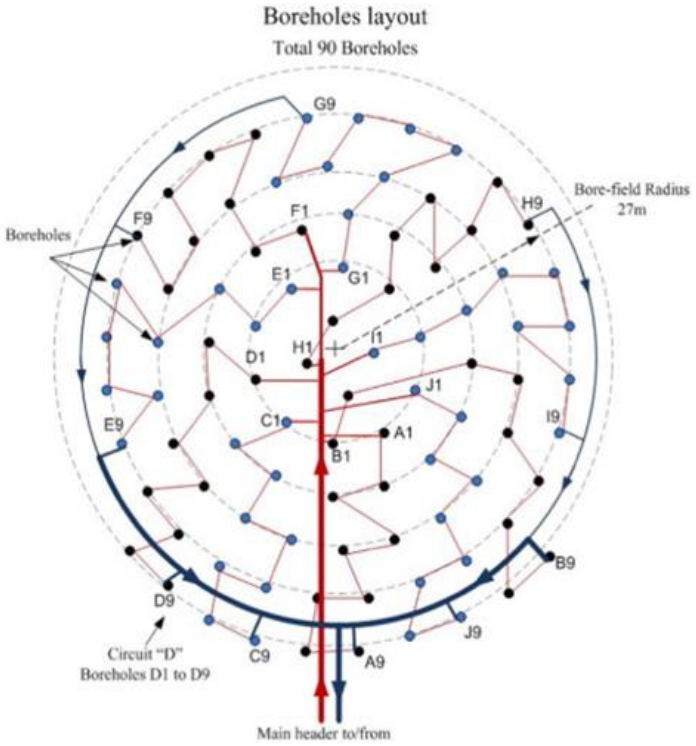

Figure 4. Circular BTES (M.Rad, S.Fung, & A.Rosen, 2017)

Considering the Hexagonal array saves up the surface area and the heat was more concentrated in the middle BHEs, which in turn reduces the cost. As a part of optimizing design, efficiency could be improved by boosting the heat load of BHEs (Gultekin, Aydin, & Sisman, 2019). (Elhashmi, Hallinan, & Chiasson, 2020) also concluded that BTES efficiency could be increased and heat losses could be decreased with an increasing load that makes solar-assisted BTES system more cost-effective in case of larger communities rather than one building. Although spherical geometrical array has the lowest surface area to volume ratio to minimize the heat, it is demanding in real-life applications (Kallesøe & Pedersen, 2019). Arrangement of geometry and borehole spacing has become important parameters with the duration of the operation (Gultekin, Aydin, & Sisman, 2019). Heat losses are minimized with the diameter of the BTES to a height of the borehole (D/H) ratio between 1 and 2, where (Lanini, Delaleux, Py, Olivès, & Nguyen, 2014) proved to have a D/H ratio as 2 for small storage applications that must not exceed 100m height of the boreholes and in (Vallin, 2019) it was studied optimal D/H ratio as 1 for applications of the height of the boreholes above 100m. In the case of high heat demand, (Vallin, 2019) mentioned medium storage applications

with a length of the borehole above 500m is the feasible solution and also possesses less influence of groundwater flow due to increased depth in crystalline bedrock. (Gultekin, Aydin, & Sisman, 2019) examined the dependency on the aspect ratio (BAR) of geometrical field arrangement, operation time, and the number of boreholes (N) affected the thermal interaction coefficient, which is the quantified value of dependency of total heat transfer of several BHEs in their borehole spacing.

In this thesis, it is found that the D/H ratio lower than 1 would save the larger mass flow rate, which might not lead to thermal losses towards the outer rings but the heat storage efficiency would be lower. In many applications, borehole spacings range between 2.5m-5m depend upon the thermal properties and array pattern of the storage medium (Gehlin, 2016). Storage temperature varies with the borehole spacing because when the distance between the heat source and circumcenter of an array increases then the temperature change decreases and its vice versa in lower borehole spacing. Lower borehole spacing extracts more power and heat in lesser time. BHE spacing plays a pivotal role in storage performance because lower BHE spacing would decrease the storage volume thereby decrease the storage efficiency whereas the larger BHE spacing would decrease the thermal interactions between the boreholes and thereby decreases the thermal performance. Hence, to exploit the maximum thermal performance optimal BHE spacing is required (Welsch B. , 2019). However in the case of thermal interaction (Gultekin, Aydin, & Sisman, 2019) proved that when BAR value (for example an array arrangement: $4(\text{row}) \times 16(\text{column})$, BAR= $\frac{4}{16} = \frac{1}{4}$) decreases, both thermal performance losses and thermal interaction coefficient decreases and at BAR$>$ $\frac{1}{3}$, effects reduce to negligible thermal performance losses and thermal interaction. Similarly, when the number of boreholes(N) becomes greater than the critical(poor) number of boreholes(N_{cb}), then the thermal interaction coefficient becomes negligent, but when its N$<$ N_{cb}, significant reliability on thermal interaction will be observed. Due to the hexagonal pattern, the distance between the circumcenter and outer ring has a shorter distance than other patterns which is more efficient.

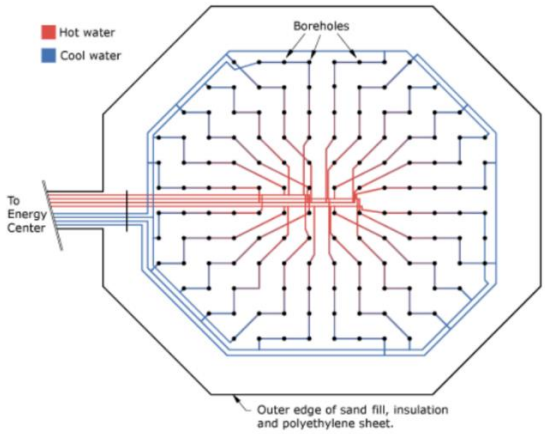

Figure 5. Hexagonal BTES in Aerial View (Kallesøe & Pedersen, 2019)

In the initial years of operation, there will be more power consumed to heat the center of the BTES system as shown in *Figure 5* which is having series in the connection that is identical to *Figure 6* but the field model has the combination of series and parallels in the recharging process to inject higher heat than it is extracted. We can observe that the heating mechanism in *Figure 5* shows that core temperatures are concentrated in the center of the BTES while gradually lessen the temperatures towards the outer rings after passing from every outlet of the ring. The lower temperatures are used according to the heating demand of the building or industries during the discharge. *Figure 7* is the real model of the BHE field taken from Heliostorage Oy projects, which shows the combination of parallel and series connection. After 4-6 years of operation, a quasi-steady state will be achieved reaching the operating temperatures, and yearly heat losses to the surface and surroundings turn stable (Skarphagen, Banks, Frengstad, & Gether, 2019). During the recharge phase, cold temperatures that are absorbed during winter are utilized in the summertime starting the cold mechanism from outer rings to the center of the BTES, so that again the core higher temperatures stay at the center region. After discharging every time there will be the heat left out which can be utilized in the recharging phase to save the energy called the thermal recovery. Thermal recovery in the design is defined by the ratio of heat recovered to the heat recharged per annum. Higher thermal recovery makes higher in the performance of the BTES by saving up the energy from an economical viewpoint.

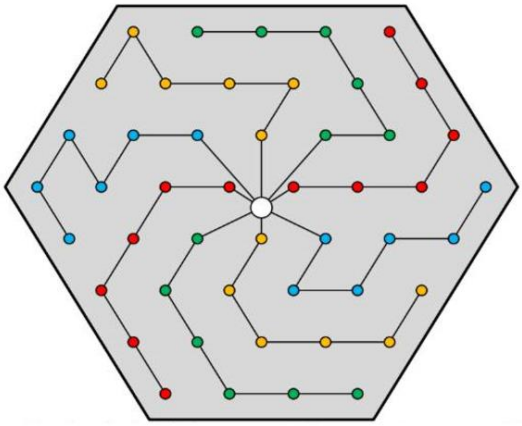

Figure 6. BTES series connection of boreholes followed in DLSC project, Canada (Kallesøe & Pedersen, 2019)

Borehole drilling followed by piping and insulation materials takes up the higher capital cost among all and some drilling methods lead to larger deviations which leads to uncertain borehole spacings or intersections at depths in BTES.

Figure 7. Parallel and Series connection of one of the Heliostorage BTES projects at Kokkola,

2.5.6 Piping Materials

Borehole Heat Exchanger(BHE) U-tube is typically made up of high-density polymer polyethylene (HDPE) or cross-linked polyethylene (PEX) with 40mm outer diameter. High-temperature BTES systems use PEX, PE of higher thermal resistance, and steel are the preferred materials (Skarphagen, Banks, Frengstad, & Gether, 2019). There is a wide range of alternative materials to HDPE for BHE use, including thermoplastics such as PVC, PEX, and reinforced PP, as well as metals such as thick-walled mild steel, galvanized steel, L-grade stainless steel, aluminum, copper, and titanium shown in *Table 3* with the range of corresponding thermal conductivities.

Table 3. Thermal conductivity (λ) of various thermoplastic piping materials (*) Boudenne et al. 2004, Heat atlas 2010, Wypych 2016, Zhao and Ye 2011, (**) New material, http://www.rtcompany.com/

Thermoplastic material	Thermal conductivity(λ) ($Wm^{-1}K^{-1}$)
Acrylonitrile butadiene styrene (ABS)	0.16
Cellulose acetate butyrate (CAB)	0.17-0.33
Polyoxymethylene (POM)	0.30
HDPE	0.46
LDPE	0.32
PEX	0.41
Thermally enhanced HDPE (**)	1.2-2.2
Polypropylene (PP)	0.23
Reinforced PP	0.15
Polyvinyl chloride (PVC)	0.16
Chlorinated polyinyl chloride (CPVC)	0.14
Polynivylidene fluoride (PVDF)	0.22
Polyamide-6 (Nylon-6)	0.22
Polybutylene (PB)	0.22
Polyphenylene oxide (PPO)	0.20
TPE	0.17

Apart from titanium and perhaps copper, local ground conditions must be considered when using metallic materials. Since the higher thermal conductivity from *Table 3* provides the HTR which results in higher thermal performance. So, Thermally enhanced HDPE from *Table 3* is a new material that may be promising for BHE use in the future when such a wide variety of pipes become commercially available in the range of materials. In each case, material selection should consider the corresponding BHE costs. In the evaluation done in this paper, HDPE, despite its low thermal conductivity, remains a very competitive option for use in every geologic environment.

Pipe material	External diameter mm	Wall thickness mm	Cost, €/m
HDPE Φ32 (internal)	32	3	1,38
HDPE Φ63	63	3,8	3,44
PEXa Φ63	63	3,8	6,88
PVC Φ63	63	3	3,08
PB	63	10,5	19,94
PP random	63	10,5	10,90
PP reinforced	63	5,8	8,04
seamless steel black	60,3	5,54	38,96
seamless steel galvanized	60,3	3,6	37,18
welded steel galvanized	60,3	2,5	28,01
seamless steel with external PE coating	60,3	2,9	23,83
seamless steel with external bitumen coating	60,3	2,9	23,67
stainless steel 304	60,3	1,5	22,00
stainless steel 316	60,3	1,5	37,41
stainless steel 304L Cheap-GSHPs quote	60	2	6,37
aluminum	63	2,5	9,76
copper	64	2	37,08
titanium, seamless	73,02	3,05	134,75

Figure 8. Range of price, wall thickness, and external diameter for commercially available pipe materials (Mendrinos, Katsantonis, & Karytsas, 2016)

Most of the piping materials shown in *Figure 8* are broadly used in thermal storage systems, provided with the commercial costs depending upon their diameters. With appropriate commercial agreements for pipes procurement, metallic solutions can also become competitive, for example in the case of 304L stainless steel and aluminum using the special quotes for cheap-GSHP's. (Mendrinos, Katsantonis, & Karytsas, 2016). The life expectancy of those materials of coaxial BHE is depicted in *Figure 9* showing that titanium material has the highest life expectancy of 1000 years though it was presented as 100 years. Predominantly used plastic underground storage piping materials like HDPE, PEXa, PVC, PP-R have a life expectancy of 75 years followed by stainless steel compositions, aluminum, and copper (Mendrinos, Katsantonis, & Karytsas, 2016).

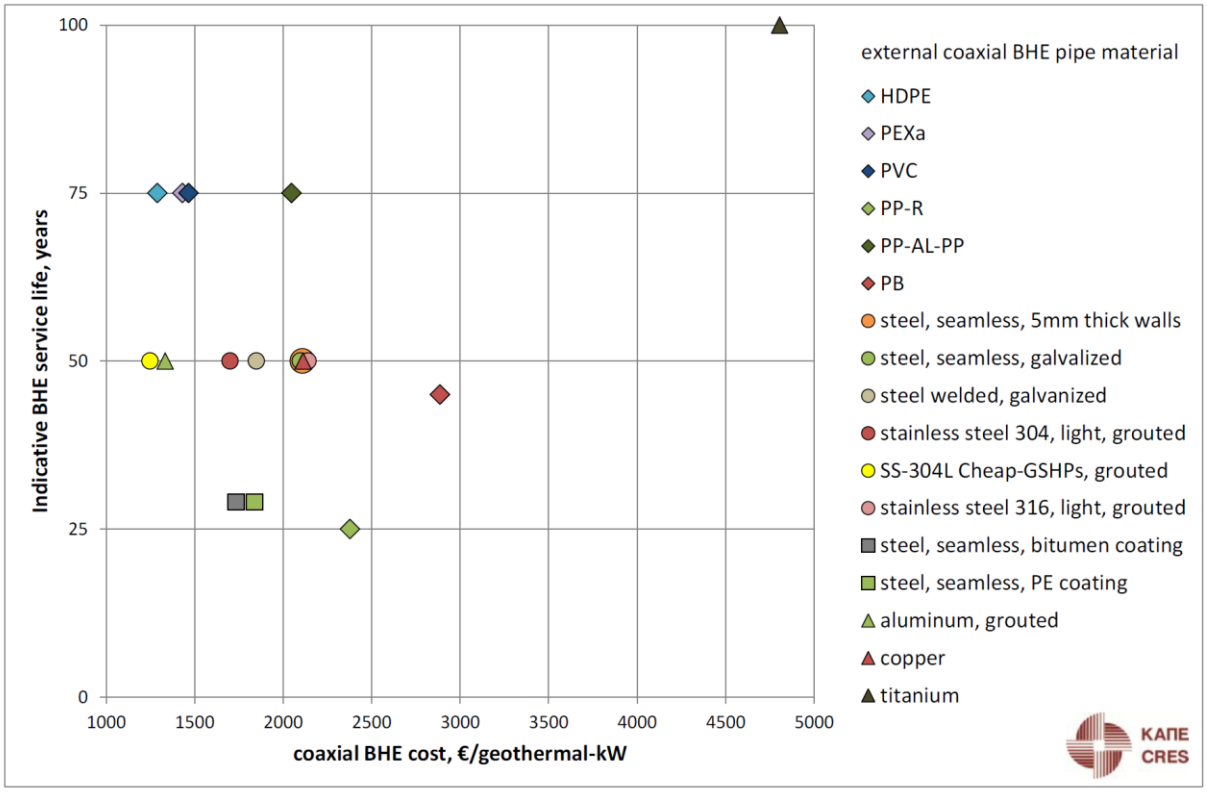

Figure 9. Expected service life (indicative) versus delivered geothermal energy costs by a coaxial BHE using an external pipe made of different market available materials (Mendrinos, Katsantonis, & Karytsas, 2016)

2.5.7 Insulation

One of the major contributors in terms of heat losses in any kind of sensible storage systems is the insulation material. Insulation materials play a significant role in tackling the heat losses. Without proper insulation around the thermal energy storage leads to higher heat losses which incur higher economic losses, especially in the case of seasonal sensible storage systems since the current research is to determine the major factors behind the heat losses and solutions to reduce it further.

Insulation materials can be external material or the natural material which is meant to cover the heat losses from any storage system due to thermophysical properties. Relative analysis of conventional insulation materials such as mineral wool, glass wool with modern products such as the vacuum insulation observed in the regard of thermophysical properties, the economic value of the materials, and footprint (Villasmil, Fischer, & Worlitschek, 2019). Glass wool and Mineral wool are the two inorganic fibrous conventional materials that occupy 60% of European market whereas organic foamy conventional materials like extruded polystyrene (XPS), expanded

polystyrene (EPS) accounts for 27% of the market. Polyurethane-polyisocyanurate (PUR-PIR) is a unique material that has high-rigid performance foam which is noticed as the transitional material between the conventional material group and super insulators group (Villasmil, Fischer, & Worlitschek, 2019). Vacuum insulation panels and silica-aerogels are the excellent super-insulators that falls in the range of $\lambda = 4 - 20\ \mathrm{mW\ m^{-1}K^{-1}}$ whereas the other conventional materials fall in the range of $\lambda = 19 - 46\ \mathrm{mW\ m^{-1}K^{-1}}$ as shown in the *Figure 10.*

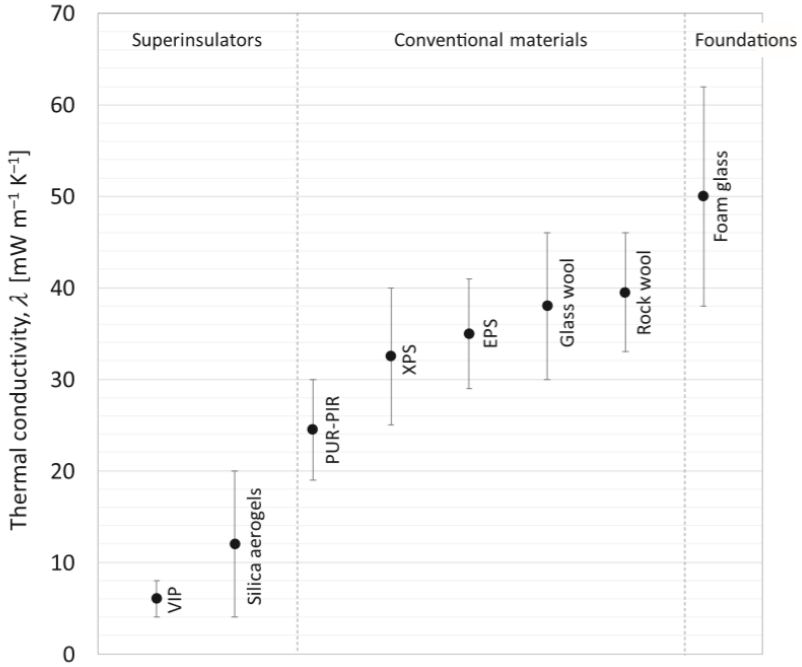

Figure 10. Thermal conductivity of different insulation materials varied by the insulation power of the material (Villasmil, Fischer, & Worlitschek, 2019)

Thermal physical properties of various insulation materials are evaluated based on the thermal resistance(R-value) which is $\frac{\mathrm{Length(L)}}{\mathrm{Thermal\ conductivity(\lambda)}}$.

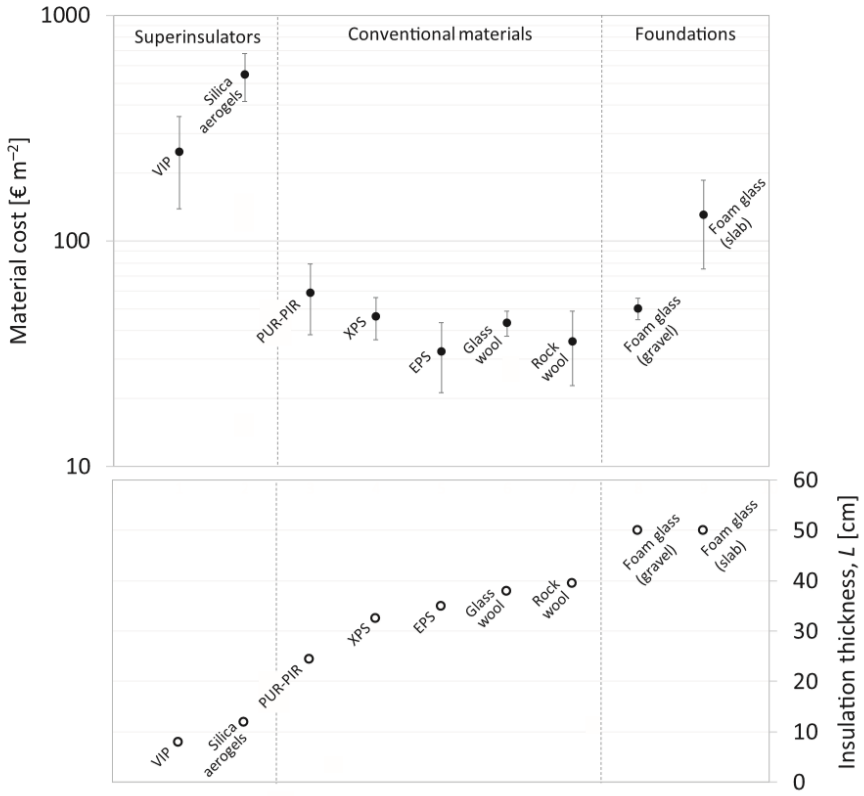

Figure 11. Price of the types of Insulation Materials, according to the thickness (Villasmil, Fischer, & Worlitschek, 2019)

From *Figure 11*, we can see that the vacuum insulation panels (VIP) occupy way less footprint but are expensive than the conventional insulation materials whereas the foundation's categorized materials are the cheapest but occupy the larger footprint with their thickness above 50cm. Vacuum insulation panels are the finest insulation materials with the lowest thermal conductivity nearly followed by silica aerogels. Silica aerogels boasts as highest translucent materials with the porosity up to 99.8%, however at higher temperatures above 200℃ insulating material of Silica aerogels will deteriorate due to the low extinction coefficient. Also, the market possibility of silica aerogels is very limited. The most favorable materials in terms of thermophysical properties, economic feasibility, and footprint are the vacuum insulated panel (VIP) and polyurethane-polyisocyanurate (PUR-PIR) because of the economic value of the footprint outperforms the extra price for these materials. Even more precise, PUR-PIR is the most value-oriented insulation material since we cannot reverse VIP once it deteriorates (Villasmil, Fischer, & Worlitschek, 2019).

2.5.8 Grout materials for borehole heat exchangers

Grout materials act as one of the major assets in thermal distribution between the boreholes and the surrounding ground. Grout thermal properties depend upon the geology and hydrogeological conditions of the site to improve the GHE efficiency. Grout materials are filled with several cement-based mortars, bentonite, silica sand, etc., between the BHEs and borehole wall that makes the stable setup in the bedrock and soil. When the low-permeability thermal enhanced grout is filled, then the heat distributes well to other boreholes that make higher thermal extraction rates during the discharging phase. Grout having higher thermal conductivity reduces the thermal resistance of GHE that enhances the thermal performance of the boreholes (Borinaga-Treviño, Pascual-Muñoz, Castro-Fresno*, & Blanco-Fernandez, 2013). Higher thermal resistance between the GHE and borehole wall struggles to distribute the heat to the ground.

Cement bentonite graphite mix (CBG) itself is the ideal grouting material that is compared with three base aggregates of cement-based mortars namely Blast Oxygen Furnace slag (BOF), Construction and Demolition Waste (CDW), and Silica sand (SS) to determine their influence on the thermal behavior of Geothermal Closed Loop Heat Exchangers in boreholes of similar geometry and geology. Hence, four TRTs were set up in four different vertical heat exchangers to study the impact of grouting material on the thermal conductivity of the ground and the borehole thermal resistance. (Borinaga-Treviño, Pascual-Muñoz, Castro-Fresno*, & Blanco-Fernandez, 2013).

Table 4. Borehole thermal resistance values from the different TRTs

Grout material in boreholes	Borehole thermal resistance($R_{b)}$	Fluid to Pipe convection resistance(R_f)	Pipe Thermal Resistance(R_p)	Thermal Resistance of the grout (R_g)	Pipe to Grout contact resistance($a_{p-g)}$
CBG	0.0714	0.0024	0.0796	0.1569	0.0467
BOF	0.0990	0.0024	0.0796	0.1830	0.1310
SS	0.0817	0.0024	0.0796	0.1030	0.1418
CDW	0.0763	0.0024	0.0796	0.1420	0.0812

Table 4 represents the units of different thermal resistances: R_b, R_f, R_p, R_g, and $a_{p\text{-}g}$ are in $\frac{m.k}{W}$. Based on the analysis of the data provided by (Borinaga-Treviño, Pascual-Muñoz, Castro-Fresno*, & Blanco-Fernandez, 2013) thermal conductivities of CBG, BOF, SS, and CDW are 2.38 $\frac{W}{m*K}$, 2.58$\frac{W}{m*K}$, 2.26$\frac{W}{m*K}$ and 2.20 $\frac{W}{m*K}$, where TRTs of three boreholes displayed mean thermal conductivity of $2.28\ Wm^{-1}K^{-1}$ with a deviation of 0.05 $Wm^{-1}K^{-1}$ and the second TRT has displayed 9% more due to the rainfall effect. Among the grouting materials from *Table 4*, cement bentonite graphite mix (CBG) has yielded better performance in thermal conductivity closely followed by the performance of construction and demolition waste (CDW) which enables to reuse of the drilling residues and construction waste efficiently to promote a circular economy. Grouting material performance in the higher thermal conductivity values do not influence the borehole thermal resistance (R_b).

3. BTES Methodology in COMSOL

The methodology that is presented here is determined to study the seasonal BTES system in an initial eight hours charging for six months, followed by sixteen hours discharging for the next consecutive six months. The analysis is studied in this methodology to find the main objective in the numerical modeling of simulation, i.e., heat losses and its factors that are reducing the efficiency of heat extraction. How much the heat we are losing every year for five years and how those heat losing factors are behaving in five years.

3.1 Numerical simulation of the in-situ design

A 3-D finite element numerical modeling and analysis has been made in the solver and Multiphysics simulation software called COMSOL Multiphysics 5.5 version. The entire numerical simulation is divided into three components apart from stating the global parameters, meshing, study, and results. In the first component, we almost define and extensively specified the selections, variables, physics, and multiphysics pertain to the numerical model. The numerical model as shown in *Figure 13* consists of a block that represents the unconsolidated rock mass and that block comprises of sub-blocks that represent the depth of the soil thickness, depth of the borehole, and depth assumption of the groundwater table (not considered in analysis). The numerical model blocks are divided by four work planes which will be comprehensively explained in the geometry section.

In the numerical modeling, post-designing the required model, we need to assign the required parameters including the few geometrical and thermal properties of the BTES. The parameters shown in *Table 5* are attributes under the global definitions, which implies that the assigned parameters are applied to multiple components. Along with the parameters, we would attribute the analytical functions for the bedrock, charging, and discharging phase under the global definitions.

The analytical function for the bedrock is defined by:

$$((T_{initial} - q_{geothermal})/(k\_bedrock * z)) - 273.15 \qquad 3.1$$

Where $T_{initial}$ denotes the initial temperature of the bedrock

z denotes the depth of the bedrock

Table 5. Parameters of BTES from the real-time input data

Name	Expression	Value	Description
BHEs	126	126	Number of BHEs
soil_thickness	22.5[m]	22.5 m	Thickness of soil layer
insulation	1.5[m]	1.5 m	Soil thickness above BHEs
r_borehole	115[mm]/2	0.0575 m	Borehole radius
H_borehole	40[m]	40 m	Borehole length
r_inner	16.3[mm]	0.0163 m	Collector pipe inner radius
r_outer	20[mm]	0.02 m	Collector pipe outer radius
k_fluid	0.615[W/(m*K)]	0.615 W/(m·K)	Thermal conductivity of working fluid
Cp_fluid	4177[J/(kg*K)]	4177 J/(kg·K)	Specific Heat Capacity of Working Fluid
rho_fluid	995.7[kg/m^3]	995.7 kg/m³	Density of working fluid
k_rock	2.47[W/(m*K)]	2.47 W/(m·K)	Bedrock Thermal conductivity, avg. value from two TRTs
Cp_rock	945.4545[J/(kg*K)]	945.45 J/(kg·K)	Specific Heat capacity of bedrock
d_borehole	2600[mm]	2.6 m	Distance between the 2 boreholes
finnfoam	20[cm]	0.2 m	Finnfoam thickness insulation layer
k_finnfoam	0.05[W/(m*K)]	0.05 W/(m·K)	Thermal conductivity of insulation
rho_finnfoam	50[kg/m^3]	50 kg/m³	Density of insulation material
Cp_finnfoam	1450[J/(kg*K)]	1450 J/(kg·K)	Specific heat capacity of insulation material
rho_rock	2750[kg/m^3]	2750 kg/m³	Bedrock density
rho_soil	2750[kg/m^3]	2750 kg/m³	Soil density
Cp_soil	945.4545[J/(kg*K)]	945.45 J/(kg·K)	Specific heat capacity of soil
k_soil	1.4[W/(m*K)]	1.4 W/(m·K)	Soil thermal conductivity
k_grout	1.6[W/(m*K)]	1.6 W/(m·K)	Thermal conductivity of BHE filling
Cp_grout	4177[J/(kg*K)]	4177 J/(kg·K)	Specific heat capacity of BHE filling
rho_grout	995.7[kg/m^3]	995.7 kg/m³	Density of BHE filling
T_init	5.70[degC]	278.85 K	Initial temperature of bedrock
Q_fluid	28.57[L/min]	4.7617E-4 m³/s	Flow rate of collector fluid during charging
Q_fluid_purku	21.42[l/min]	3.57E-4 m³/s	Volumetric flow rate during heat discharge

The analytical functions for the charging and discharging are defined by the sine function formula for the charging as well as the discharging phases. The primary conditions for the charging phase are eight hours charging every day for six months and consecutive six months is to recover from the discharging phase with sixteen hours each day. Analytical function for the charging and discharging through sine waveform defined by:

$$T_{initial} + 6.0 \sin((2 * \pi / a(\text{year})) * t(\text{seconds}, \text{minutes}, \text{hours}, \text{days}) \quad 3.2$$

Units of time vary according to our requirement

3.2 Geometry

The geometry of the 3-D model is the primary and core part of the simulation design and process. We can either design the model in various 3D designing mechanical software's like AutoCAD, Solidworks, Siemens NX, Catia, etc. and in other forms of designing extensions that we can import through the third party applications under the geometry section, or we can design the 3D simulation model in the COMSOL Multiphysics software itself. In this research, the 3D simulation model of BTES geometry was designed and executed in COMSOL Multiphysics.

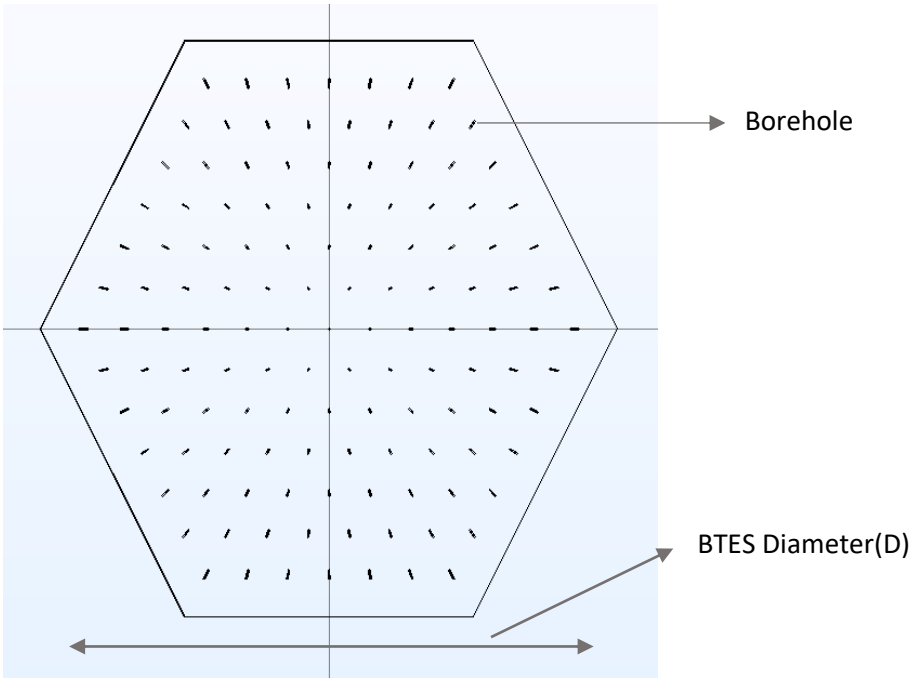

Figure 12. Top view of Hexagonal geometry designed in a different component of the COMSOL

Geometry was designed in the separate components 2 and 3 apart from the main component 1 and imported the corresponding into component 1, where we assign the local attributes. The main aim of the model is to build in the hexagonal shape BTES as per the field scale criteria shown in *Figure 12*. In component 2, the surface area of the rough field scale will be taken into account for the simulation with the side length of 150 m for a square-shaped surface, where the BTES system is built in the center of the area. Then the circles (boreholes) of 115mm diameter each are placed with the spacing of 2.6m between the circles in the hexagonal pattern. The requirement for the BTES system is to build six rings of boreholes with a total of 126 boreholes, including the core central borehole in the hexagonal pattern. To complete the geometry in component

2, circles would be subtracted from the square-shaped simulation field to form the boreholes. In component 3, the hexagonal shape is built from the vector measurements under the geometry section as we can see in *Figure 12*. The component 2 and component 3 will be imported into the primary component 1 under the geometry section at appropriate work planes. In the geometry section of component 1, the simulation model is formed based on the four work planes. The geometry of the work plane one would import the geometry of component 2, i.e. the simulation field area with the boreholes. This work plane one will be extruded till the height of the borehole as shown in the which forms as an upper block.

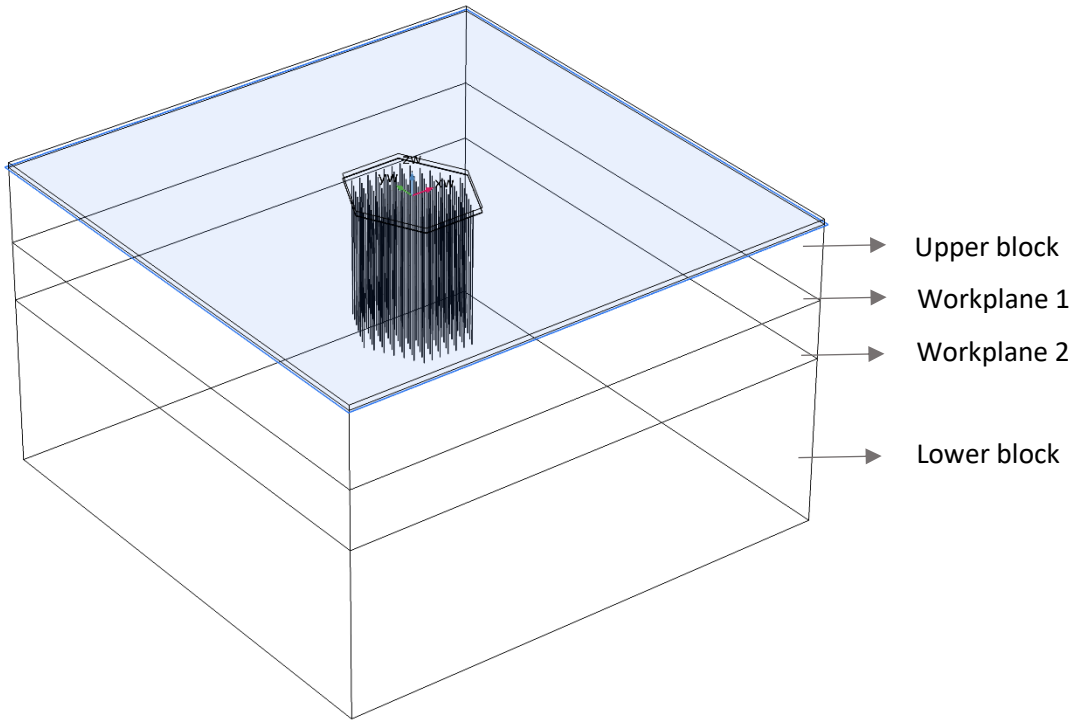

Figure 13. 3D view of BTES geometry in blocks divided into work planes according to allotment of physical and thermal characteristics

As shown in *Figure 13*, work plane 2 represents the depth of the soil thickness, where the bedrock underneath the soil is represented by the blocks. In *Figure 14*, there was a plane like structure below the work plane two which represents the depth of the boreholes, and underneath the final block, extension represents the bedrock depth. There will be another block on the top of the work plane one that represents the insulation layer on top of the soil surface.

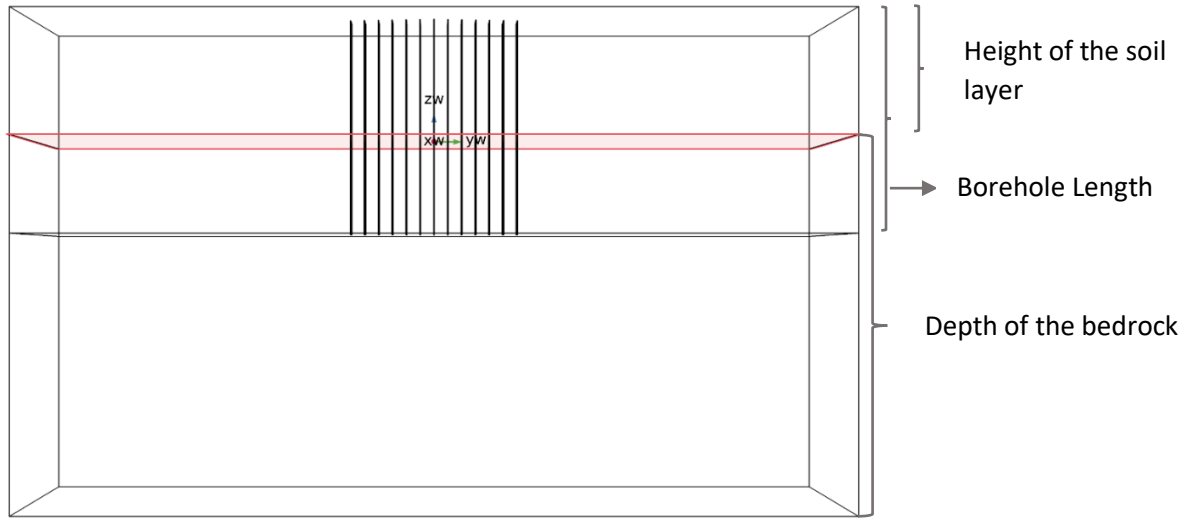

Figure 14. Selection of 2nd work plane in BTES geometry of COMSOL that representing soil height without finnfoam material

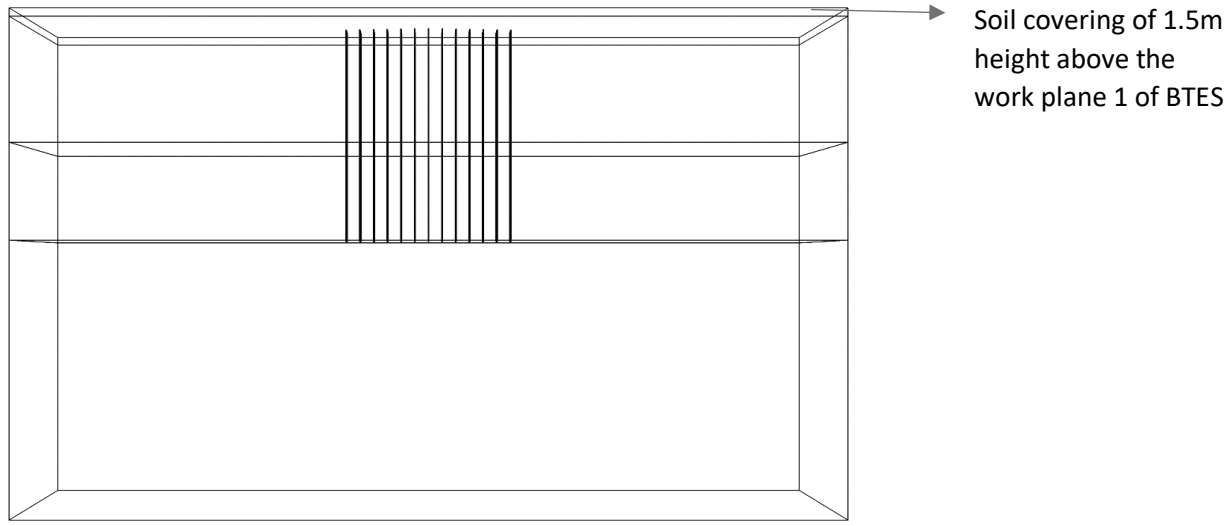

Figure 15. Side view of all the work planes in COMSOL component without finnfoam material on top of the boreholes

Under the geometry section of the work plane 3, the hexagonal geometry of component 3 will be imported, which represents the hexagonal pattern on the boreholes of the BTES system. The hexagonal borders will be extruded, which acts as the foam material for the BTES insulation. Insulation on top of the soil is insulated up to the level of 1.5m above the work plane 1 as shown in *Figure 15*. Usually, the foam material is used at a basic thickness of 10cm. In the following model, the parameters are optimized to minimize heat losses. Work plane four would represent the insulation layer of the hexagonal pattern from the imported geometry of component 3 from *Figure 16*.

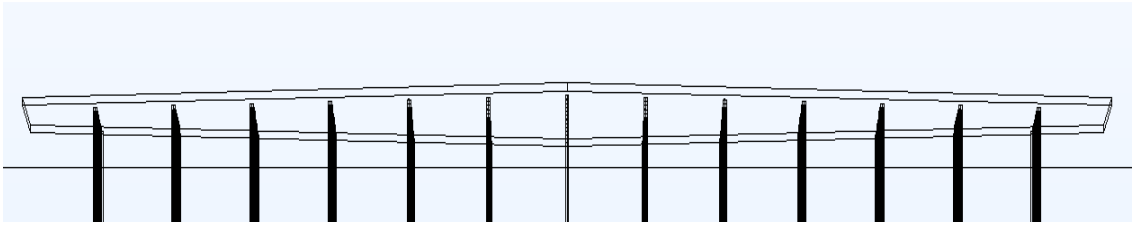

Figure 16. Insulation foam material in work plane 3 on top of boreholes in BTES subsystem to prevent the heat losses

3.3 Variables and Selections

Post-assembling of components 2 and 3 in component 1, we have to assign local variables to component 1 under the definitions. These local variables are correlated to component 1 geometry such as attributing the temperature of the fluid during injection and extraction from ring 1, ring 6, and other different temperatures. Heat losses during charging and discharging can be assigned with the expressions from the global parameters.

Selections are the components that we select and label and later use it depend upon the various operations. Primarily in selections, the required components will be chosen, labeled to check it for the other operations such as edge probe, average temperature operations of the rings during the charging and discharging phases seasonally in a 180-days breakdown cycle. In *Figure 17*, all BHEs are selected to easily apply physics and multiphysics processes to all the boreholes and to mesh them separately into discrete units.

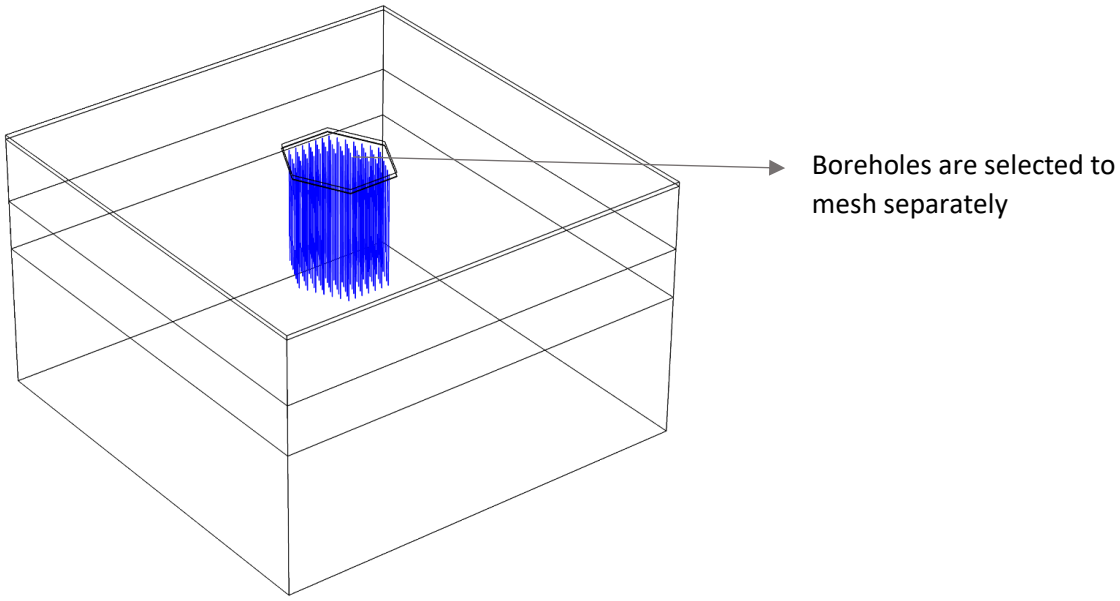

Figure 17. BHEs are selected from the component selection of the 3D geometry of the COMSOL simulation. Convective heat transfer had taken place from the selected boreholes through grout to soil

In *Figure 18*, it is visible how the component, like boundaries of the boreholes of ring one, is selected and labeled. Similarly, such a selection of boundaries needs to be done on boreholes of other rings as well. So that these boundary selections of any ring can be used instantly to know the temperature at the boundaries in various operations

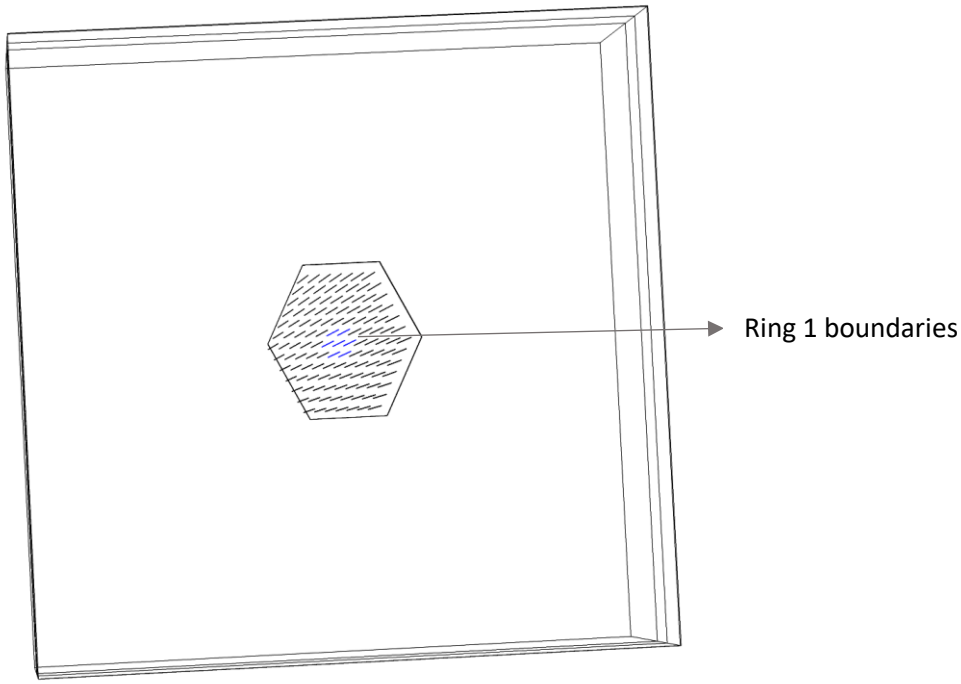

Figure 18. Boundaries of the ring 1 are selected from the component selections so that ring 1 will be assigned with coefficient form of partial differential equation.

Edges of the boreholes of different rings are selected independently, and these edges will be called later at various operations by its label of selections. For example, in *Figure 19*, the edges of each borehole in ring one are selected from the previous selection of edges to examine the development of average temperature of boreholes on ring one during injection from day 1 to day 180 and from day 181 to day 365 during extraction. Again, the same edges from the list of selections can be used for the average operation of boreholes of ring1 to find out the average temperature of ring one during the injection phase and extraction phase as well.

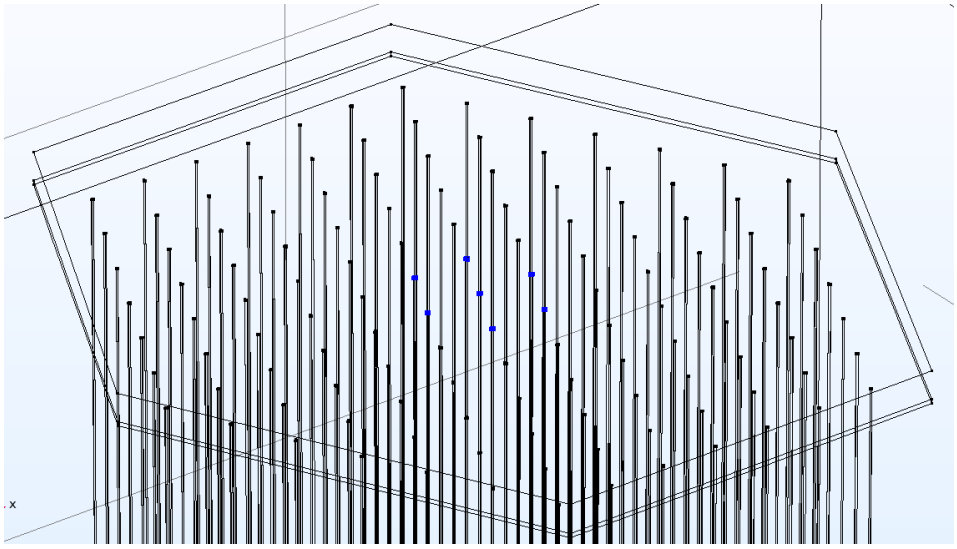

Figure 19. Edges of the Ring 1 are selected to find an average value of the borehole edges in ring 1

Figure 20 is similar to the *Figure 19*, but edges of the boreholes are called from the ring 6 of the selections, which is the outer ring in this model to examine the development of average temperatures of boreholes in the outer ring during injection from day 1 to day 180 and from day 181 to day 365 during extraction. The same selection of boreholes of ring six can also be utilized for the average operation of the temperature of ring six during injection and extraction phases. The operator name in operation can also be used as the local variables in the expression. In this way, once the required components are selected and labeled, they can be called at multiple operations without the selection of each component again.

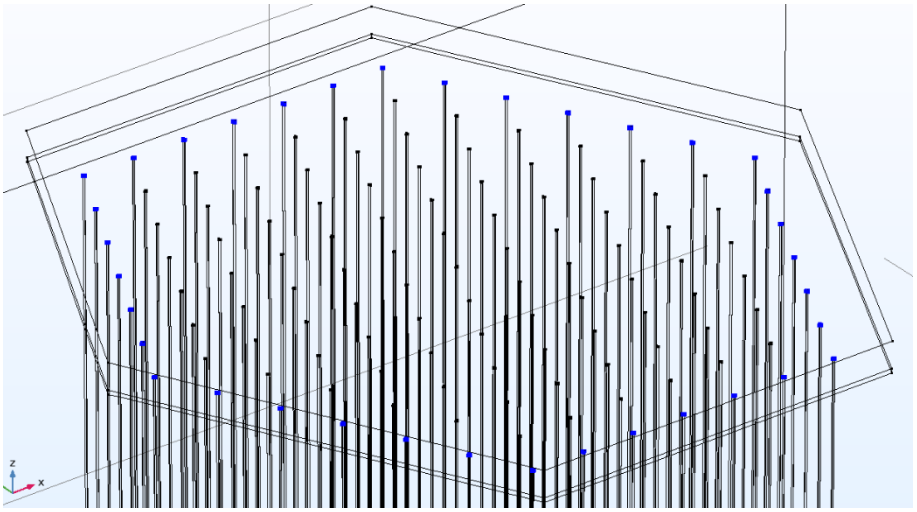

Figure 20. Edges of the Ring 6 are selected to find the average value of borehole edges in ring 6

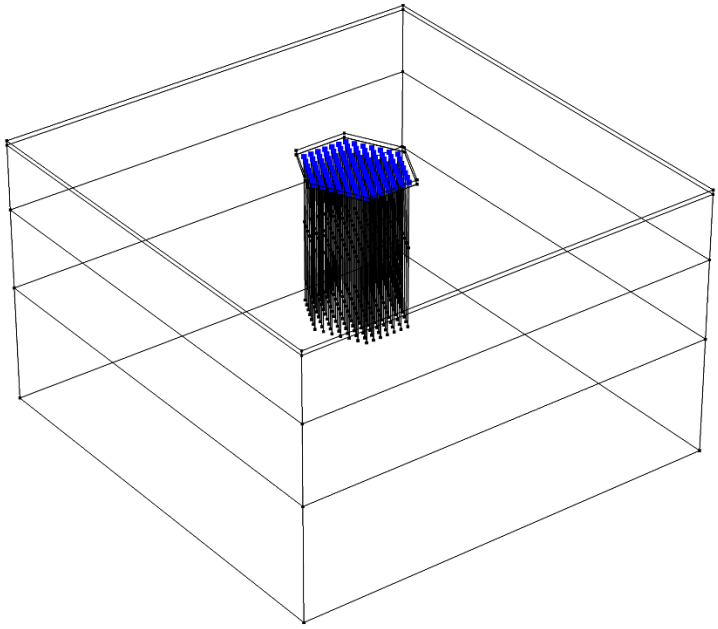

Figure 21. Edges of all the rings are selected in the selections to find an average value of the borehole edges

From *Figure 21*, the edges of the boreholes in all the rings are selected for the average operation to find out the average temperature of all the rings during the injection phase and extraction phase as well.

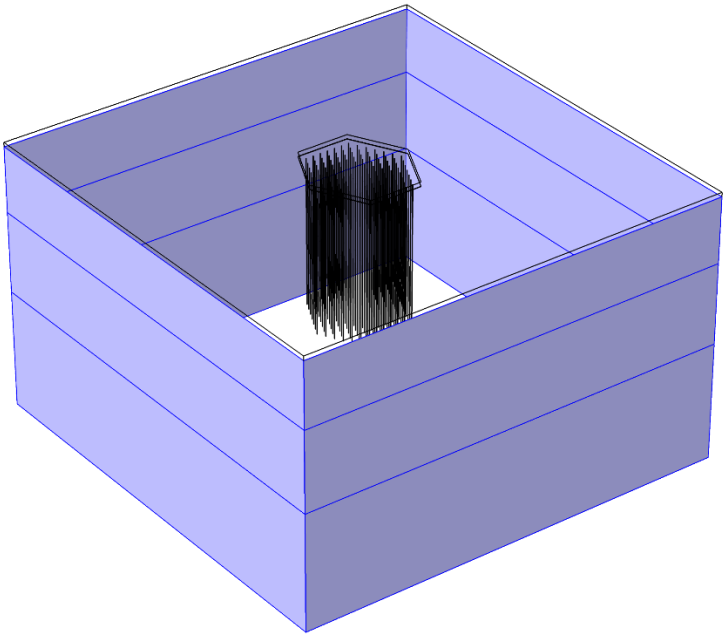

Figure 22. Boundaries of the BTES field selected to find the average value of the surrounding boundaries

In *Figure 22*, boundaries of the field scale are selected for the average operation to find out the average temperature of the boundaries of the field scale around during injection

and extraction phases. In *Figure 23*, the boundary of the lower insulation layer on top of the soil is selected for the average operation to check the average temperature at the lower insulation layer during the injection and extraction phases. Likewise, many such selections of edges, boundaries, and domains will be assigned to various components of the model.

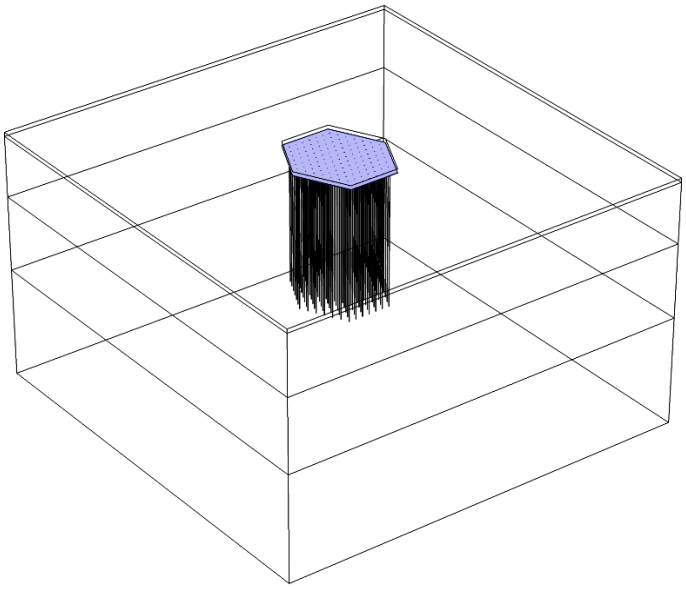

Figure 23. A lower insulation layer was selected in COMSOL to find the average heat characteristics and provide the separate meshing.

3.4 Physics

Physics interfaces use the finite element method within the COMSOL Multiphysics to solve the fundamental partial differential equations. The physics of the simulated model is divided into charging and discharging phases. The procedure of choosing the partial differential operations under the physics of the charging phase and discharging are in a similar line, but the selections and dependent variable would vary from each other. Both in charging and discharging phases, the common selection would be all the boundaries of BHEs in the geometry. The finite element method discretizes the boundaries, domains into simpler and smaller ones known as elements. In determining the physics of charging and discharging phases, we need to solve the partial differential equation for BHEs. The solution comes from computation modeling and solving all the equations of the elements of the model. The solution from the equation of the elements would result in the solution to a partial differential equation. So, the predefined coefficient form of the partial differential equation for the elements of the boundaries of BHEs of

geometry would solve the mathematical operation of a partial differential equation of physics of charging and discharging. The equations within each element are also called as the shape functions in the physics interface. Since the solution to the partial differential equation is a sum of the shape function of elements, linear order would emerge from the linear sum of the elements. The physics interfaces need not be similar because they can use various shape functions which implies it can have unique discretization settings that can manage the degree of order, shape functions that are using for the dependent variables. In charging, dependent variables are assumed as T1, T2, Tg, whereby assuming T1, T2 as the variable for the fluid inlet, fluid outlet, and Tg as the variable for the grout. In the case of discharging, dependent temperatures are assumed as T1p, T2p, Tgp whereby assuming T1p, T2p as the variable for the fluid inlet, fluid outlet, and Tgp as the variable for the grout. The elements that represent the discrete units of boundaries of the geometry goes linear (first-order) and are spatial in the distribution in BHEs of the 3D geometry and uses the language function.

Under the coefficient of boundary form to find the partial differentiation solution of all the BHEs, we need to solve the coefficient form of partial differential equations to every ring individually from the selection of boundaries of each ring.
Initial values of the three dependent variables of the physics interface of charging are the dependent variables of the partial differential equation of BHEs during discharging, i.e., T1=T1p, T2=T2p, Tg=Tgp
The equation of the partial differentiation of all the boundaries of rings in the BTES system is governed by:

$$e_a \frac{\partial^2 u}{\partial t^2} + d_a \frac{\partial u}{\partial t} + \nabla.(-c\nabla u - \alpha u + \gamma) + \beta.\nabla u + au = f \qquad 3.3$$

e_a *is the mass coefficient*

d_a *is the damping coefficient or mass coefficient*

c *is the diffusion coefficient*

α *is a conservative flux convection coefficient*

a *is the absorption coefficient*

γ *is the conservative flux term*

f *is the source term*

where,

$$u = [T1, T2, Tg]^T \quad 3.4$$

$$\nabla = \left[\frac{\partial}{\partial x}, \frac{\partial}{\partial y}, \frac{\partial}{\partial z}\right] \quad 3.5$$

3.4.1 Case of charging:

Charging of the BHEs goes by ascending order of rings starting from the core center of ring 1. We need to choose the Dirichlet boundary condition so that the prescribed value of the dependent variable in each ring from the individual selection of each ring in six rings is taken and the corresponding variable value would be fixed along the inlet edges of the boreholes ranging from ring 1 to ring 6. The variable value will be imposed in each inlet edge selection of rings, and it is governed by the time-dependent injection assuming:

$$g_{reaction} = -\mu \quad 3.6$$

$$\mu = [\mu 1, \mu 2, \mu 3]^T \quad 3.7$$

In ring 1, the prescribed initial value injected temperature is set as 70℃ in the local variable section of component 1. Following the BTES mechanism, an average temperature value of the boreholes in the ring one will be acting as the prescribed inlet variable value to the ring 2, an average temperature value of the boreholes in the ring two will act as the inlet variable value to the ring 3, an average temperature value of the boreholes in the ring three will be the inlet variable value to the ring 4, an average temperature value of the boreholes in the ring four will be the inlet variable value to the ring five and final assigned inlet value to ring six inlet value will be the average temperature value from ring 5.

In COMSOL Multiphysics, we can define the partial differential equation of the boundary of the domain by stating and solving the coefficients for derivates of a different order which results in the coefficient form partial differential equation. These

derivates are typically up to the second-order in both time and space without any combination of an order of derivates.

$$e_a \frac{\partial^2 u}{\partial t^2} + d_a \frac{\partial u}{\partial t} - \nabla.(c\nabla u + \alpha u - \gamma) + \beta.\nabla u + au = f \qquad 3.8$$

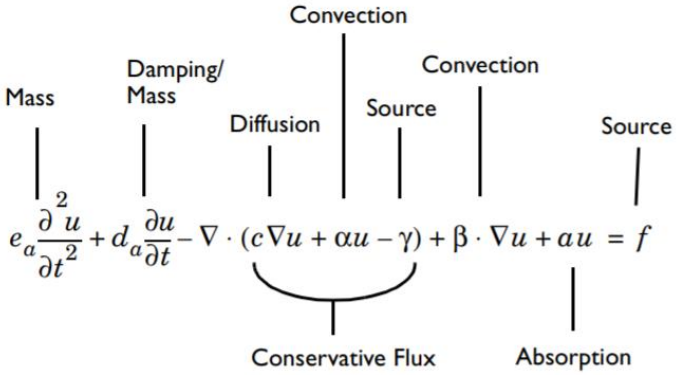

Figure 24. A partial differential equation in coefficient form

To solve the partial differential equation in coefficient form along the boundaries of the domain in each ring, we need to state each coefficient in the partial differential equation of *Figure 24* to the charging dependent variables: fluid inlet T1, fluid outlet T2, ground temperature Tg

3.4.2 Case of discharging:

Discharging of the BHEs goes by descending order of rings with extraction from the outer ring 6. We need to choose the Dirichlet boundary condition so that the prescribed value of the dependent variable in each ring from the individual selection of each ring in 6 rings is taken and the corresponding variable value would be fixed along the inlet edges of the boreholes ranging from ring 6 to ring 1. Since the dependent variables are T1p, T2p, Tgp. The variable value will be imposed in each inlet edge selection of rings, and it is governed by the time-dependent injection equation:

$$\mathrm{u} = [\mathrm{T1p}, \mathrm{T2p}, \mathrm{Tgp}]^{\mathrm{T}} \qquad 3.9$$

$$\mathrm{g}_{\mathrm{reaction}} = -\mu$$

$$\mu = [\mu 1, \mu 2, \mu 3]^{T}$$

A ring 6, the prescribed initial value extracted temperature is set as 20℃ in the local variable section of component 1. Following the BTES mechanism, an average extracted temperature value of the boreholes in the ring six will be acting as the prescribed inlet variable value to the ring 5, an average temperature value of the boreholes in the ring five will act as the inlet variable value to the ring 4, an average temperature value of the boreholes in the ring four will be the inlet variable value to the ring 3, an average temperature value of the boreholes in the ring three will be the inlet variable value to the ring two and final assigned inlet core higher temperatures to ring one inlet value will be the average temperature value from ring 2.

In COMSOL Multiphysics, we can define the partial differential equation of the boundary of the domain by stating and solving the coefficients for derivates of a different order which results in the coefficient form partial differential equation. These derivates are typically up to the second-order in both time and space without any combination of an order of derivates similar as eq. 3.8.

$$e_a \frac{\partial^2 u}{\partial t^2} + d_a \frac{\partial u}{\partial t} - \nabla.(c\nabla u + \alpha u - \gamma) + \beta.\nabla u + au = f$$

To solve the partial differential equation in coefficient form along the boundaries of the domain in each ring, we need to state each coefficient in the partial differential equation of *Figure 24* to the discharging dependent variables: fluid inlet T1p, fluid outlet T2p, ground temperature Tgp.

a. c = diffusion coefficient

where,

In the case of **charging**, the Diffusion coefficient of T1 = Diffusion coefficient of T2 = k_{fluid} $Wm^{-1}K^{-1}$, Diffusion coefficient Tg = k_{grout} $Wm^{-1}K^{-1}$

In the case of **discharging**, the Diffusion coefficient of T1p = Diffusion coefficient of T2p = k_{fluid} $Wm^{-1}K^{-1}$, Diffusion coefficient Tgp = k_{grout} $Wm^{-1}K^{-1}$

b. a = absorption coefficient

where in the case of **charging** absorption coefficient for T1=T2=Tg = 0 $Wm^{-3}K^{-1}$

where in case of **discharging** absorption coefficient for T1p=T2p=Tgp = 0 $Wm^{-3}K^{-1}$

c. f = source term

In case of **charging,**

$$\text{source for T1} = \frac{\left[\text{b\_fluid\_to\_grout} * \left(T_g - T_1\right) * \text{dS\_pipe}\right]}{[\text{dV\_pipe}]} \frac{W}{m^3}$$

$$\text{source for T2} = \frac{\left[\text{b\_fluid\_to\_grout} * \left(T_g - T_2\right) * \text{dS\_pipe}\right]}{[\text{dV\_pipe}]} \frac{W}{m^3} \quad 3.10$$

$$\begin{aligned}\text{source for Tg} = & \frac{\left[\text{b\_fluid\_to\_grout} * \left(T_1 - T_g\right) * \text{dS\_pipe}\right]}{[\text{dV\_grout}]} \\ & + \frac{\left[\text{b\_fluid\_to\_grout} * \left(T_2 - T_g\right) * \text{dS\_pipe}\right]}{[\text{dV\_grout}]} \\ & + \frac{\left[\text{b\_grout\_to\_soil} * \left(T_s - T_g\right) * \text{dS\_grout}\right]}{[\text{dV\_grout}]} \frac{W}{m^3}\end{aligned} \quad 3.11$$

$$\text{b\_fluid\_to\_grout} = 1/\left(R_{fp} * 2 * \text{pi} * r_{outer}\right) W m^{-2} K^{-1} \quad 3.12$$

where $R_{fp} = R_{pipe} + R_{fluid}$

In the case of **discharging,**

$$\text{source for T1p} = \frac{\left[\text{b\_fluid\_to\_grout\_purku} * \left(T_{gp} - T_{1p}\right) * \text{dS\_pipe}\right]}{[\text{dV\_pipe}]} \frac{W}{m^3} \quad 3.13$$

$$\text{source for T2p} = \frac{\left[\text{b\_fluid\_to\_grout\_purku} * \left(T_{gp} - T_{2p}\right) * \text{dS\_pipe}\right]}{[\text{dV\_pipe}]} \frac{W}{m^3} \quad 3.14$$

$$\begin{aligned}\text{source for Tgp} = & \frac{\left[\text{b\_fluid\_to\_grou\_purkut} * \left(T_{1p} - T_{gp}\right) * \text{dS\_pipe}\right]}{[\text{dV\_grout}]} \\ & + \frac{\left[\text{b\_fluid\_to\_grout\_purku} * \left(T_{2p} - T_{gp}\right) * \text{dS\_pipe}\right]}{[\text{dV\_grout}]} \\ & + \frac{\left[\text{b\_grout\_to\_soil\_purku} * \left(T_p - T_{gp}\right) * \text{dS\_grout}\right]}{[\text{dV\_grout}]} \frac{W}{m^3}\end{aligned} \quad 3.15$$

In discharging,

$$b\_fluid\_to\_grout\_purku = 1/\left(R_{fp\_purku} * 2 * pi * r_{outer}\right) Wm^{-2}K^{-1} \quad 3.16$$

where $R_{fp\_purku} = R_{pipe} + R_{fluid\_purku}$

For both charging and discharging,

$$R_{pipe} = \log\left(\frac{r_{outer}}{r_{inner}}\right)/(2 * pi * k_{pipe}) \quad 3.17$$

In **charging,**

$$R_{fluid} = 1/(2 * pi * r_{inner} * h_{fluid}) \quad 3.18$$

$$h_{fluid} = Nu_{fluid} * k_{fluid}/(2 * r_{inner}) \quad 3.19$$

$$Nu_{fluid} = 0.023 * Re_{fluid}^{0.8} * Pr_{fluid}^{0.3} \quad 3.20$$

In **discharging,**

$$R_{fluid\_purku} = 1/(2 * pi * r_{inner} * h_{fluid\_purku}) \quad 3.21$$

$$h_{fluid\_purku} = Nu_{fluid\_purku} * k_{fluid}/(2 * r_{inner}) \quad 3.22$$

$$Nu_{fluid\_purku} = 0.023 * Re_{fluid\_purku}^{0.8} * Pr_{fluid}^{0.3} \quad 3.23$$

For both **charging and discharging**,

$$dS\_pipe = 2 * pi * r_{outer} * dz \quad 3.24$$

$$dV\_pipe = pi * (r_{inner}^2) * dz \quad 3.25$$

$$dV\_grout = pi * r_{borehole}^2 * dz - 2 * pi * r_{outer}^2 * dz \quad 3.26$$

d. e_a = Mass coefficient

For charging assume,

$$e_a \text{ of } T1 = e_a \text{ of } T2 = e_a \text{ of } Tg = 0 \frac{kg}{m.s.K}$$

For discharging assume,

$$e_a \text{ of } T1p = e_a \text{ of } T2p = e_a \text{ of } Tgp = 0 \frac{kg}{m.s.K}$$

e. d_a = damping or mass coefficient

$$d_a \text{ of } T1, T2, T1p, T2p = rho\_fluid * Cp\_fluid \; Jm^{-3}K^{-1}$$

$$d_a \text{ of } Tg, Tgp = rho\_grout * Cp\_grout \; Jm^{-3}K^{-1} \quad 3.27$$

f. α = Conservative Flux convection coefficient

$$\alpha \text{ of } T1, T2, Tg, T1p, T2p, Tgp = 0 \frac{W}{m^2K}$$

g. β = Convection coefficient

$$\beta \text{ of } T1, T1p = \left(\frac{-v\_fluid}{\frac{\text{No. of boreholes in the current ring}}{\text{No. of boreholes in ring 1}}} \right) * rho\_fluid * Cp\_fluid \frac{W}{m^2K}$$

-ve sign indicates the flow goes in the downward direction

$$\beta \text{ of } T2, T2p = \left(\frac{v\_fluid}{\frac{\text{No. of boreholes in the current ring}}{\text{No. of boreholes in ring 1}}} \right) * rho\_fluid * Cp\_fluid \frac{W}{m^2K} \quad 3.28$$

+Ve sign indicates the flow goes in the upward direction

$$\beta \text{ of } Tg, Tgp = 0 \frac{W}{m^2 K}$$

$$\mathbf{h}.\gamma = \text{Conservative Heat flux}$$

$$\gamma \text{ of } T1, T2, Tg, T1p, T2p, Tgp = 0 \ \frac{W}{m^2}$$

Post-solving the partial differential equation of all the boundaries of rings in the coefficient form, we need to assign the constant value to the outlet fluid variable T2 in case of charging and T2p in the discharging phase as well at the ends of the boreholes in the Dirichlet boundary condition, which will be the inlet variable to towards the outlet of all boreholes.

3.5 Multiphysics

Usually, Multiphysics refers to the interaction of multiple physical properties. In COMSOL Multiphysics, we must approach by the underlying concepts and physical phenomena of the built geometry. The approach towards the simulation begins with initial principles of fluid transport development, fluid mechanics, heat transfer mechanism, and solid mechanics, etc., as some of the connections of the COMSOL software. We must mesh all the connections in a steady way to solve the simulation depending upon the needs of the study.

In this case of the BTES system, we have the two phases to perform the interaction among the physical properties and study for certain periods to observe the simulation phenomena, and we need to select all the domains around the geometry manually as shown in *Figure 25* in both charging and discharging phases as well.

3.5.1 Case of Charging

The required heat injection equation during charging of the bedrock in solid is governed by 3.29

$$\rho C_p \frac{\partial T_s}{\partial t} + \rho C_p u.\nabla T_s + \nabla.q = Q + Q_{ted} \qquad 3.29$$

where

$$q = -k\nabla T_s \quad 3.30$$

The reference temperature for the simulated geometrical model is stated at 293.15K with the linear discretization with the dependent surface temperature variable as T_s. Depending upon the theory behind a certain physical state of the BTES system, we must define the parameters of each physical component. Starting with the solid mechanics as clearly shown in *Figure 25* that the domain of the surrounding bedrock is selected to define the thermal parameters for surrounding bedrock, likewise, the domain of only finnfoam insulation material is chosen to define finnfoam physical parameters. For the solid mechanics of surrounding bedrock and finnfoam insulation material, the equation governed as the heat injection equation during the charging phase as mentioned above. Heat conduction and thermodynamics of solid state of bedrock are defined by the user-defined parameters that include thermal conductivity of the rock a during heat conduction, density and specific heat capacity of rock at constant pressure under the thermodynamics of the material whereas solid-state of finnfoam insulation material are defined by the user-defined parameters that include thermal conductivity of the finnfoam material during heat conduction, density and specific heat capacity of finnfoam material at constant pressure under the thermodynamics.

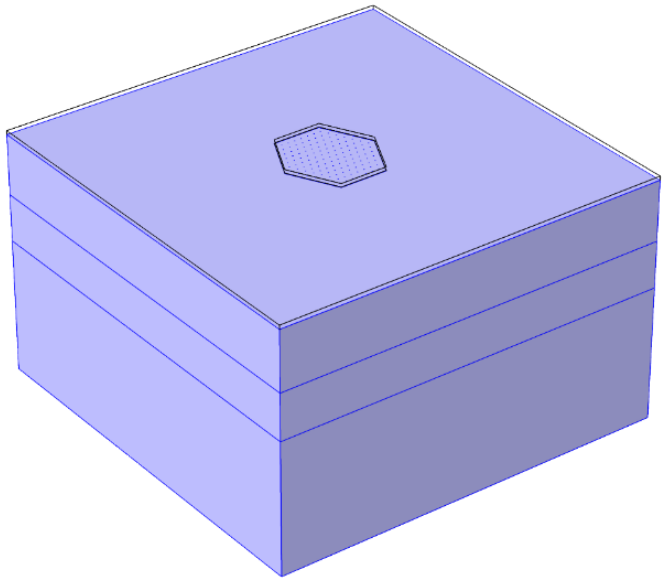

Figure 25. Domains of BTES subsystem without insulation layer on a top surface is selected to assign the thermal properties around the bedrock.

Initial values must be stated as per the charging phase phenomena by selecting all the domains and initial value temperature variable of $T_s = T_p(\text{outlet})$ in kelvin. Thermal insulation around the sides of the surrounding bedrock is assumed as $-n.q = 0$ because there is no thermally insulating material around the bedrock.

During the convective heat transfer of the BTES, there will be heat flux as selected in figure i.e., HTR per unit surface area per unit time that takes among the BHEs. To resolve the heat flux of the BHEs, we can choose the non-solid material assuming the below equations 3.31 and 3.32

$$-n.q = q_0 \tag{3.31}$$

$$q_0 = h(T_{ext} - T_s) \tag{3.32}$$

Where,

h is defined as the heat transfer coefficient on the borehole wall, which is equivalent to the heat transfer coefficient from grout to soil $\frac{W}{m^2K}$

T_{ext} is defined as the external temperature which is the ground temperature during charging in summer ~T_g

T_s is defined as the inlet temperature variable during charging

During the inward heat transfer of the BTES, there will be heat flux from *Figure 26* i.e., HTR per unit surface area per unit time that takes among the BHEs surface. To resolve the inward heat flux of the ground area below the height of BHEs, we can choose the non-solid material assuming the eq. 3.31

$$-n.q = q_0$$

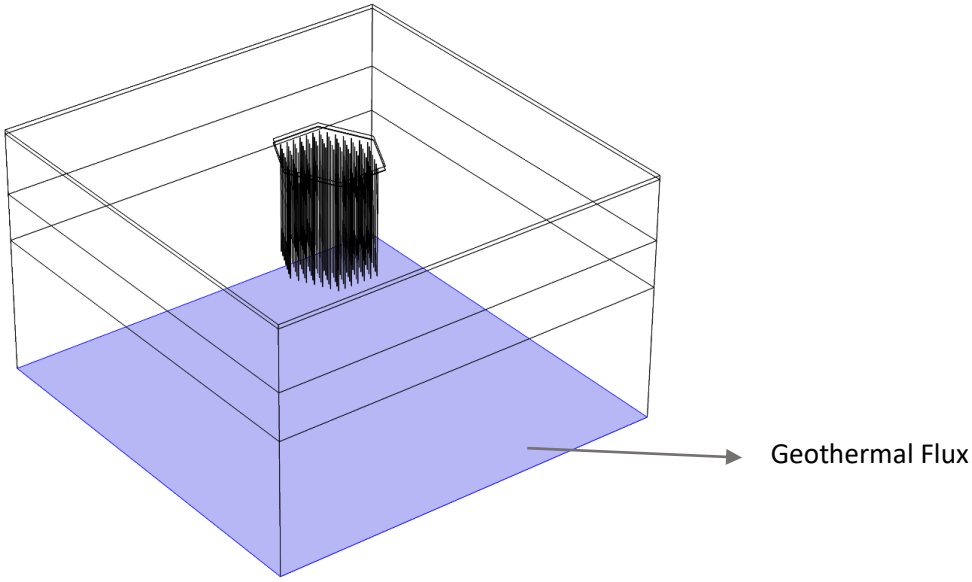

Figure 26. Inward Heat Flux in the ground represents the geothermal flux and its gradient around

Where,

q_o is the geothermal heat flux of the ground in W/m^2

In solid mechanics, there is the soil insulation layer on top of the finnfoam insulation material as shown in *Figure 27* which typically has the height that ranges between 1.5m-2m. The required heat injection equation during charging of the bedrock in solid is governed similar as eq. 3.29 and eq. 3.30

$$\rho C_p \frac{\partial T_s}{\partial t} + \rho C_p u.\nabla T_s + \nabla.q = Q + Q_{ted}$$

$$q = -k\nabla T_s$$

The solid-state of the soil insulation layer on top of finnfoam material is defined by the user-defined parameters that include thermal conductivity of the coil insulation layer during heat conduction, density, and specific heat capacity of the soil layer at constant pressure under the thermodynamics.

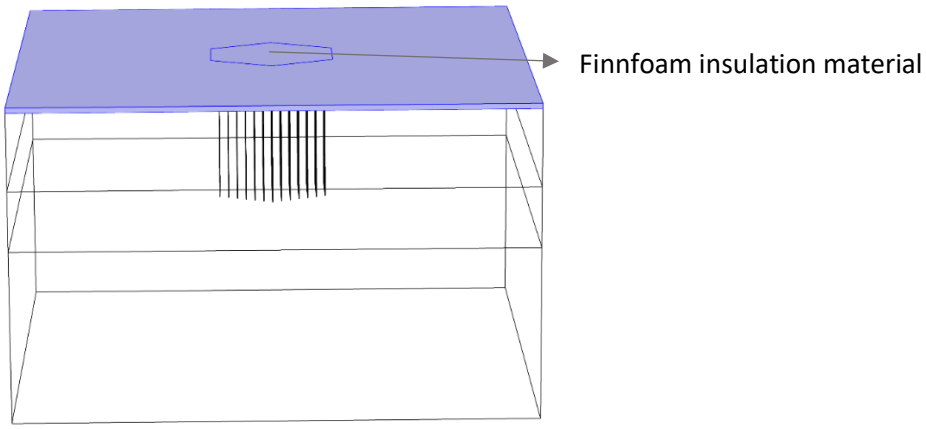

Figure 27. Soil Insulation Layer of tope of the BTES which is usually at the depth of 1-1.5m beneath the ground

The ground surface temperature of the BTES system while charging phase is assumed as

$$T_s = T_0$$

$$T_0 = T_{surface(t)}$$

Where $T_{surface(t)}$ in the charging case,

$$T_{surface(t)} = T_{initial} + 6.0\sin((2 * \pi / a(\text{year})) * (t(\text{days}) * t(\text{charging hours})/t(\text{total hours})) \quad 3.33$$

In the research, the charging phase starts from 1st day and goes till the 180th of the year for eight hours per day.

3.5.2 Case of Discharging

The required heat extraction equation during discharging of the bedrock in solid is governed as similar to eq. 3.29 and eq. 3.30 but here 'T_p' denotes outlet temperature variable in discharging phase

$$\rho C_p u.\nabla T_p + \nabla.q = Q + Q_{ted} \quad 3.34$$

$$q = -k\nabla T_p \quad 3.35$$

The equations of the discharging case are dependent upon the charging cycle of BTES. The reference temperature for the simulated geometrical model is stated at 293.15K with the linear discretization with the dependent surface temperature variable as T_p. Depending upon the theory behind the certain physical state of the BTES system, we must define the parameters of each physical component. Starting with the solid mechanics as clearly shown in *Figure 25*. The domain of the surrounding bedrock is selected to define its physical parameters, likewise, the domain of only finnfoam insulation material is chosen to define finnfoam physical parameters. For the solid mechanics of surrounding bedrock and finnfoam insulation material, the equation is governed as the heat extraction equation that is time-dependent upon the study of the injection equation during the charging phase as mentioned above. Heat conduction and thermodynamics of solid state of bedrock are defined by the user-defined parameters that include thermal conductivity of the rock a during heat conduction, density, and specific heat capacity of rock at constant pressure under the thermodynamics of the

material whereas solid-state of finnfoam insulation material are defined by the user-defined parameters that include thermal conductivity of the finnfoam material during heat conduction, density and specific heat capacity of finnfoam material at constant pressure under the thermodynamics.

Initial values must be stated as per the discharging phase phenomena by selecting all the domains and initial value temperature variable of $T_p = T_s(\text{inlet})$ in kelvin. Thermal insulation around the sides of the surrounding bedrock even during discharging is assumed as $-n.q = 0$ because there is no thermally insulating material around the bedrock, so the heat losses around the bedrock are not considered.

During the convective heat transfer of the BTES, there will be heat flux, i.e., HTR per unit surface area per unit time that takes among the BHEs. In order to solve the heat flux of the BHEs, we can choose the non-solid material assuming the equation as 3.31

$$-n.q = q_0$$

$$q_0 = h(T_{ext} - T_p) \qquad 3.36$$

Where,

h is defined as the heat transfer coefficient on the borehole wall, which is equivalent to the heat transfer coefficient from grout to the soil during discharging in $\frac{W}{m^2K}$

T_{ext} is defined as the external temperature which is the ground temperature during discharging in winter ~ T_{gp} in K

T_p is the outlet temperature variable during discharge

During the inward heat transfer of the BTES, there will be heat flux i.e., HTR per unit surface area per unit time that takes among the BHEs surface. In order to solve the inward heat flux of the ground area below the height of BHEs, we can choose the non-solid material assuming the equation as 3.31

$$-n.q = q_0$$

In the solid mechanics, there is the soil insulation layer on top of the finnfoam insulation material as shown in the fig. which typically has the height that ranges between 1.5m-2m. The required heat extraction equation during discharging of the bedrock in solid is governed by equation 3.34 and 3.35

$$\rho C_p u.\nabla T_p + \nabla.q = Q + Q_{ted}$$

$$q = -k\nabla T_p$$

Solid-state of soil insulation layer on top of finnfoam material is defined by the user-defined parameters that include thermal conductivity of the coil insulation layer during heat conduction, density, and specific heat capacity of soil layer at constant pressure under the thermodynamics. Ground surface temperature $T_{discharge(t)}$ of the BTES system while discharging phase is assumed as

$$T_p = T_0$$

$$T_0 = T_{discharge(t)}$$

Where $T_{discharge(t)}$ in the charging case,

$$T_{discharge(t)} = T_{initial} + 6.0\sin((2 * \pi / a(\text{year})) * (t(\text{days}) * t(\text{charging hours})/t(\text{total hours})) \quad 3.37$$

In the research, the discharging phase starts from 181st day and goes until the end of the year for sixteen hours per day.

3.6 Mesh

Creating the problem is described by the partial differential equation, and the solution can be called by the mathematical model through the finite element method. The finite element method is based on the discretization of model geometry into discrete units called elements. The elements are connected through the points called nodes. It mainly serves two purposes: point one represents the geometry and point two represents the solution field.

The meshing can be built in two ways: 1. Automating with the physics-controlled mesh and 2. User-defined meshing. Many factors should be considered while meshing the geometry model, which are the functionalities and features of the mesh in COMSOL Multiphysics. The factors that are categorized into:

3.6.1 Meshing sequence order

Meshing typically built in the sequential order and the sequential order of building operation and local attributes that play an important role in generating the mesh without errors. In every sequence, there is an individual mesh generation node that represents the element type where we can modify the number of elements and order of elements. In the user-defined meshing, we can create according to the needs of the geometry and can add attributes to the mesh generator nodes. In geometry, we had begun with an edge node for boreholes.

3.6.2 Element type

The element type used in the model divides the geometry into discrete units according to their shape. In 1D models, these are called intervals whereas, in the 2D models, geometry will be subdivided into triangles and quadrilaterals. Usually in 3D models, geometry will be divided into tetrahedrons, hexahedrons, pyramids, and prisms with the default being tetrahedron element shape. In COMSOL Multiphysics, regular hexahedrons are quadrilateral that swept along a certain distance. Similarly, in the prism, triangular elements are swept along a certain distance.

3.6.3 Element size and distribution

We can do user-defined meshing either by editing the physics-controlled mesh or by creating the user-defined mesh from starting. While editing the physics-controlled mesh, we can change the size of the mesh node. Usually, the coarser mesh would provide approximate results but takes less computation effort, memory, and simulating time whereas finer mesh would provide accurate results but takes a lot of effort in computing, memory, and simulating time. For example, when we add a triangular type to the mesh and apply it to the larger domain and we add a quadrilateral type to a smaller domain. After building, all we can observe the uniform sizing and alignment. If we want to make triangular elements extra fine through the sub-node settings and by applying to them to larger domain, thereby building all make the quadrilateral elements in smaller domains reduced in size towards the shared boundary with the larger domain to accommodate extra fine mesh in a larger domain. If we change the order of the mesh nodes, thereby building all makes the smaller domain to accommodate coarser mesh by growing the element size towards the shared boundary in a larger domain. The exact alignment happens due to the automatic continuous mesh adjustment through the form union in the geometry finalization method. This is the principle behind how every meshing sequence and element size affects the meshing.

In the BTES system, meshing had begun with the finer mesh sizing due to dominant element size in the geometry mode that takes control over the major portion of the geometry and will be set under the predefined set of global size node as shown in *Figure 28.*

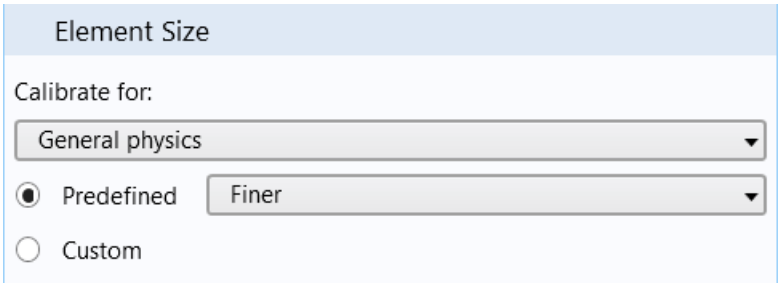

Figure 28. Element size window for providing meshing size

Then we must concentrate on other specific parts of geometry that need accurate results from the meshing through local size sub-node settings. So, we have chosen the boreholes with the meshing of the edges. The meshing over edges of the boreholes is distributed with fixed six elements to provide the fine results of borehole simulation where the major operation takes place. Thereby, building all provides the finer mesh over the remaining parts of the geometry.

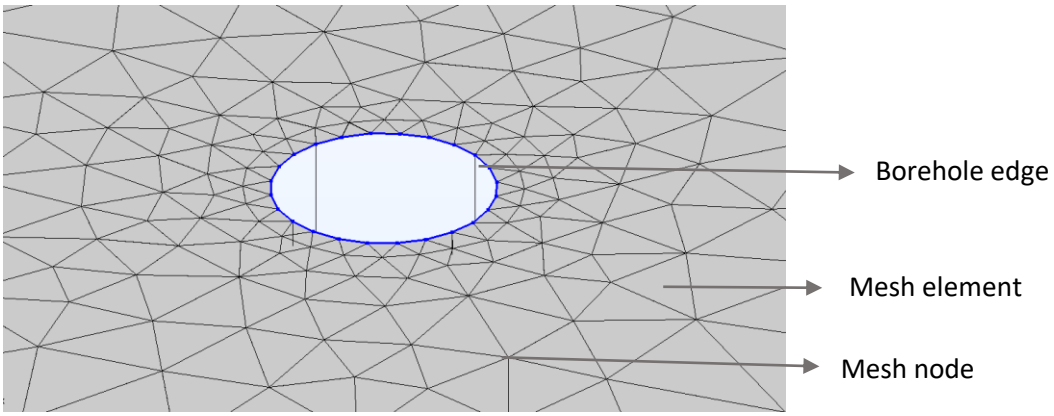

Figure 29. Tetrahedral mesh on the surface to accommodate edge mesh in the borehole and borehole edge was unselected for different meshing since the tetrahedral mesh on the larger areas of the model.

In the remaining bigger domains, the tetrahedral element type was selected for 3D shapes of the geometry that includes soil insulation, finnfoam material, and underground geometry block below the boreholes. Since the order of the meshing sequence begins with the edge mesh node for borehole meshing, the elements in borehole mesh would be accommodated with six elements that share the boundary with a bigger domain of soil insulation surface accommodated by finer mesh shown in *Figure 29*. The finer mesh elements in the soil insulation get reduced computationally as it approaches the borehole edges and aligned automatically due to usage of form union finalization method in the geometry. *Figure 30* clears shows how the meshing of the ground surface which is having tetrahedral elements was accomodated to reduce to

fit the size of the predefined finer borehole elements while approaching the boundary of the BTES.

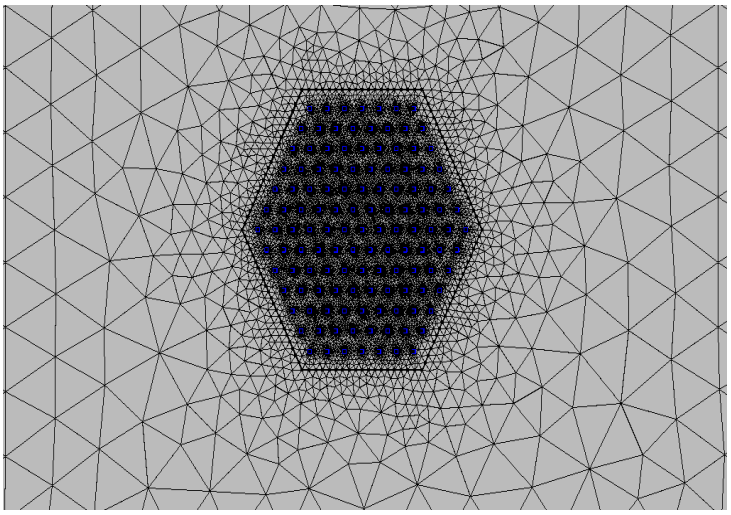

Figure 30. Top view of the tetrahedral mesh on the ground surface to accommodate all the borehole edges and

In 3D shaped domains, as shown in *Figure 31*, we usually choose the tetrahedral element type and size of the elements differ in the bigger domains with the influence of the sequence of other mesh nodes and its element sizing under the sub-nodes setting.

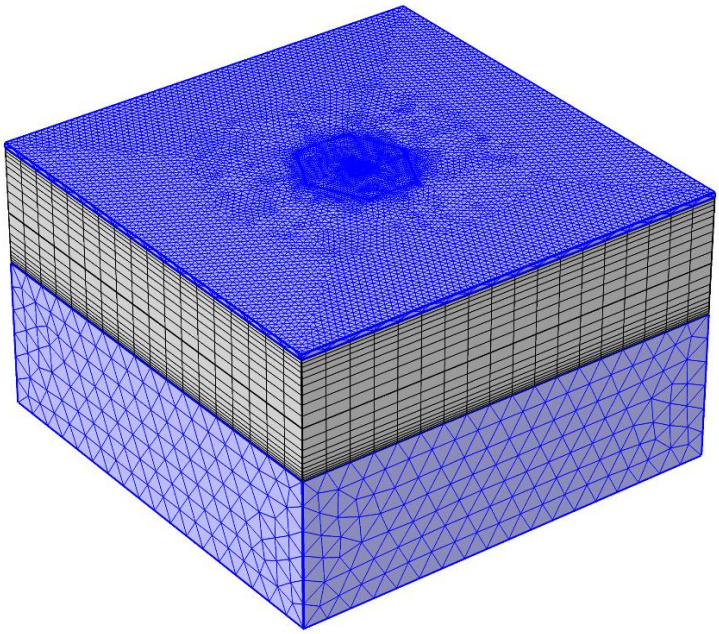

Figure 31. Tetrahedral mesh selection finer on the top surface, normal on the bottom, and swept mesh in the middle

3.6.4 Element order and mesh quality

There are two ways to reduce the memory of computation. As we discussed, one way is to reduce the size of the elements, and the other one is to reduce the number of

elements. If we reduce the number of elements, this will enable us to lessen the memory that is needed to resolve the problem. To reduce the number of elements in the geometry, we can use swept mesh and applying it domains of the lower block of underground and as well as a top insulation layer. To use a swept mesh effectively, we need to create a surface mesh that will be utilized to sweep through the respective domains. We have added the triangular surface mesh just on top of the boreholes below the insulated soil layer and applied the swept mesh to it. Thereby building the mesh, it was swept through the respective domains of the lower block of underground and as well as the top insulation layer with the finer meshing of the boreholes resolved. *Figure 32* shows how the swept mesh inside the boreholes swept along the depth of the boreholes and edges of boreholes have finer mesh.

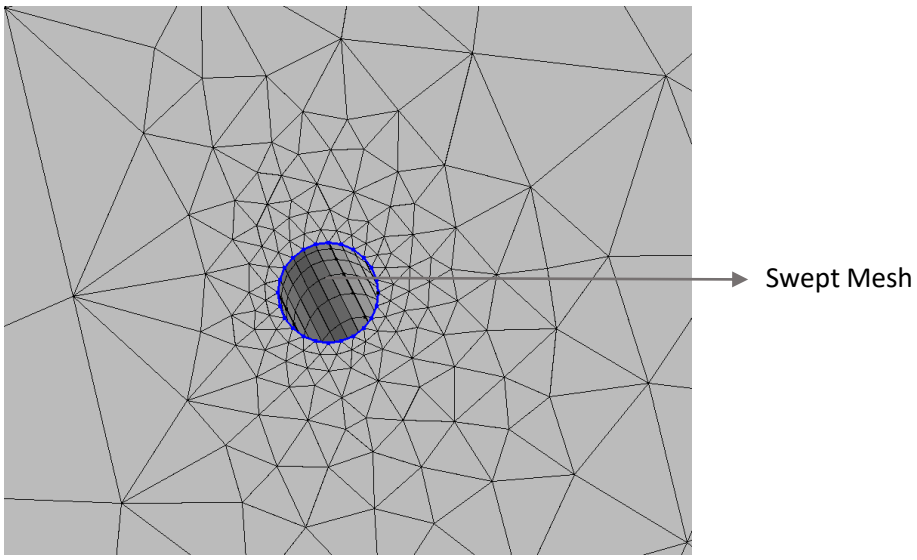

Figure 32. Swept mesh inside each of the borehole and tetrahedral mesh accumulated towards the edges of the borehole

To have more precise control in reducing the memory of the borehole, we can add the distribute sub-node. In distribution, we can clearly state the distribution type, element order, and element ratio under the distribution section. A lesser number of elements saves up memory and computation time. In this way, we can modify the resolution to each domain according to the needs of resolving the problem. We can add several meshes with different sequence type meshes and can choose the suitable mesh under the mesh selection in the study of the COMSOL. We can validate the element quality from the study of the geometry model by toggling the adaptive mesh refinement in the time-dependent study. We can overview the generated mesh statistics and element

histogram quality in the mesh node shown in *Figure 33*. From the mesh statistics we can refine the meshing with the type and size of the elements. Increase in the size and number of elements would increase the complexity and prone to higher errors. Statitsics would show the how the quality of the mesh histogram and could be optimised in the results.

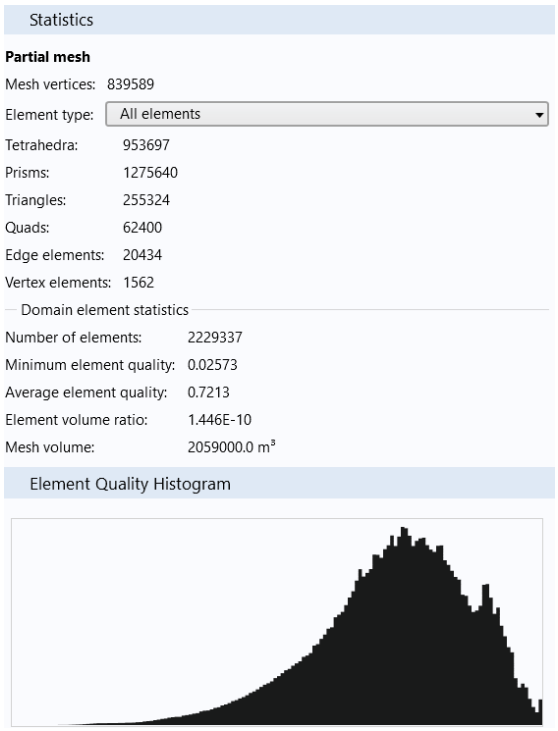

Figure 33. Mesh statistics of a 3D subsystem of BTES model that defines the type, number, and quality of elements.

The simulation time and memory are correlated to the number of degrees of freedom in the geometry model. It is often desirable to be able to estimate the number of degrees of freedom based on the number of elements in the model. In physics interfaces, each dependent variable is present in all nodes in the mesh, which implies that the number of degrees of freedom is provided by the number of nodes multiplied by the number of dependent variables.

4. Results

In this research, three-dimensional in-situ seasonal borehole thermal energy storage was simulated using the finite element method and analysis, solver, and Multiphysics simulation software called COMSOL. The purpose of the simulation is to produce near to accurate results of the thermodynamic performance of the subsystem (Lanahan & Tabares-Velasco, 2017). The simulated model used the temperatures of time-dependent study of injection, which will act as the continuous values to the consecutive time-dependent studies for the next five year period. Several studies were taken to examine the thermal performance and heat loss simulation phenomena over 5 years during eight hours of injection per day for six months followed by six months for sixteen hours per day in an annual cycle. Though we have developed the study for five years, we will be discussing the analysis of period one and period five extensively, since the development of simulation during charging and discharging of all the periods looks similar even though data inside the simulation changes. The remaining simulations of the second, third, and fourth-year will be included under 8. Appendix.

Along with the investigation of time-dependent studies of five years, an extensive study on the major factors of BTES model heat losses are investigated and how they are affected with varying parameters. THE simulated BTES model has six rings with 126 boreholes that have an inlet flow of 200 l/min in the center ring during the charging phase and outflow from the center has 150 l/min during the discharging phase.

4.1 Period 1 Analysis

During the initial period, the injection temperature to the BTES system from the solar collectors was set at 70℃. Inlet flows during the charging phase for eight hours are set at 200 hours l/min in the center borehole which will be divided into the other rings that are connected in series as well as the parallel between the boreholes each ring. In the injection phase, the charging gradually increases from ring 1 to ring 6 during the first 180 days for eight hours every day. From *Figure 34*, it was clear that the lowest charging power starting at 70kW and gradually decreases to zero is consumed by ring 1 that consists of 7 boreholes, including the center borehole. Similarly, ring 2 has 12 boreholes consumes power at 175kW from the day 1 along with the additional charging power of ring 1 and gradually reduces to near zero, ring 3 has 18 boreholes consumes

power at 300kW from the day 1 along with the charging of ring 1 and ring 2, ring 4 has 24 boreholes consumes power at 400kW from the day 1 along with the charging of ring 1, ring 2, ring 3 that gradually decreases the power to 60kW at the end of 180th day, ring 5 has 30 boreholes consumer power at 560kW from the day 1 along with the charging of ring1, ring 2, ring 3, and ring 4 that gradually decreases the power to 110kW, Ring 6 has 36 boreholes consumer power at 680kW from the day 1 along with the charging of ring 1, ring 2, ring 3, and ring 4, and ring 5 that gradually decreases the power to 200kW. Ring 1 consumes the lowest power due to the initial charging of the lowest number of BHEs. Power consumption increases as we increase each ring radially that are connected in series and boreholes in each ring are in parallel. By the time it reaches it ring 6 which has 36 boreholes power needs to higher as the power passes from ring 1 to ring 6 during summer.

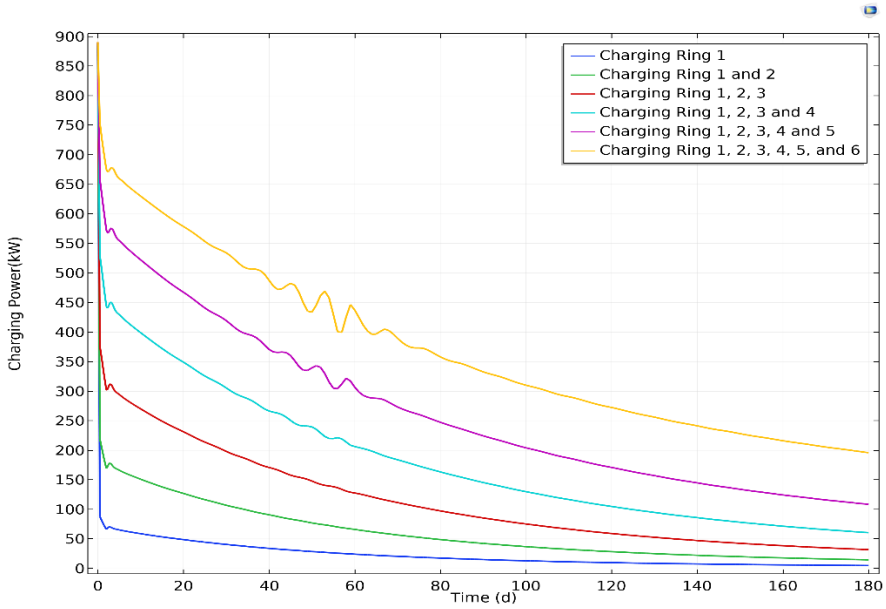

Figure 34. Power injection (charging) in the first six months for the first year. Ring 1 shows the least power consumption and the remaining rings combined with ring 6 show the highest power consumption.

Injection temperature at the center core of the BTES would be sent peak at 70℃ during charging which involves the other 6 boreholes of ring 1, which is shown in *Figure 35*. So usually there are higher temperatures concentrates in the ring 1 during injection which reaches 69℃ by the end of day 180 begun from 65℃ that was injected into the BTES system after convective heat losses on the day 1. From the ring 1, outlet higher temperatures will be sent as the inlet temperatures to ring 2 where the temperatures reach up to 68℃ by the end of day 180, that begun at 58℃ on day 1. The outlet temperatures from the ring 2 will be sent as the inlet temperatures to ring 3 where the temperatures reach up to 67℃ by the end of day 180 that begun at 47℃ on the day 1.

The outlet temperatures from the ring 3 will be sent as the inlet temperatures to ring 4 where the temperatures reach up to 65℃ by the end of day 180 that begun at 38℃ on the day 1. Similarly, outlet temperatures from the ring 4 will be sent as the inlet temperatures to ring 5 where the temperatures reach up to 62℃ by the end of day 180 that begun at 28℃ on the day 1. Finally, outlet temperatures from the ring 5 will be sent as the inlet temperatures to ring 6 where the temperatures reach up to 55℃ by the end of day 180 that begun at 21℃ on the day 1. Though we inject at temperatures of 70℃, there will be convective heat losses from the pipes when it reaches the ring 1. There will be convective heat losses from the BHEs along the passage of each ring and major thermophysical properties of the materials and surrounding effect the degree of heat losses.

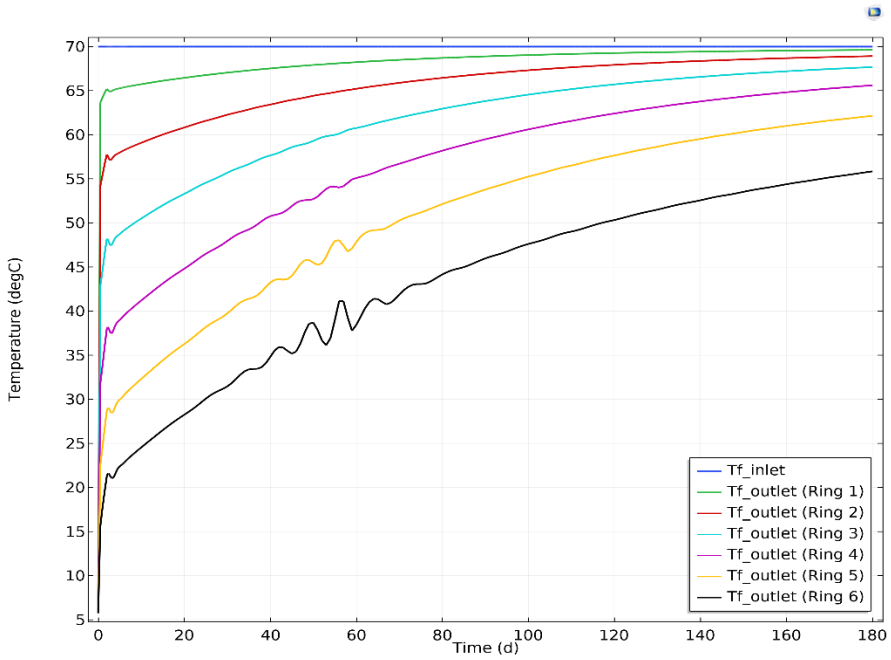

Figure 35. Temperature injection(charging) in the first six months for the first year. Ring 1 received the highest temperature from injection and the last outer Ring 6 receives the least temperature.

As we know that boreholes are connected in series in their respective ring and parallel in connection to other rings, the fluid mass flow rate from the input parameter is limited to the number of boreholes because the total mass flow rate is the same to the BTES system. If we observe all the figures, fluctuations in ring 5 and ring 6 are due to the key reason that the mass flow rate is reduced by the increased number of boreholes in the increasing ring which makes the fluid flow rate struggle at larger rings. Indeed, supporting factors include the length of the BHEs, the radius of the inner and outer radius of the collector pipes which are affiliated to convective heat losses. The convective heat losses are caused due to hydrogeological conditions, thermal and

physical properties within and around the system. Insufficient flow rate to a larger level-headed radius of the inner and outer radius of the collector pipe makes the flow struggle at outer rings. This is due to the mechanism of pipe parallel and series connectivity which makes the flow to distribute through each ring. Turbulent inlet flow at 70℃ in the collector pipe which is drilled at the center of the BTES would continue to distribute through the complete length of BHEs in each ring. One of the optimal ways to reduce the fluctuations at outer rings to enable smooth flow is by increasing the higher inlet flow rate during injection, which is directly proportional to the number of rings. Another optimal way is to decrease the length of the borehole, which is directly proportional to the injection flow rate. Another strategic way is to adjust the radius of the collector pipe by limiting the radius to a good extent in a way that reaches to outer ring 5 and 6 in an even course.

During the extraction phase of *Figure 36* in winter, higher temperatures are extracted from the ring 1, and the temperatures decrease moderately in other rings. The outlet flow rate in the collector pipe during the extraction phase was assumed as 150 l/min after the convective heat losses in the BTES. So, 75% of the inlet flow rate was assumed to be extracted from the BTES is the approximation based on the previous projects of Heliostorage Oy. During winter, rings 6,5,4,3,2, and 1 discharge at sixteen hours per day provides the highest power at nearly 340kW on day 181 which gradually decreases nearly to 40kW at the end of day 365. As extraction temperatures from the outer ring 6 acts as the input temperatures to the descending ring order, the power from the rings 6,5,4,3,2 discharges at sixteen hours per day at nearly 330kW on the day 181 and gradually falls to 38kW at the end of the day 365. Similarly, power extraction rings 6,5,4,3 has nearly 270kW on day 181, which gradually decreases to 36kW at the end of day 365. This shows that ring 1 followed by ring 2 has the highest power extraction capability due to its higher temperatures which are visible in the result of temperatures in the simulation. Due to this, there is a drop in the power extraction after disengagement from ring 2. Again, power from the rings 6,5,4 has nearly 269kW on day 181 which gradually decreases to 36kW at the end of day 365 which implies that ring 3 and ring 4 are almost on the similar lines of power production. Post disengagement from ring 4, there is a drop in power extraction from the ring 5 as discharging power stands at 190kW from ring 6,5 on the day 181 and drops nearly to 30kW on the day 365. Ring 6 alone produces the power at 100kW on day 181 and gradually decreases approximately to 20kW on day 365, which is a significant drop in

power discharge from the ring 5. The power efficiency of BTES for 1st period attains up to 37.83%.

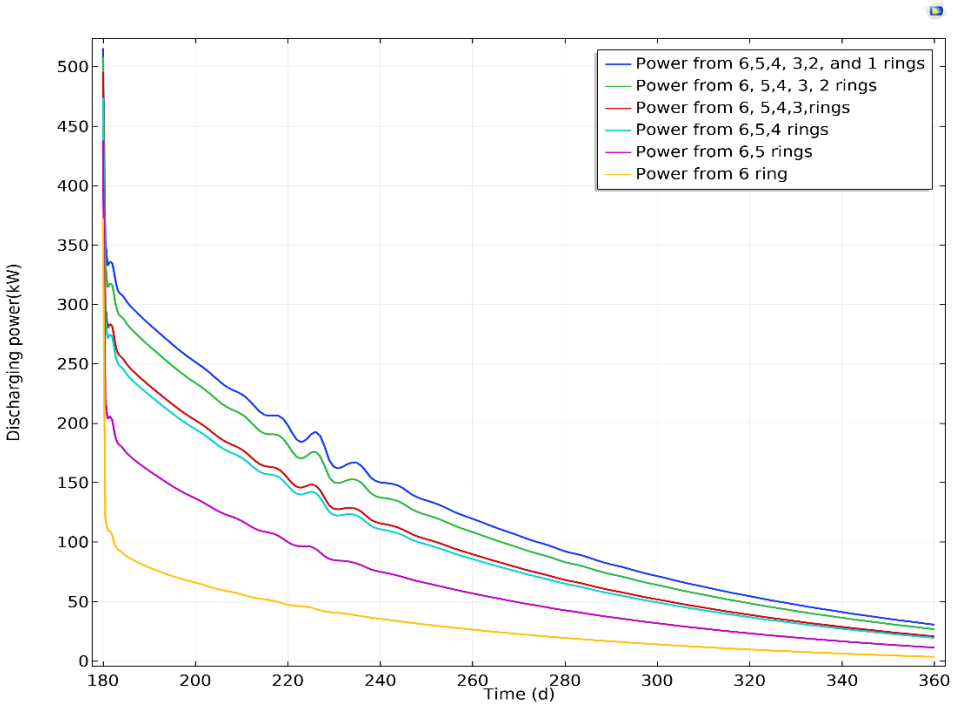

Figure 36. Power extraction (discharging) in the last six months for the first year. Ring 6 supplies the least power and the remaining rings combined with Ring 1 produce the highest power.

During winter, the inlet temperature from *Figure 37* in the outer ring 6 outlets was assumed as the 20℃. Discharging temperatures from ring 6 serves as the inlet temperatures to ring 5. Generally, temperatures in outer ring 6 are lowest among all rings during injection as well as extraction. Discharging temperature from ring 6 stands at 30℃ on day 181 and gradually reduces to 20℃ by the end of day 365. Discharging temperature from ring 5 stands at 40℃ on day 181 and descends to 22℃ on day 365. Extracted temperatures from Ring 4 and Ring 3 stand at 46℃ and 47℃ on day 181 and both the rings have the near-identical temperature that ends at 23℃ by the end of day 365. Similarly, Ring 2 and Ring 1 has the higher temperatures at 50℃ and 51℃ are extracted at high colder temperatures in winter and ends at 24℃ by the end 365. The fluctuations in Ring 1,2,3,4 and slightly at ring 5 were due to convective heat losses which lead to undersupplied extracted flow rate during the discharging phase, which begins from the outlet of ring 6. The core temperature by the end of the 1st annual period reaches 22.94℃. Thermal recovery from the ring 1 retrieves up to 40.34%. in the initial year of heating the BTES.

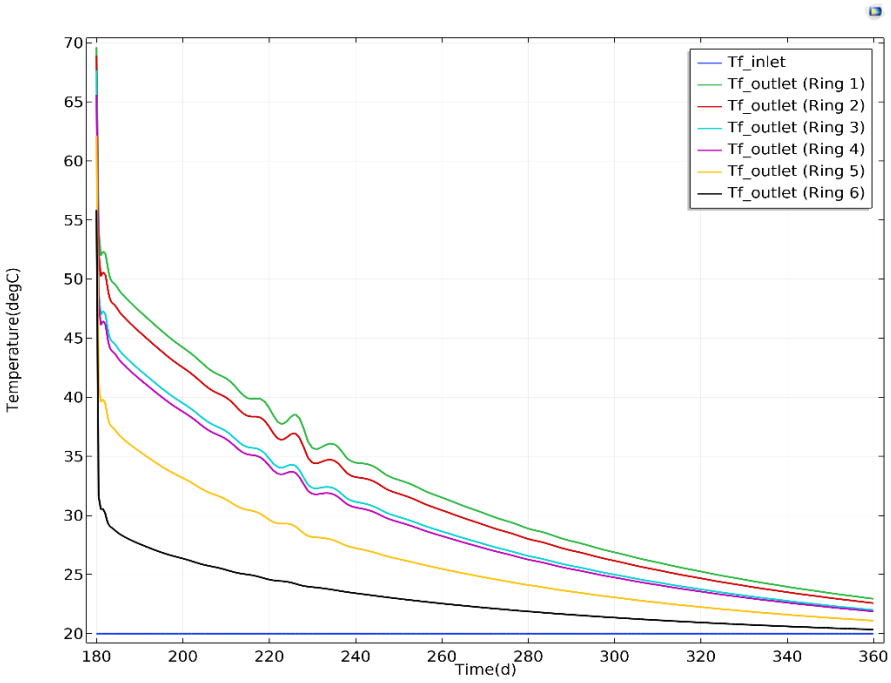

Figure 37. Extraction temperatures(discharging) in the last six months for the first year. Temperatures from the ring 6 supply the least temperature whereas Ring 1 supplies the highest core temperature.

4.2 Period 5 Analysis

In the final period of *Figure 38*, the lowest charging power starting at 50kW and gradually decreases to zero is consumed by ring 1 that consists of 7 boreholes, including the center borehole. Similarly, ring 2 has 12 boreholes consumes power at 125kW from the day 1440 along with the additional charging power of ring 1 and gradually reduces to near zero, ring 3 has 18 boreholes consumes power at 200kW from the day 1440 along with the charging of ring 1 and ring 2, ring 4 has 24 boreholes consumes power at 300kW from the day 1440 along with the charging of ring 1, ring 2, ring 3 that gradually decreases the power to 50kW at the end of 1620th day, Ring 5 has 30 boreholes consumer power at 400kW from the day 1440 along with the charging of ring1, ring 2, ring 3, and ring 4 that gradually decreases the power to 90kW, Ring 6 has 36 boreholes consumer power at 480kW from the day 1440 along with the charging of ring 1, ring 2, ring 3, and ring 4, and ring 5 that gradually decreases the power to 150kW. Ring 1 consumes the lowest power due to the initial charging of the lowest number of BHEs. Power consumption increases as we increase each ring radially that are connected in series and boreholes in each ring are in parallel. By the time it reaches it ring 6 which has 36 boreholes power needs to higher as the power passes from ring 1 to ring 6 during summer.

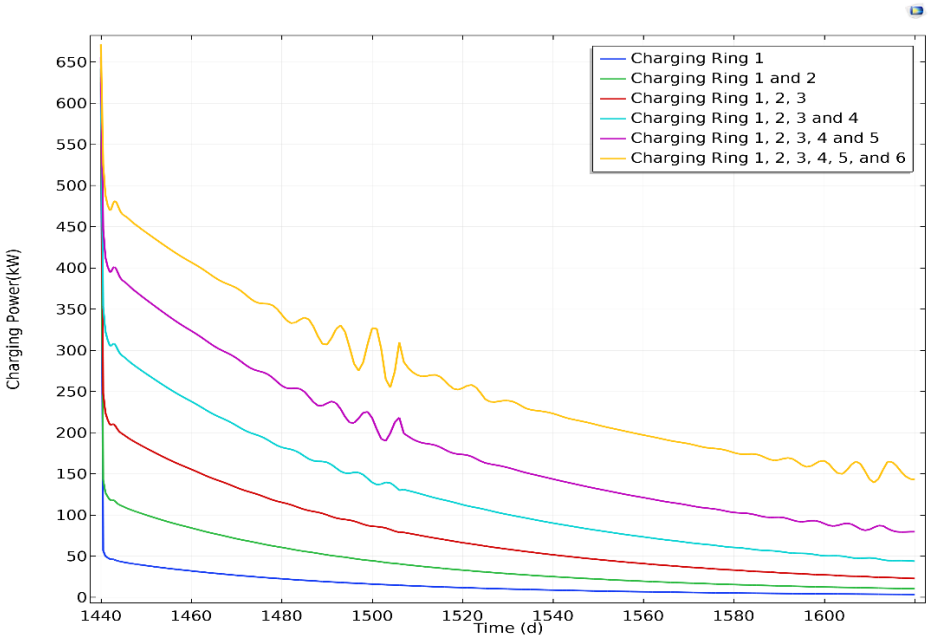

Figure 38. Power injection(charging) in the first six months for the fifth year. Ring 1 shows the least power consumption and the remaining rings combined with Ring 6 show the highest power consumption.

In the final period, the injection temperature shown in *Figure 39* sent to the center core of the BTES would be a peak at 70℃ during charging which involves the other 6 boreholes of ring 1. So usually there are higher temperatures concentrates in the ring 1 during injection which reaches 69℃ by the end of day 1620 begun from 66℃ that was injected into BTES after convective heat losses on the day 1440. From the ring 1, outlet higher temperatures will be sent as the inlet temperatures to ring 2 where the temperatures reach up to 68℃ by the end of day 1620, begun at 62℃ that was injected into ring 2 after convective heat losses on day 1440. The outlet temperatures from the ring 2 will be sent as the inlet temperatures to ring 3 where the temperatures reach up to 67℃ by the end of day 1620 begun at 55℃ that was injected into ring 3 after convective heat losses on the day 1440. The outlet temperatures from the ring 3 will be sent as the inlet temperatures to ring 4 where the temperatures reach up to 66℃ by the end of day 1620 begun at 48℃ that was injected into ring 4 after convective heat losses on the day 1440. Similarly, outlet temperatures from the ring 4 will be sent as the inlet temperatures to ring 5 where the temperatures reach up to 64℃ by the end of day 1620 begun at 41℃ that was injected into ring 5 after convective heat losses on the day 1440. Finally, outlet temperatures from the ring 5 will be sent as the inlet temperatures to ring 6 where the temperatures reach up to 60℃ by the end of day 1620 that begun at 35℃ on the day 1440. There will be convective heat losses from the BHEs along the passage

of each ring and major thermophysical properties of the materials and surrounding effect the degree of heat losses.

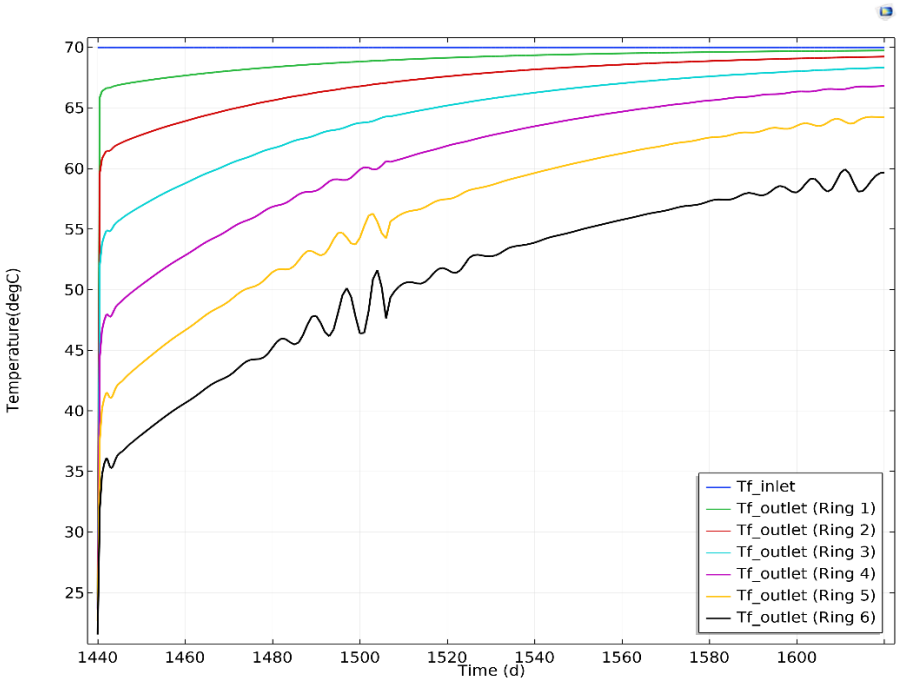

Figure 39. Injection Temperatures(charging) in the first six months for the fifth year. Ring 1 received the highest temperature from injection and the last outer Ring 6 receives the least temperature.

As explained in period 1 analysis, fluctuations in ring 4, ring 5, and ring 6 happened due to various factors such as flow rate, length of the BHEs, the radius of the inner and outer radius of the collector pipes which are affiliated to convective heat losses in the fifth consecutive year. The convective heat losses are caused due to hydrogeological conditions, thermal and physical properties within and around the system. Insufficient flow rate to a larger level-headed radius of the inner and outer radius of the collector pipe makes the flow struggle at outer rings. This is due to the mechanism of pipe parallel and series connectivity which makes the flow to distribute through each ring. Turbulent inlet flow at 70°C in the collector pipe which is drilled at the center of the BTES would continue to distribute through the complete length of BHEs in each ring. One of the optimal ways to reduce the fluctuations at outer rings in order to enable smooth flow is by increasing the higher inlet flow rate during injection, which is directly proportional to the number of rings. Another optimal way is to decrease the length of the borehole, which is directly proportional to the injection flow rate. Another strategic way is to

adjust the radius of the collector pipe by limiting the radius to a good extent in a way that reaches outer ring 4, ring 5, and 6 in an even course.

During the extraction phase in winter from *Figure 40*, higher temperatures are extracted from the ring 1 and the temperatures decrease moderately in other rings. The outlet flow rate in the collector pipe during the extraction phase was assumed as 150 l/min after the convective heat losses in the BTES. So, 75% of the inlet flow rate was assumed to be extracted from the BTES is the approximation based on the previous projects of Heliostorage Oy. During winter, rings 6,5,4,3,2, and 1 discharge at sixteen hours per day provides the highest power at nearly 360kW on day 1621 which gradually decreases nearly to 50kW at the end of day 1800. As extraction temperatures from the outer ring 6 acts as an input temperature to the descending ring order, the power from the rings 6,5,4,3,2 discharges at sixteen hours per day at nearly 330kW on the day 1621 and gradually falls to 50kW at the end of the day 1800. Similarly, power extraction rings 6,5,4,3 has nearly 320kW on day 1621, which gradually decreases to 50kW at the end of the day 1800. This shows that ring 1 followed by ring 2 has the highest power extraction capability due to its higher temperatures which are visible in the result of temperatures in the simulation. Due to this, there is a drop in the power extraction after disengagement from ring 2. Again, power from the rings 6,5,4 has nearly 300kW on day 1621 which gradually decreases to 50kW at the end of day 1800 which implies that ring 3 and ring 4 are almost on the same lines of producing power. Post disengagement from the ring 4, there is a drop in power extraction from the ring 5 as discharging power stands at 240kW from ring 6,5 on the day 1621 and drops nearly to 30kW on the day 1800. Ring 6 alone produces the power at 140kW on day 1621 and gradually decreases approximately to 20kW on day 1800, which is a significant drop in power discharge from the ring 5. The power efficiency of BTES for the 5^{th} year attains up to 62.02%, which is a significant drop from 1^{st} year's power efficiency of 37.83%.

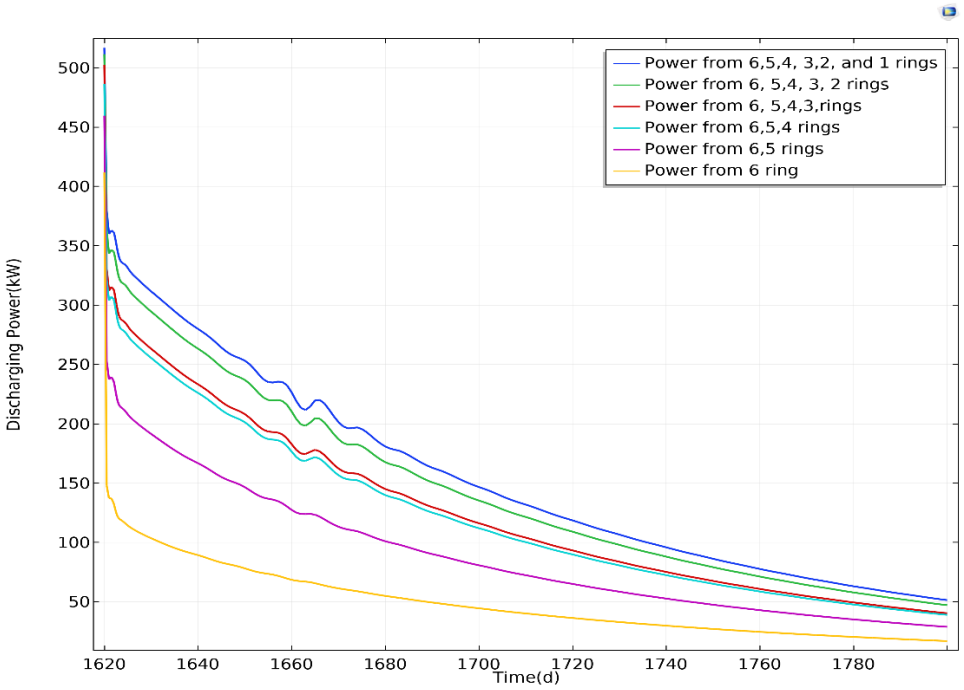

Figure 40. Power extraction(discharging) in the last six months for the fifth year. Ring 6 supplies the least power and the remaining rings combined with Ring 1 produce the highest power.

During the fifth year of the extraction phase from *Figure 41*, the inlet temperature in the outer ring 6 outlets was assumed as the 20℃. Discharging temperatures from ring 6 serves as the inlet temperatures to ring 5. Generally, temperatures in outer ring 6 are lowest among all rings during injection as well as extraction. Discharging temperature from ring 6 stands at 34℃ on the day 1621 and gradually reduces to 23℃ by the end of day 1800. Discharging temperature from ring 5 stands at 43℃ on the day 1621 and descends to 24℃ on day 1800. Extracted temperatures from Ring 4 and Ring 3 stand at 50℃ and 51℃ on day 1621 and both the rings have the near-identical temperature that ends at 24℃ by the end of day 1800. Similarly, Ring 2 and Ring 1 have higher temperatures at 54℃, and 55℃ are extracted at high colder temperatures in winter and end at 25℃ by the end of 1800. The fluctuations in Ring 1,2,3,4 and slightly at ring 5 were due to convective heat losses which lead to an inadequate extracted flow rate during the discharging phase, which begins from the outlet of ring 6. The core temperature by the end of the final annual period reaches at 25℃. Thermal recovery from ring 1 retrieves up to 75.43% which has increased from initial year recovery but becomes near stable due to less difference in temperatures. After a stable point, it reaches the quasi-steady state which means heat loss becomes static.

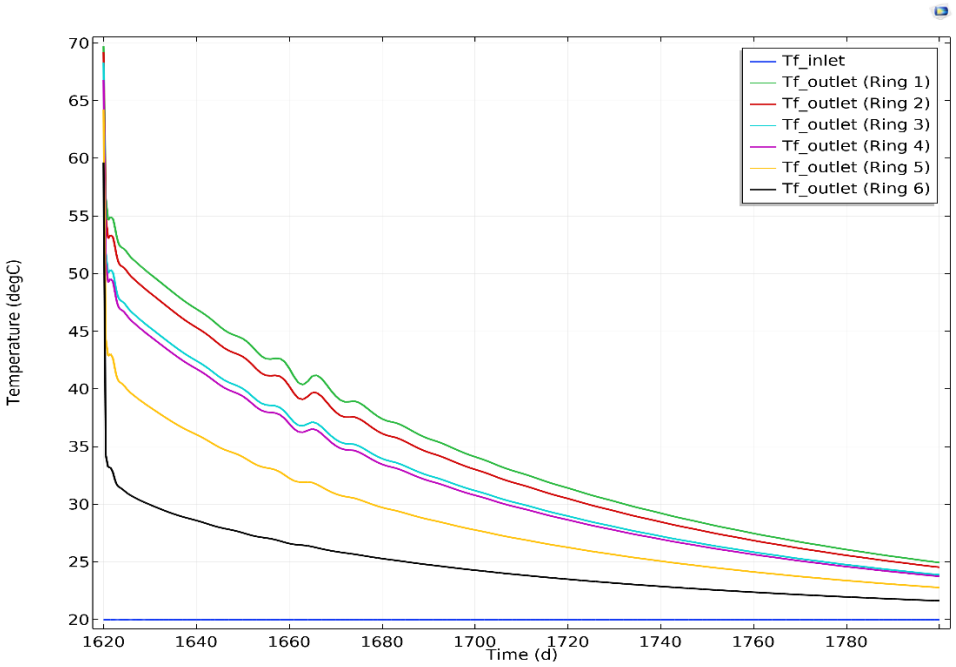

Figure 41. Extraction temperatures(discharging) in the last six months for the fifth year. Ring 6 supply the least temperature and Ring 1 supply highest temperature.

4.3 Thermal conductivities of the rock analysis

Thermal conductivity analysis is conducted on a six-ring BTES system that has the same length of the borehole to the diameter of the BTES. Major contributors to the considerable heat losses are taken and investigated on their variance in BTES simulation on parametric changes. Thermal conductivity of the bedrock is one of the factors prompting heat losses along with the thermal conductivities of soil. Investigated samples are studied from thermal conductivity $\lambda = 1\ \mathrm{Wm^{-1}K^{-1}}$ to $\lambda = 4\mathrm{Wm^{-1}K^{-1}}$ and results are shown below in *Figure 42*. There is a significant rise of heat loss from 5.5kWh to 6.5kWh with thermal conductivity $(\lambda) = 1\mathrm{Wm^{-1}K^{-1}}$ to $\lambda = 1.5\mathrm{Wm^{-1}K^{-1}}$, followed by a rise of heat loss from 6.5−7.1kWh at thermal conductivity $(\lambda) = 1.5\mathrm{Wm^{-1}K^{-1}}$ to $\lambda = 2\mathrm{Wm^{-1}K^{-1}}$. The difference between the rise of heat losses have dropped gradually following the thermal conductivity $\lambda = 2\mathrm{Wm^{-1}K^{-1}}$. After crossing thermal conductivity $\lambda = 2.5\mathrm{Wm^{-1}K^{-1}}$ increase of heat losses have become minimal and did not show much difference. So, the thermal conductivities of the bedrock between the range of $(\lambda) = 1 - 2\mathrm{Wm^{-1}K^{-1}}$ shows the minimal heat losses which are the optimal geographic condition to BTES and post $\lambda = 2.5\mathrm{Wm^{-1}K^{-1}}$there is no significant increase in heat losses to the BTES.

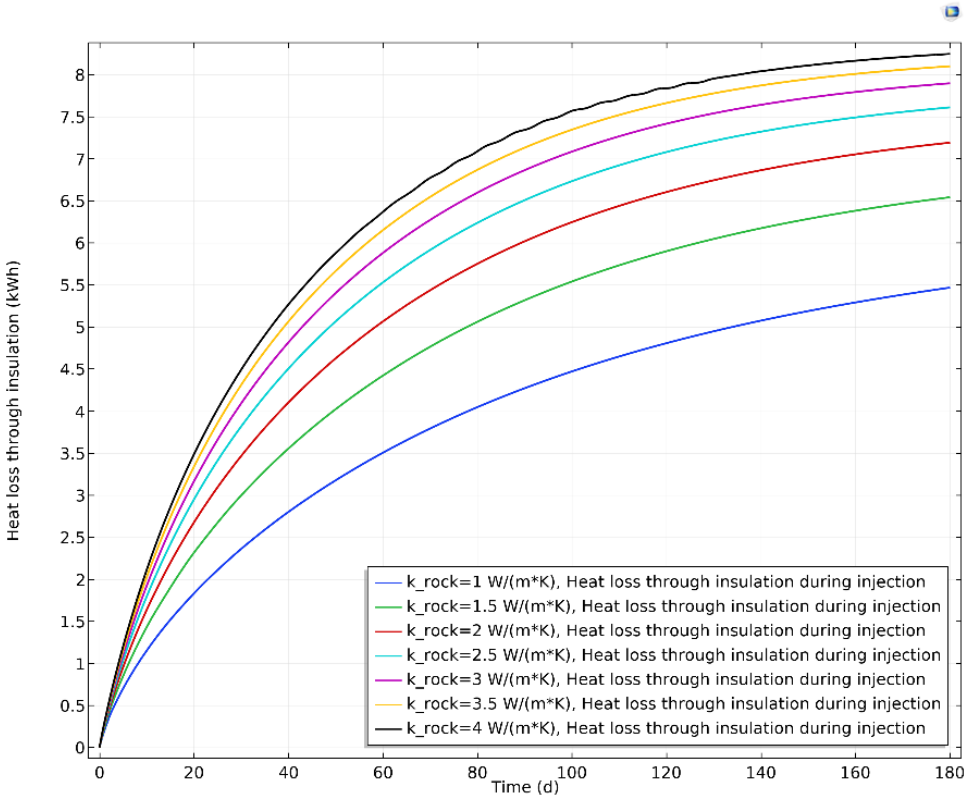

Figure 42. Analysis of various thermal conductivity values of the rock from k_rock =1-4 W/mK

4.4 Thermal conductivities of the soil analysis

The thermal conductivity of the soil is one of the factors prompting heat losses along with the thermal conductivities of rock. Investigated samples are studied from thermal conductivity $\lambda = 1\mathrm{Wm^{-1}K^{-1}}$ to $\lambda = 4\mathrm{Wm^{-1}K^{-1}}$ and results are shown below in *Figure 43*. Heat losses in soil composition have higher heat loss values than the heat losses in bedrock composition to the BTES. There is a notable rise of heat loss from 7 kWh to 7.6 kWh by thermal conductivity $(\lambda) = 1\mathrm{Wm^{-1}K^{-1}}$ to $\lambda = 1.5\mathrm{Wm^{-1}K^{-1}}$, followed by the slight rise of heat loss from 7.6kWh to 8.1kWh at thermal conductivity $(\lambda) = 1.5\mathrm{Wm^{-1}K^{-1}}$ to $\lambda = 2\mathrm{Wm^{-1}K^{-1}}$. The difference between the rise of heat losses have reduced post thermal conductivity $\lambda = 2\mathrm{Wm^{-1}K^{-1}}$. After crossing thermal conductivity $\lambda = 2.5\mathrm{Wm^{-1}K^{-1}}$ increase of heat losses did not show much difference. *Figure 43* analysis explains that the geographical location having thermal conductivities of the soil between the range of $(\lambda) = 1 - 2\mathrm{Wm^{-1}K^{-1}}$ results in minimal heat losses which are optimal to the BTES but heat losses are higher compared to the thermal conductivity of the bedrock and post $\lambda = 2.5\mathrm{Wm^{-1}K^{-1}}$ there is no effect on increase in heat losses.

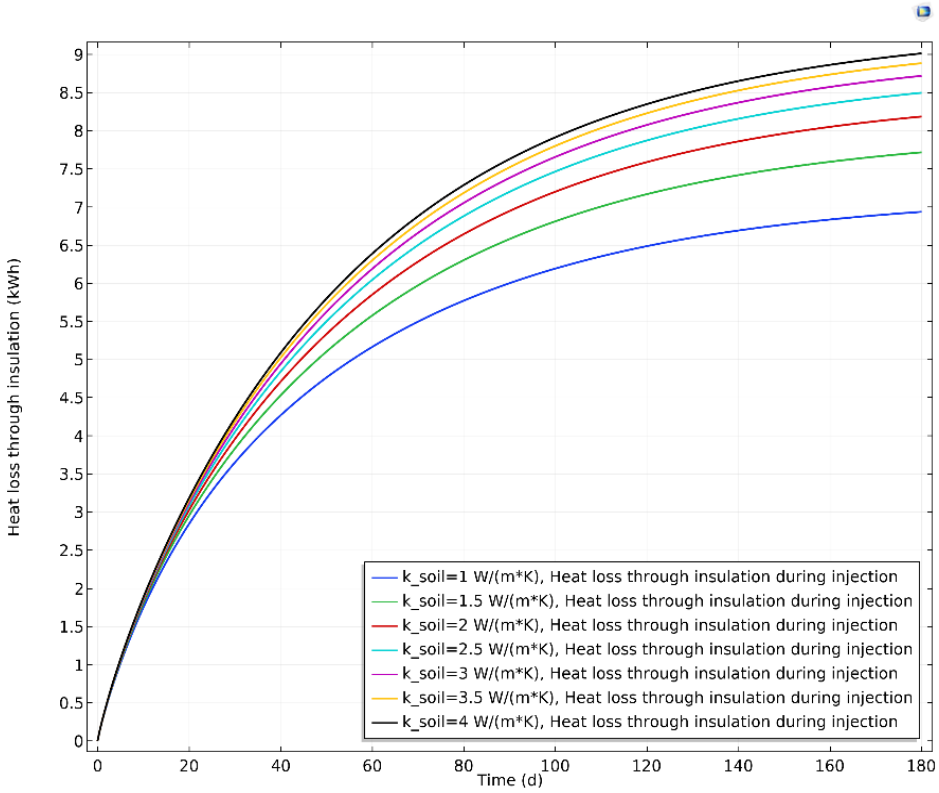

Figure 43. Analysis of various thermal conductivity values of the soil ranging from k_soil=1-4 W/mK

4.5 Thickness of the finnfoam analysis

Another major element in contributing to the heat losses of BTES is the insulation material thickness shown in *Figure 44*. The insulation foam material of a thickness of 30cm shows the least amount of heat losses approximately at 3.8kWh among other sizes due to its higher resistance from the top of the BTES. Insulation foam material thickness of 20cm shows the moderate level of heat losses approximately at 5.1kWh from the top of BTES while the insulation thickness of 10cm depicts the large increase in heat losses to 7.7kWh but economically cheap with less resistance. Insulation foam material thickness of 20cm, estimated at 35% heat loss savings from the typical material thickness at 10cm. So the insulation material thickness at 20cm is the optimal one to cover the top of the BTES to have better resistance capability and cost-effective option.

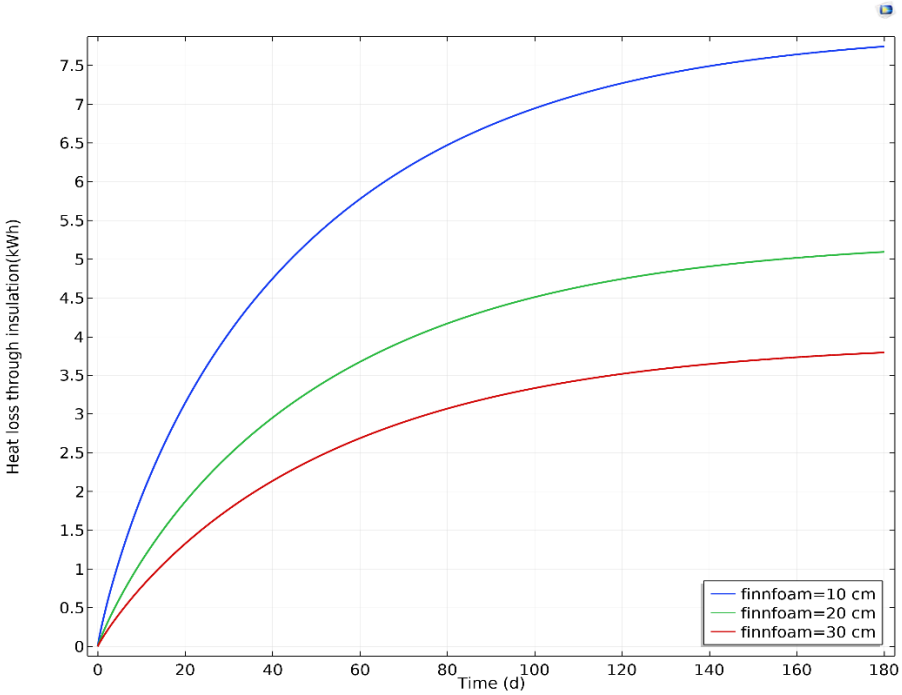

Figure 44. Analysis of various thickness sizes of insulation foam ranging from a thickness of 10cm to 30cm.

4.6 Economical Value

The Economic value of the BTES system is calculated based on the (Mauthner & Herkel, 2016). The cost of constructing the BTES systems in terms of €/m3 can be estimated using the correlation 4.1, based on the equivalent water volume V_{eq} of the BTES. The cost curve of the BTES was computed based on in-situ parameters that are optimized with heat loss factors.

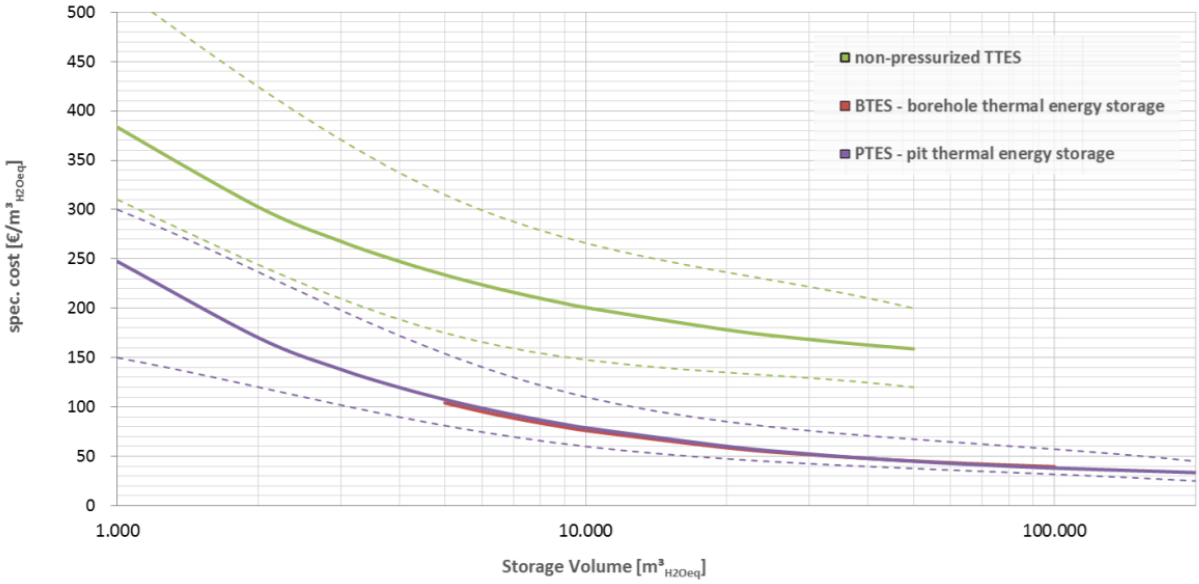

Figure 45. Cost curve of 3 types of sensible heat storages: TTES, BTES, and PTES excluding the VAT and subsidies (Mauthner & Herkel, 2016)

From *Figure 45*, it was observed that the BTES is the most cost-effective seasonal thermal energy storage, especially in large seasonal BTES.

$$C_{BTES} = 25330 * {V_{eq}}^{-0.685} + 30 \quad 4.1$$

$$V_{eq} = \text{Base} * \text{Height} \quad 4.2$$

The price of the simulated BTES based on the in-situ geometrical parameters using the equation 4.1 is $C_{BTES} = €47.4/m^3$. Higher borehole spacing ($\geq 4m$) increases pose the expensive cost on BTES systems which is feasible at a higher thermal conductivity of bedrock ($\lambda = 3 - 4\frac{W}{mK}$). It is viable to have the borehole spacing of 3.5m to build the cost-effective BTES in moderate thermal conductivities of rock and soil so that thermal distribution would reach in a steady wat to the outer rings.

4.7 Exergy Analysis

Exergy is the optimal use of work recovered from the system as it reversibly comes into equilibrium with the environment. Exergy analysis is the taken on basis of the combination of thermodynamic first and second laws. Energy is neither created nor destroyed whereas exergy destroys the energy if the energy is lost permanently. The difference between the amount of energy available in the system and the environment provides the available exergy. In this simulated model of five years, we have already defined the thermal recovery efficiency but the quality of energy that is recovered is not yet measured. Exergy is the measure to knows its quality of heat being used from the system. From the (I & M. A., 2012), the exergy of the six ring BTES with 126 boreholes for the core temperature ring is resolved by the 4.3

$$\Delta E_x = m_f * C_p[(T_1 - T_2) - T_0\left(\ln\left(\frac{T_1}{T2}\right)\right) \quad 4.3$$

Exergy efficiency in the initial year is 57.40% which should lower among all the years because the exergy difference is higher between the charging and discharging phases. In the second year, exergy efficiency would reach by 73.04% because the thermal recovery is more in the recharging phase. By the third-year exergy efficiency reaches 74.96% and in the fifth year, it reaches 75.52% that implies exergy difference in recharging and recovering are minimizing which means heat losses are reducing to the stabilized level.

5. Discussion

As a part of this research, there was some quick analysis observed and performed from various studies and numerical methodology of this work. The six-ring BTES model has 126 boreholes with 2.6m borehole spacing between the boreholes in each ring. The boreholes in each ring are parallelly connected and radially connected in series to order have the good extraction rates. The investigated parameters include the BTES diameter(D) to Length (L) ratio, the thermal conductivity of soil, the thermal conductivity of rock, insulation foam material thickness under unsaturated conditions. Considering the optimum measures of thermal conductivity of soil at $\lambda_{soil} = 1.4 \frac{\mathrm{W}}{\mathrm{m*K}}$, the thermal conductivity of rock $\lambda_{rock} = 2.47 \frac{\mathrm{W}}{\mathrm{m*K}}$, BTES (D/H=1), insulation foam thickness at $20\mathrm{cm}$, and studies of simulation have taken place for five years in six months charging followed by six months discharging phase.

A comparative approach on a calibrated numerical model of the in-situ BTES system in Paskov to evaluate HTR and thermal recovery performed by (Rapantova, et al., 2016) using FEFLOW software simulation, the sixteen operational boreholes of depth 60m arranged in a square-shaped array with 2.5m borehole spacing in Paskov could retrieve optimal thermal recovery up to 65% by the end of the three-year operation. Similarly, (Siren, Janiszewski, Uotinen, & Oosterbaan, 2017) simulated the BTES system of $6425\mathrm{m}^3$ capacity for 10 year period that consists of 64 boreholes yielded a 62.8% thermal recovery rate by the final year of operation. In five year period, BTES's power efficiency from all the rings combined have been remarkably increased from 37.83% in the first year to 59% in the third year due to initial temperature rise from 5℃ of bedrock to 70℃, and in the fifth year, it had gone up to 62.02%. Heat recovery efficiency from the center ring accounts for higher temperatures has been increased each year from 40.34% in the first year to 74.62% in the third year with an exergy efficiency of 74.9%, and in the fifth year, it has gone up to 75.43% with the exergy efficiency of 75.5%. The optimal thermal recovery could be achieved by minimizing the heat losses with optimized geometrical changes according to the provided material properties. These results are might be due to the different approach and subsystem simulation by considering the optimal parameters after analyzing the major factors that

support the heat losses to resist improving efficiency every year. (Nilsson & Rohdin, 2019) shown how the poor estimation of design parameters affects the BTES temperatures when the recovered heat is not higher due to lower injection temperatures which resulted in just 19% efficiency over 6 years of operation.

Due to the increased borehole spacing, the fluid mass flow rate struggle to reach the increased outer boreholes, and (Vallin, 2019) shown that borehole spacing of more than 4m needs the highest mass flow rate to the system capacity during charging as well as discharging to reach the longer distanced boreholes and indeed heat extraction rate will not be increased which strategically needs to minimize the number of boreholes. The thermal conductivity of the bedrock is dependent on BHE arrangement and spacing which results in fluctuation of the fluid mass flow rate. (Wołoszyn, 2018) provided a strategic way to reach a higher efficiency rate is by increasing the inlet mass flow rate to an optimal level during charging and ensure the lowest mass flow rate during discharging. Decreasing thermal conductivities of bedrock allows the thermal plumes to concentrate in the center of BTES and thereby increase the higher thermal gradients around the BHEs during the discharging phase in winter which in turn increases the power efficiency. For the thermal conductivity range of rock 3-4 $\mathrm{Wm^{-1}K^{-1}}$optimum borehole spacing of $3.5 - 4\mathrm{m}$ is an optimal measure as well as a higher mass flow rate to minimize the heat losses because the thermal interaction acts as an important element in equivalent thermal distribution between the BHEs. For the thermal conductivity values of rock at less than 2.45 $\mathrm{Wm^{-1}K^{-1}}$ optimum borehole spacing of $1.5 - 3.5\mathrm{m}$ can achieve a higher efficiency rate (Wołoszyn, 2018). But (Nilsson & Rohdin, 2019) concluded that heat extraction rates at a higher temperature dependent on the mass flow rate increases in the case of borehole spacing $3 - 4\mathrm{m}$. An increase in soil thermal conductivity does not show the significant increase in heat losses compared to the increase in thermal conductivity of bedrock because the lower thermal conductivity of bedrock has lower heat loss values compared to the lower thermal conductivity of the soil. However, (Yu, Li, Yao, Nielsen, & Heller, 2020) concluded from the Thermal response test (TRT) that for every $0.1\mathrm{Wm^{-1}K^{-1}}$, rise in soil thermal conductivity will increase the HTR by 0.67W.

Indeed, poor insulation material and thinner density on the top of the BTES may decrease the thermal resistance from the boreholes, which results in convective heat losses. High soil permeability associated with convective heat losses leads to a decrease in BTES power efficiency and thermal recovery rate because the heat goes away from the boreholes in the upward direction from the BTES system (Catolico, Ge, & S. McCartney, 2016). An increase in thermal conductivity of the ground gives the optimal heat extraction rates in lesser time but decreases in efficiency due to heat losses. The distance between the borehole in a TRT and the surrounding ground must be within the 1m to have the effect of fluid temperatures (Yu, Li, Yao, Nielsen, & Heller, 2020). Fluid temperature is one of the influential parameters in the BTES because for every 1℃ rise of average fluid temperature will result in $-6.03\ \mathrm{kWm^{-1}}$ rise of average HTR per meter (Yu, Li, Yao, Nielsen, & Heller, 2020). Thermal interaction between the boreholes is dependent on the heat flux in the BHEs, borehole spacing, geometry aspect ratio, and operation duration.

Hexagonal geometry has a minimal surface area among other geometries like linear, square, and circle. Since minimal surface area and optimal volume is the core design strategy for BTES to increase heat efficiency. D/H ratio between 1-2 is the effective design ratio range to minimize the heat losses and the optimal D/H ratio should be 1 for the high-scale BTES system. Storage efficiency may reduce due to the higher hydraulic gradient because of groundwater movement removes the stored heat through advection. Lower temperature BTES system has lower heat losses than the high-temperature BTES system. In meshing the model, higher solution accuracy arises from higher discretization without the need of changing the elements whereas the lower solution accuracy arises from, the lower discretization. At higher accuracy solutions follows the higher computational price and time.

6. Conclusion

A BTES field model is designed based on numerical modeling using finite element analysis method based software COMSOL. The numerical solutions provide the outflow and inflow of the heat in the BTES, and the method was developed based on the validated data of the static model. Numerical solutions deliver the near accurate results, but the memory and time take high cost. The geometry was studied as the whole system of heat injection and heat extraction phenomena.

The main objectives of this master's thesis were to find out the quantity of heat loss, thermal recovery, and its effect on thermal performance during discharge every year and strategic ways to regulate the heat losses to increase the efficiency in an economic sense. Design parameter changes according to the heat loss subscribers are one of the strategic ways to deal with heat losses. The results proved that the thermal conductivity of the rock, the thermal conductivity of soil, insulation material thickness, BHE arrangement acts as the major subscribers to the storage heat losses considering the fluid injection and extraction temperatures. However, groundwater influence on unsaturated ground conditions was not extensively studied in this research, although studies show heat losses due to advection. D/H ratio, mass flow rate, and collector pipe inner and outer radius are some of the important factors to consider in designing cost-effective geometry.

Thermal conductivity of the soil influences the higher losses but a lower rise in heat losses in the soil compared to the thermal conductivity of bedrock that influences have lower heat losses but a higher rise in varying thermal conductivity values. Under typical parameters, heat losses amount up to 7.7 kWh every year under normal conditions without optimal parametric changes for the same geometry. It is recommended to optimize the BHE spacing at a higher thermal conductivity of bedrock or soil accordingly.

This master's thesis designed a six-ring seasonal BTES system with eight hours charging per day for the first six months and followed by sixteen hours discharging per day for consecutive six months in an annual cycle. Under the optimized parameters, the

simulated model is developed for five years is found to generate an average of 184.5kW thermal energy at peak load and 37.75℃ at the core temperature in the final year from the central ring of BTES with D/H ratio as 1. The thermal recovery is achieved up to 75% at the end of the fifth year of operation and heat losses could be minimized to 5.5kWh. From the eq. 4.1, the specific cost of this model comes to €47.3/m^3 excluding the drilling costs, construction, insulation material costs, and other external costs. However, the financial viability of the optimized design parameters needs to be investigated in further studies thoroughly.

7. References

Alva, G., Lin, Y., & Fang, G. (2018). An overview of thermal energy storage systems. *Energy*, 341-378. doi:https://doi.org/10.1016/j.energy.2017.12.037

ARANER. (2020, 01 25). *What materials should your TES tank be built in?* Retrieved from Arana: https://www.araner.com/blog/what-materials-should-your-tes-tank-be-built-in/

Bakema, G., Snijders, A., & Nordell, B. (1995). *Underground Thermal Energy Storage- State of the art 1994.* Arnhem, Netherlands: IF Technology bv.

Bauer, D., Heidemann, W., Müller-Steinhagen, H., & Diersch, H.-J. (2011). Thermal resistance and capacity models for borehole heat exchangers. *35*, 312-320. doi:https://doi.org/10.1002/er.1689

Borinaga-Treviño, R., Pascual-Muñoz, P., Castro-Fresno*, D., & Blanco-Fernandez, E. (2013). Borehole thermal response and thermal resistance of four different grouting materials measured with a TRT. *Applied Thermal Engineering, 53*(1), 13-20. doi:https://doi.org/10.1016/j.applthermaleng.2012.12.036

Cai, S., Zhang, B., Cui, T., Guo, H., & Huxford, J. (2019, July 18). Mesoscopic study of the effective thermal conductivity of dry and moist soil. *International Journal of Refrigeration, 98*, 171-181. doi:https://doi.org/10.1016/j.ijrefrig.2018.10.023

Catolico, N., Ge, S., & S. McCartney, J. (2016). Numerical Modeling of a Soil-Borehole Thermal Energy Storage System. *Vadose Zone Journal, 15*(1). doi:10.2136/vzj2015.05.0078

Ciampi, G., Rosato, A., & Sibilio, S. (2018). Thermo-economic sensitivity analysis by dynamic simulations of a small Italian solar district heating system with a seasonal borehole thermal energy storage. *Energy, 143*, 757-771. doi:https://doi.org/10.1016/j.energy.2017.11.029

Delgado, B. M., Kotireddy, R., Cao, S., Hasan, A., Hoes, P.-J., Hensen, J., & Sirén, K. (2018). Lifecycle cost and CO2 emissions of residential heat and electricity prosumers in Finland and the Netherlands. *Energy Conversion and Management, 160*, 495-508. doi:https://doi.org/10.1016/j.enconman.2018.01.069

Diersch, H.-J., Bauer, D., Heidemann, W., R¨ uhaak, W., & Sch¨atzl, P. (2011). Finite element modeling of borehole heatexchanger systems Part 2. Numerical simulation. *Computers & Geosciences, 37*, 1136-1147. doi:https://doi.org/10.1016/j.cageo.2010.08.002

Dinker, A., Agarwal, M., & Agarwal, G. (2017). Heat storage materials, geometry and applications: A review. *Journal of Energy Institute*, 1-11. doi:https://doi.org/10.1016/j.joei.2015.10.002

Eklöf, C., & Gehlin, S. (1996). *A Mobile Equipment for Thermal Response Test.* Luleå: Luleå University of Technology.

Elhashmi, R., Hallinan, K., & Chiasson, A. (2020). Low-energy opportunity for multi-family residences: A review and simulation-based study of a solar borehole thermal energy storage system. *Energy*, 117870. doi:https://doi.org/10.1016/j.energy.2020.117870

Energy, U. (2020, March 25). *Applied Hydrogeology Geothermal Innovation*. Retrieved from Underground Energy: https://underground-energy.com/our-technology/btes/

Eurostatistics. (2020, May 7). *Renewable Energy Statistics.* Retrieved from Eurostat: https://ec.europa.eu/eurostat/statistics-explained/index.php/Renewable_energy_statistics#Over_one_fifth_of_energy_used_for_heating_and_cooling_from_renewable_sources

Fisch, M., Guigas, M., & Dalenback, J. (1998). A Review of large-scale solar heating systems in Europe. *Sol. Energy*, 355-366. doi:https://doi.org/10.1016/S0038-092X(98)00103-0

Flynn, C., & S, K. (2015). Influence of location and design on the performance of a solar district heating system equipped with borehole seasonal storage. *Renewable Energy, 81*, 377-388. doi:https://doi.org/10.1016/j.renene.2015.03.036

Fong, M., Alzoubi, M., Sasmito, A. P., & Kurnia, J. C. (2019). Performance Evaluation of Ground-Coupled Seasonal Thermal Energy Storage with High Resolution Weather Data: Case Study of Calgary, Canada. *10th International Conference on Applied Energy (ICAE2018), 22-25 August 2018. 158*, pp. 4980–4985. Hong Kong, China: Energy Procedia.

Gehlin, S. (2016). Borehole Thermal Energy Storage. In S. Gehlin, *Advances in Ground-Source Heat Pump Systems* (pp. 295-327). Lund, Sweden: Elsiever Ltd. doi:https://doi.org/10.1016/B978-0-08-100311-4.00011-X

Giordano, N., Comina, C., Mandrone, G., & Cagni, A. (2016). Borehole thermal energy storage (BTES). First results from the injection phase of a living lab in Torino (NW Italy). *Renewable Energy, 86*, 993-1008. doi:https://doi.org/10.1016/j.renene.2015.08.052

Gultekin, A., Aydin, M., & Sisman, A. (2014). Determination of Optimal Distance Between Boreholes. *Thirty-Ninth Workshop on Geothermal Reservoir Engineering* (pp. 1-8). California, USA: Stanford University.

Gultekin, A., Aydin, M., & Sisman, A. (2019). Effects of arrangement geometry and number of boreholes on thermal interaction coefficient of multi-borehole heat exchangers. *App. Energy*, 163-170. doi:https://doi.org/10.1016/j.apenergy.2019.01.027

Hirth, L. (2013). The market value of variable renewables *,** The effect of solar wind power variability on their relative price. *Energy Economics*, 218-236. doi:https://doi.org/10.1016/j.eneco.2013.02.004

Hirvonen, J., Rehman, H., & Sirén, K. (2018). Techno-economic optimization and analysis of a high latitude solar district heating system with seasonal storage, considering different community sizes. *Solar Energy, 162*, 472-488. doi:https://doi.org/10.1016/j.solener.2018.01.052

Honkonen, M. (2016). *Thermal energy storage concepts and their feasibility.* Aalto University, Civil Engineering. Espoo: School of Engineering.

I, D., & M. A., R. (2012). Chapter 1: Thermodynamic Fundamentals. In D. I, *Exergy: Energy, environment and sustainable development* (pp. 1-19). Ontario: Elsevier Ltd.

Janiszewski, M. (2019). *Techno-economic aspects of seasonal underground storage of solar thermal energy in hard crystalline rocks.* Aalto University, Civil Engineering. Espoo: School of Engineering.

Janiszewski, M., Hernández, E., Siren, T., Uotinen, L., Kukkonen, I., & Rinne, M. (2018). In Situ Experiment and Numerical Model Validation of a Borehole Heat Exchanger in Shallow Hard Crystalline Rock. *Energies, 11*(4), 963. doi:doi:10.3390/en11040963

Janiszewski, M., Honkonen, A., Kukkonen, M., Uotinen, L., Siren, T., & Rinne, M. (2016). Feasibility of underground seasonal storage of solar heat in Finland. *International Conference on Geo-mechanics, Geo-energy and Geo-resources* (pp. 959-965). Melbourne: Conference Proceedings.

Javed, S., Ørnes, I. R., Myrup, M., & Dokkaa, T. H. (2019). Design optimization of the borehole system for a plus-Energy kindergarten in Oslo, Norway. *ARCHITECTURAL ENGINEERING AND DESIGN MANAGEMENT , 15*(3), 181-195. doi:10.1080/17452007.2018.1555088

Kallesøe, A., & Pedersen, T. (2019). *Underground Thermal Energy Storage (UTES).* GeoThermica.

Kim, D., & Oh, S. (2019). Relationship between the thermal properties and degree of saturation of cementitious grouts used in vertical borehole heat exchangers. *Energy & Buildings, 201*, 1-9. doi:https://doi.org/10.1016/j.enbuild.2019.07.017

Kizilkan, O., & Dincer, I. (2015). Borehole thermal energy storage system for heating applications: Thermodynamic performance assessment. *Energy Conversion and Management, 90*, 53-61. doi:https://doi.org/10.1016/j.enconman.2014.10.043

Lanahan, M., & Tabares-Velasco, P. C. (2017). Seasonal Thermal-Energy Storage: A Critical Review on BTES Systems, Modeling, and System Design for Higher System Efficiency. *Energies, 10*(6). doi:https://doi.org/10.3390/en10060743

Lanini, S., Delaleux, F., Py, X., Olivès, R., & Nguyen, D. (2014). Improvement of borehole thermal energy storage design based based on experimental and modelling results. *Energy and Buildings, 77*, 393-400. doi:https://doi.org/10.1016/j.enbuild.2014.03.056

Liu, J., Wang, F., Cai, W., Wang, Z., & Li, C. (2020). Numerical investigation on the effects of geological parameters and layered subsurface on the thermal performance of medium-deep borehole heat exchanger. *Renewable Energy*, 384-399. doi:https://doi.org/10.1016/j.renene.2019.11.158

M.Rad, F., S.Fung, A., & A.Rosen, M. (2017). An integrated model for designing a solar community heating systemwith borehole thermal storage. *Energy for Sustainable Development*, 6-15. doi:https://doi.org/10.1016/j.esd.2016.10.003

Majuri, P. (2018). Technologies and environmental impacts of ground heat exchangers in Finland. *Geothermics, 73*, 124-132. doi:https://doi.org/10.1016/j.geothermics.2017.08.010

Manh Do, T., Kim, H.-K., Kim, M.-J., & Kim, Y.-S. (2020). Utilization of controlled low strength material (CLSM) as a novel grout for geothermal systems: Laboratory and field experiments. *Journal of Building Engineering, 29*. doi:https://doi.org/10.1016/j.jobe.2019.101110

Mauthner, F., & Herkel, S. (2016). *TECHNOLOGY AND DEMONSTRATORS C1: Classification and benchmarking of solar thermal systems in urban environments.* Europe: Solar Heating & Cooling Programme International Energy Agency. doi:10.13140/RG.2.2.31437.28648

Mendrinos, D., Katsantonis, S., & Karytsas, C. (2016). Pipe materials for borehole heat exchangers. *European Geothermal Congress 2016.* Strasbourg.

Mikkelsen, P. (2002, December). *Geosense.co.uk.* Retrieved April 9, 2020, from https://www.geosense.co.uk/media/BlockAttributeValueFile/132/file/CementBentonitegroutbackfillforboreholeinstruments.pdf

Nguyen, A., Pasquier, A., & Marcotte, D. (2017). Borehole thermal energy storage systems under the influence of groundwater flow and time-varying surface temperature. *Geothermics, 66*, 110-118. doi:https://doi.org/10.1016/j.geothermics.2016.11.002

Nilsson, E., & Rohdin, P. (2019). Empirical Validation and Numerical Predictions of an Industrial Borehole Thermal Energy Storage System. *Energies, 12*, 2263. doi:https://doi.org/10.3390/en12122263

Nilsson, E., & Rohdin, P. (2019). Performance evaluation of an industrial borehole thermal energy storage (BTES) project - Experiences from the first seven years of operation. *Renewable Energy*, 1022-1034. doi:https://doi.org/10.1016/j.renene.2019.05.020

Nordell, B. (1994). *Borehole Heat Store Design Optimization.* Luleå University of Technology. Luleå: Division of Water Resources Engineering. Retrieved 02 22, 2020 from https://www.ltu.se/cms_fs/1.5013!/file/FINAL_NORDELL_PHD_red.pdf

Nordell, B. (2000). Large Scale Thermal Energy Storage. *in: Proceedings of Winter Cities.* Sweden: Energy and Environment. doi:https://doi.org/10.1088/2040-8978/13/5/055203

Nordell, B., Grein, M., & Kharseh , M. (2007). Large-scale Utilisation of Renewable Energy Requires Energy Storage. *International Conference for Renewable Energies and Sustainable Development* (p. 6). Algeria: Université Abou Bakr BELKAID – TLEMCEN.

Penttinen, S. (2000). *ELECTRICAL AND HYDRAULIC CLASSIFICATION OF FOREST TILL SOlLS IN CENTRAL LAPLAND, FINLAND.* Espoo: Geological Survey of Finland, Bulletin 398.

Rapantova, N., Pospisil, P., Koziorek, J., Vojcinak, P., Grycz, D., & Rozehnal, Z. (2016). Optimisation of experimental operation of borehole thermal energy storage. *Applied Energy*, 464-476. doi:https://doi.org/10.1016/j.apenergy.2016.08.091

Reuss, M. (2015). The use of borehole thermal energy storage (BTES) systems. In M. Reuss, *Advances in Thermal Energy Storage Systems* (pp. 117-147). Germany: Bavarian Center for Applied Energy Research (ZAE Bayern). doi:http://dx.doi.org/10.1533/9781782420965.1.117

Ringkjøb, H.-K., Haugan, P., & Solbrekke, I. (2018). A review of modelling tools for energy and electricity systems with large shares of variable renewables. *Renewable and Sustainable Reviews*, 440-459. doi:https://doi.org/10.1016/j.rser.2018.08.002

Shah, S., Aye, L., & Rismanchi, B. (2020). Simulated performance of a borehole-coupled heat pump seasonal solar thermal storage system for space heating in cold climate. *Solar Energy*, 365-385. doi:https://doi.org/10.1016/j.solener.2020.03.111

Siren, T., Janiszewski, M., Uotinen, L., & Oosterbaan, H. (2017). Modelling of Borehole Solar Energy Storage Concept in High Latitudes. *2017 YSRM Young Scholars' Symposium on Rock Mechanics* (pp. 369-372). Jeju, Korea: 5th International Symposium on New Development in Rock Engineering - an ISRM Specialised Conference.

Skarphagen, H., Banks, D., Frengstad, B. S., & Gether, H. (2019). Design Considerations for Borehole Thermal Energy Storage (BTES): A Review with Emphasis on Convective Heat Transfer. *Geofluids, 2019*, 1-26.

Sliwa, T., & Rosen, M. A. (2017). Efficiency analysis of borehole heat exchangers as grout varies via thermal response test simulations. *Geothermics, 69*, 132-138. doi:https://doi.org/10.1016/j.geothermics.2017.05.004

Sommerfeldt, N., & Madani, H. (2019). In-depth techno-economic analysis of PV/Thermal plus ground source heat pump systems for multi-family houses in a heating dominated climate. *Solar Energy, 190*, 44-62. doi:https://doi.org/10.1016/j.solener.2019.07.080

Tulus, V., Boer, D., Cabeza, L. F., Jiménez, L., & Guillén-Gosálbez, G. (2016, November 1). Enhanced thermal energy supply via central solar heating plants with seasonal storage: A multi-objective optimization approach. *Applied Energy, 181*, 549-561. doi:https://doi.org/10.1016/j.apenergy.2016.08.037

Underground Energy. (2020, Jan 10). *Applied Hydrogeology Geothermal Innovation*. Retrieved from Underground Energy: https://underground-energy.com/our-technology/btes/

Vallin, S. (2019). *Modelling and optimization study on a high-temperature borehole thermal energy storage concept driven by power plant waste heat.* Aalto University, Mechanical . Espoo: School of Engineering.

Villasmil, W., Fischer, L. J., & Worlitschek, J. (2019). A review and evaluation of thermal insulation materials and methods for thermal energy storage systems. *Renewable and Sustainable Energy Reviews, 103*, 71-84. doi:https://doi.org/10.1016/j.rser.2018.12.040

Wei, W., Gu, C., Huo, D., Blond, S., & Yan, X. (2018, Nov 28). Optimal Borehole Energy Storage Charging Strategy in a Low Carbon Space Heat System. *IEEE Access, 6*, 76176-76186. doi:10.1109/ACCESS.2018.2883798

Welsch, B. (2019). *Technical, Environmental and Economic Assessment of Medium Deep Borehole Thermal Energy Storage Systems.* Darmstadt, Germany: Technische Universität Darmstadt.

Welsch, B., Göllner-Völker, L., Schulte, D. O., Bär, K., Sass, I., & Schebek, L. (2018). Environmental and economic assessment of borehole thermal energy storage in district heating systems. *Applied Energy*, 73-90. doi:https://doi.org/10.1016/j.apenergy.2018.02.011

Wołoszyn, J. (2018). Global sensitivity analysis of borehole thermal energy storage efficiency on the heat exchanger arrangement. *Energy Conversion and Management, 116*, 106-119. doi:https://doi.org/10.1016/j.enconman.2018.04.009

Woloszyn, J. (2020). Global sensitivity analysis of borehole thermal energy storage efficiency for seventeen material, design and operating parameters. *Renewable Energy*, 545-559. doi:https://doi.org/10.1016/j.renene.2020.05.047

Xu, J., Wang, R., & Li, Y. (2014). A review of available technologies for seasonal thermal energy storage. *Solar Energy, 103*, 610-638. doi:https://doi.org/10.1016/j.solener.2013.06.006

Ying, L., & Seth, B. (2016). Characterization of the effects of borehole configuration and interference with long term ground temperature modelling of ground soirce heat pumps. *App. Energy*, 1032-1047. doi:https://doi.org/10.1016/j.apenergy.2016.07.048

Yu, X., Li, H., Yao, S., Nielsen, V., & Heller, A. (2020). Development of an efficient numerical model and analysis of heat transfer performance for borehole heat exchanger. *Renewable Energy*, 189-197. doi:https://doi.org/10.1016/j.renene.2020.01.044

Zhang, C., Wang, X., Sun, P., Kong, X., & Sun, S. (2020). Effect of depth and fluid flow rate on estimate for borehole thermal resistance of single U-pipe borehole heat exchanger. *Renewable Energy*, 2399-2408. doi:https://doi.org/10.1016/j.renene.2019.10.036

Zhu, L., & Chen, S. (2018). Sensitivity Analysis on Borehole Thermal Energy Storage Under Intermittent Operation Mode. *10th International Conference on Applied Energy (ICAE2018), 22-25 August 2018. 158*, pp. 4655–4663. Hong Kong, China: Energy Procedia.

Zhu, L., Chen, S., Yang, Y., Tian, W., Sun, Y., & Lyu, M. (2019, December). Global sensitivity analysis on borehole thermal energy storage performances under intermittent operation mode in the first charging phase. *Renewable Energy, 143*, 183-198. doi:https://doi.org/10.1016/j.renene.2019.05.010

8. Appendix

8.1 Simulation Results

8.1.1 Period 2

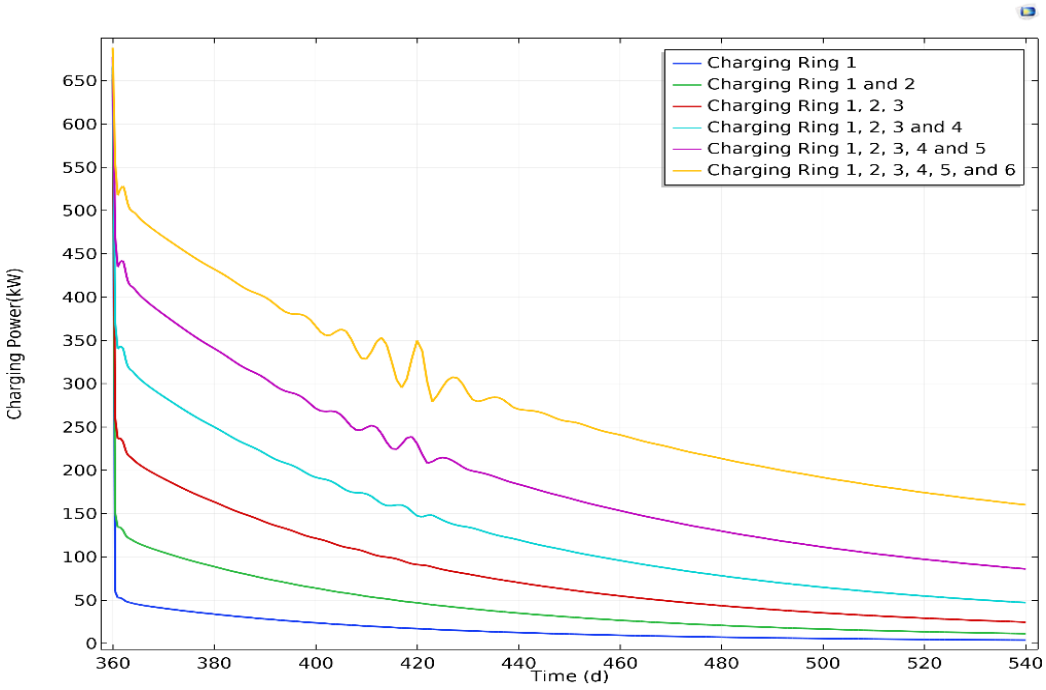

Figure 46. Power injection(charging) in the first six months for the second year

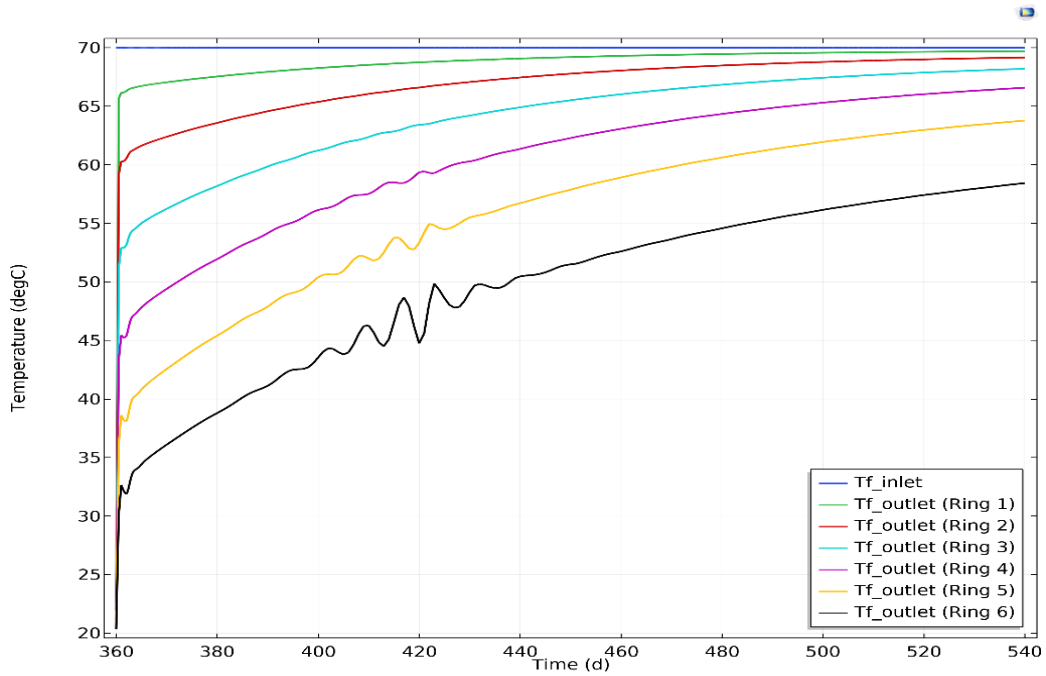

Figure 47. Injection temperatures(charging) in the first six months for the second year

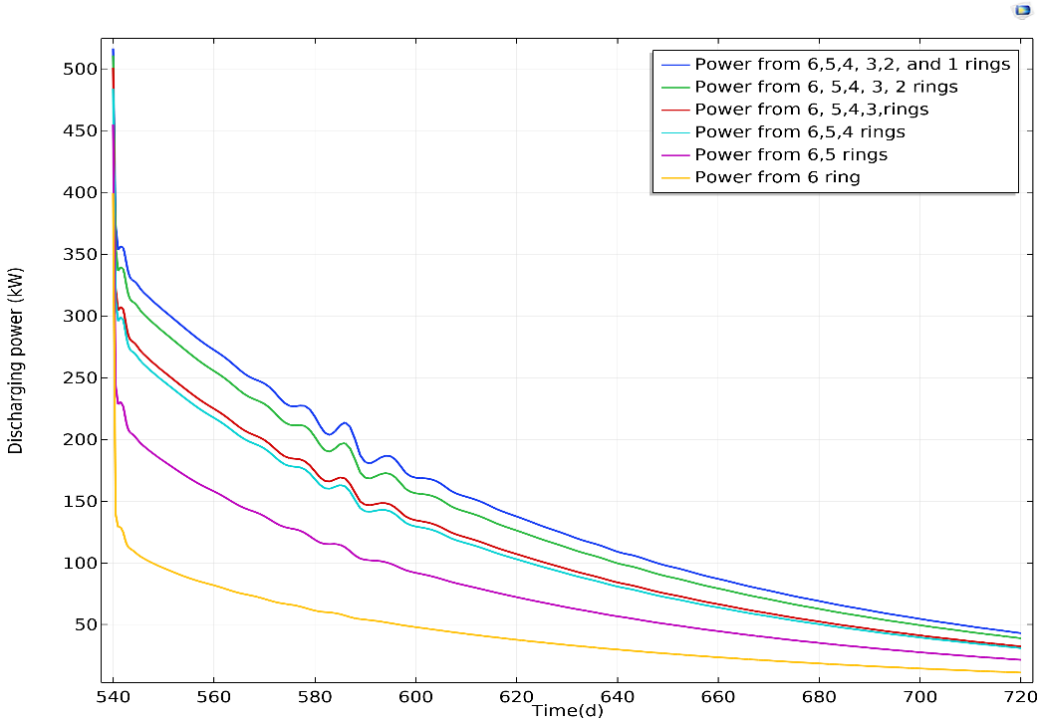

Figure 48. Power extraction(discharging) in the last six months for the second year

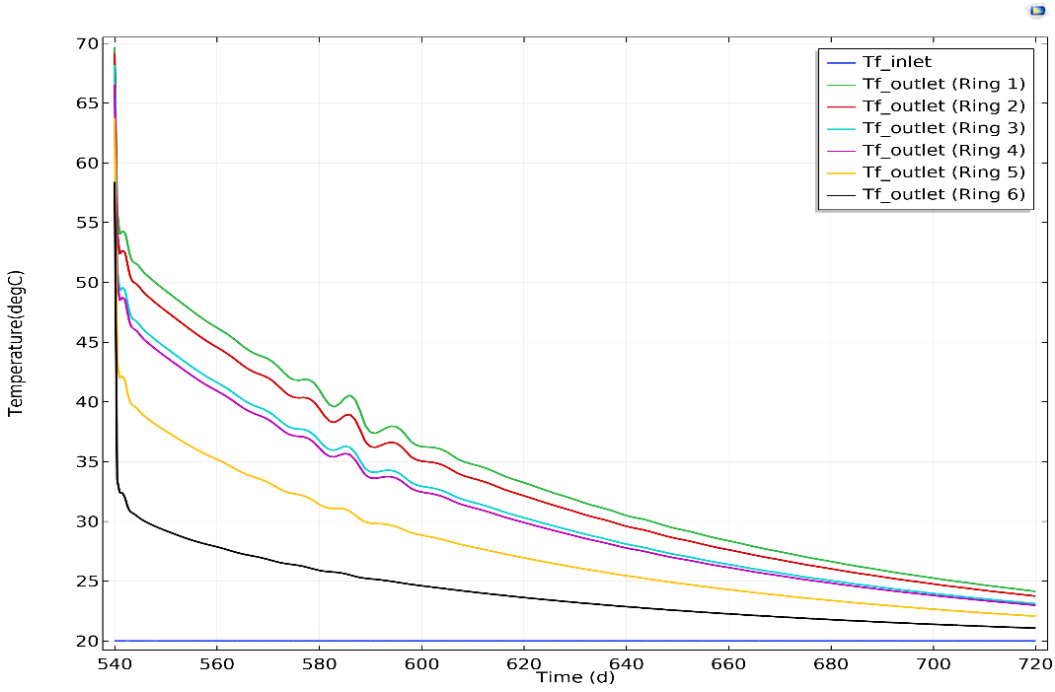

Figure 49. Extraction temperatures(discharging) in the last six months for the second year

8.1.2 Period 3

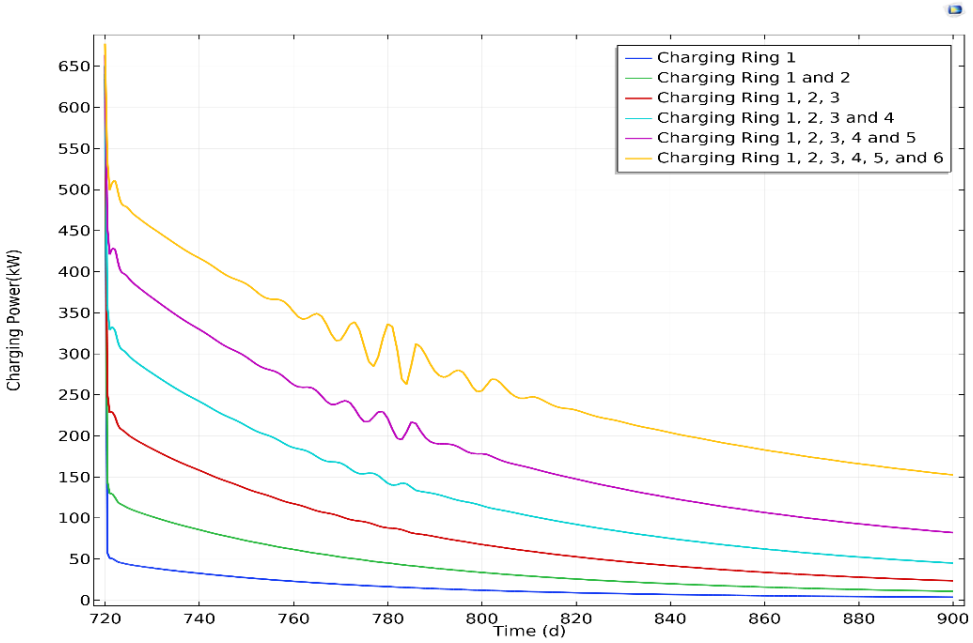

Figure 50. Power injection(charging) in the first six months for the third year

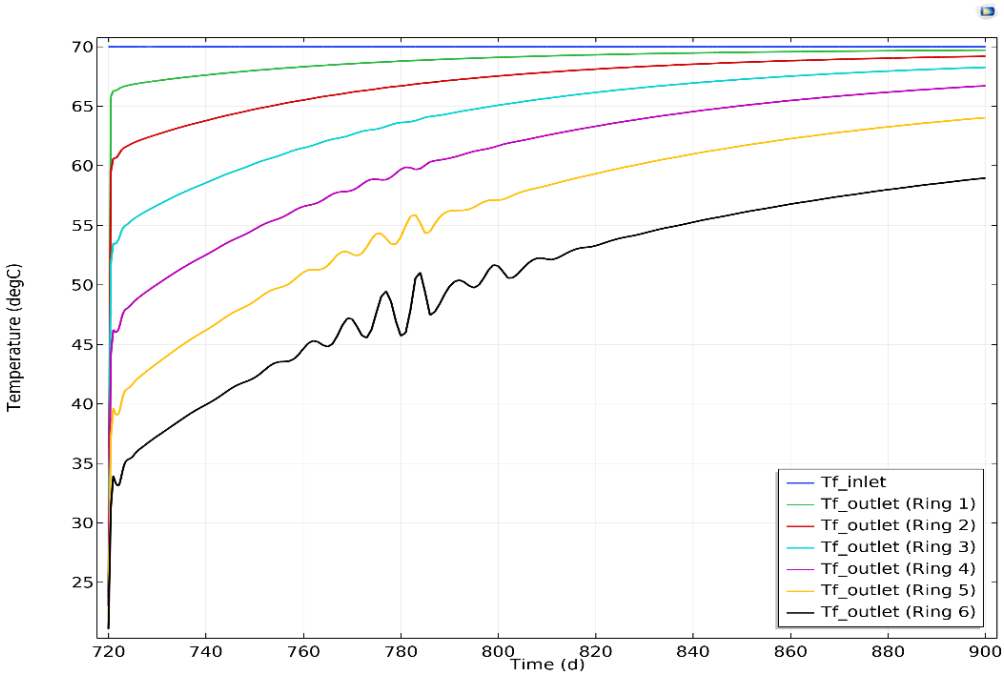

Figure 51. Injection temperatures(charging) in the first six months for the third year

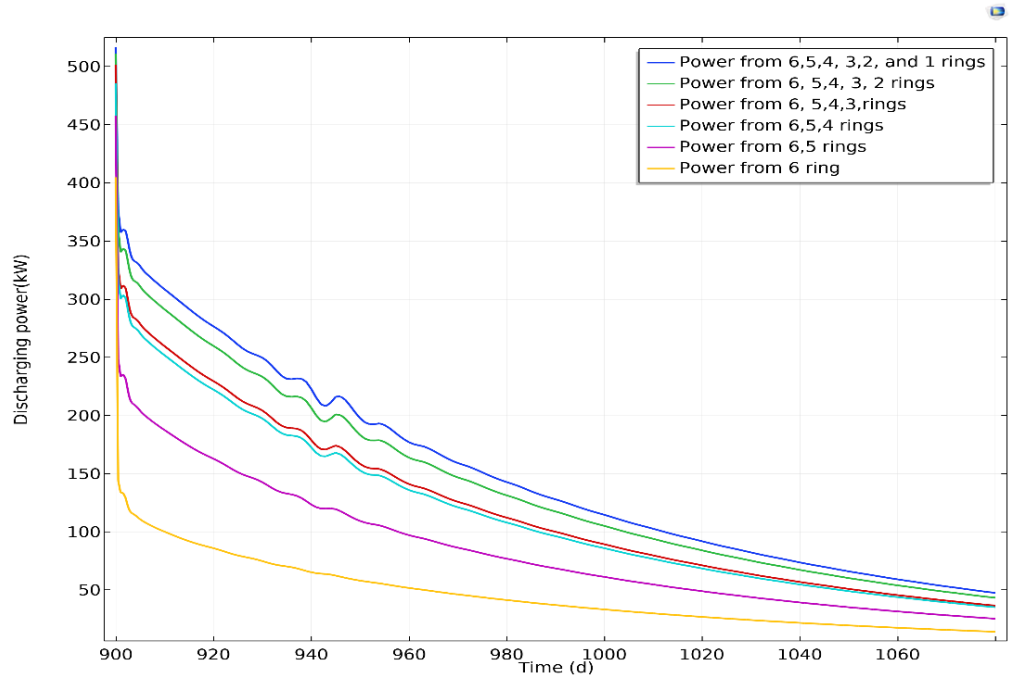

Figure 52. Power extraction(discharging) in the last six months for the third year

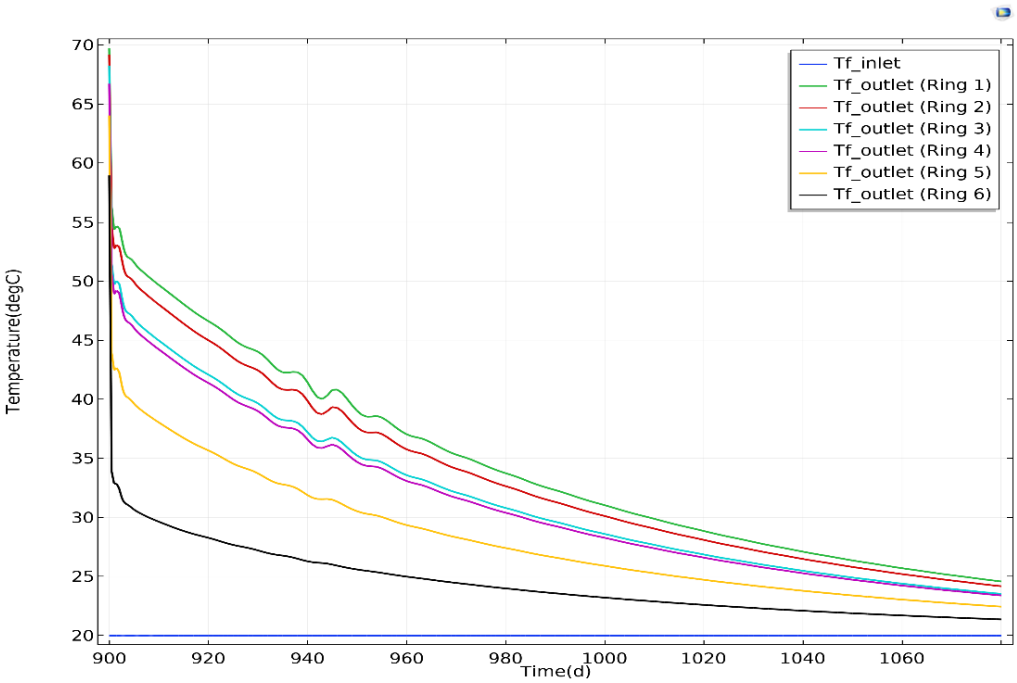

Figure 53. Extraction temperatures(discharging) in the last six months for the third year

8.1.3 Period 4

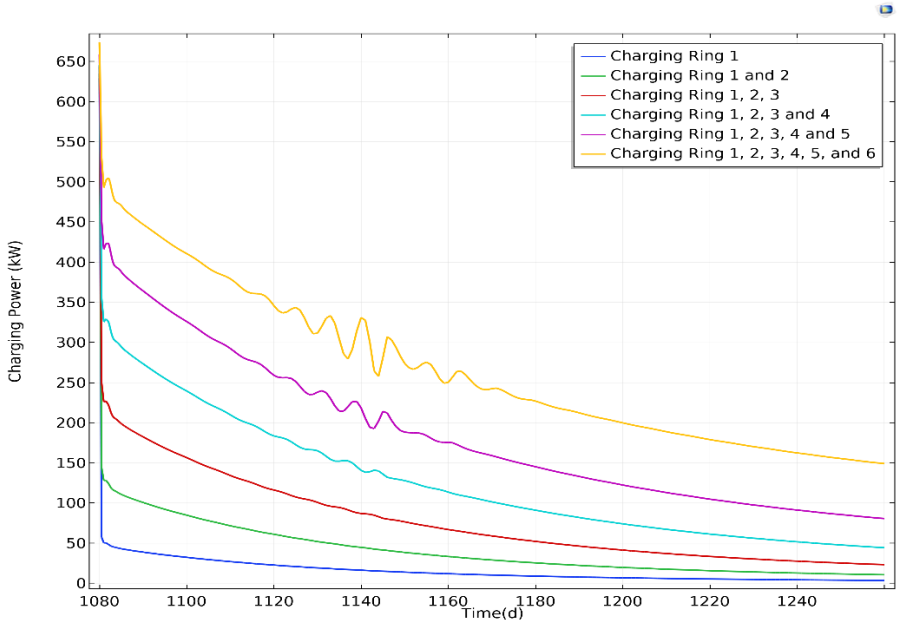

Figure 54. Power injection(charging) in the first six months for the fourth year

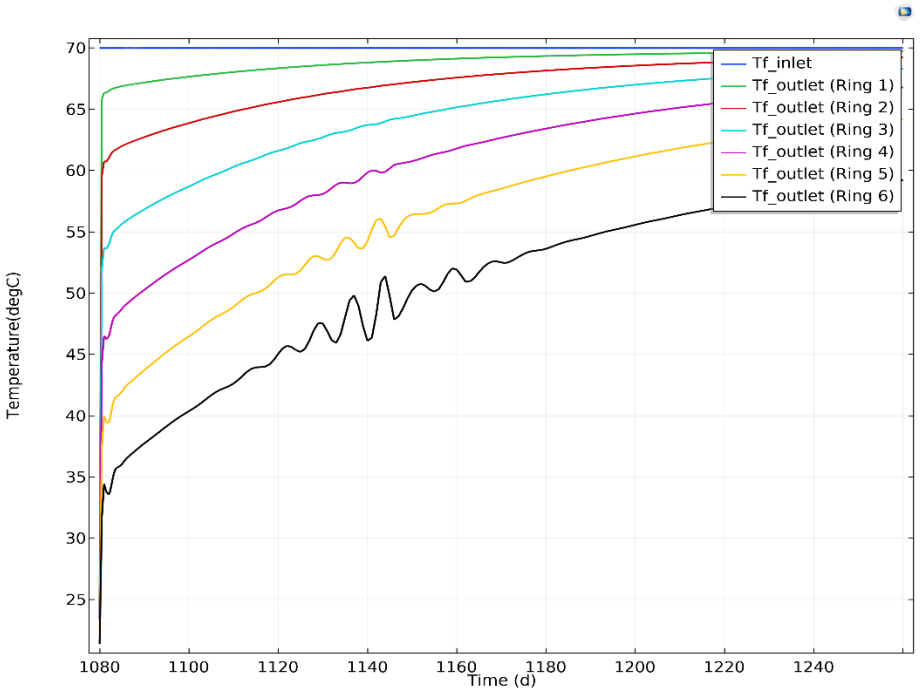

Figure 55. Injection temperatures(charging) in the first six months for the fourth year

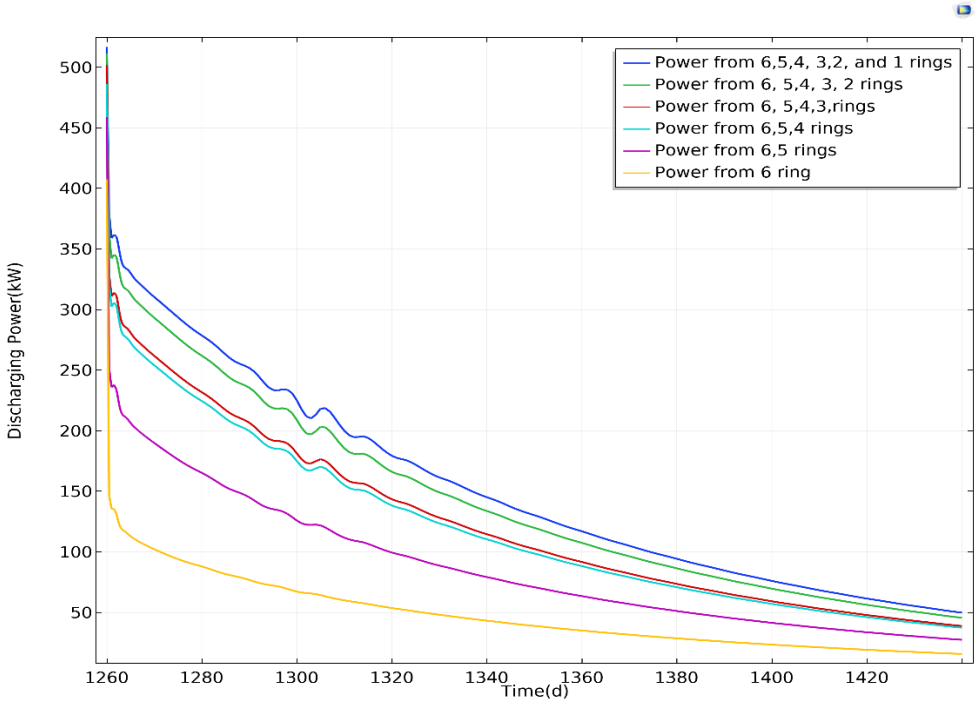

Figure 56. Power extraction(discharging) in the last six months for the fourth year

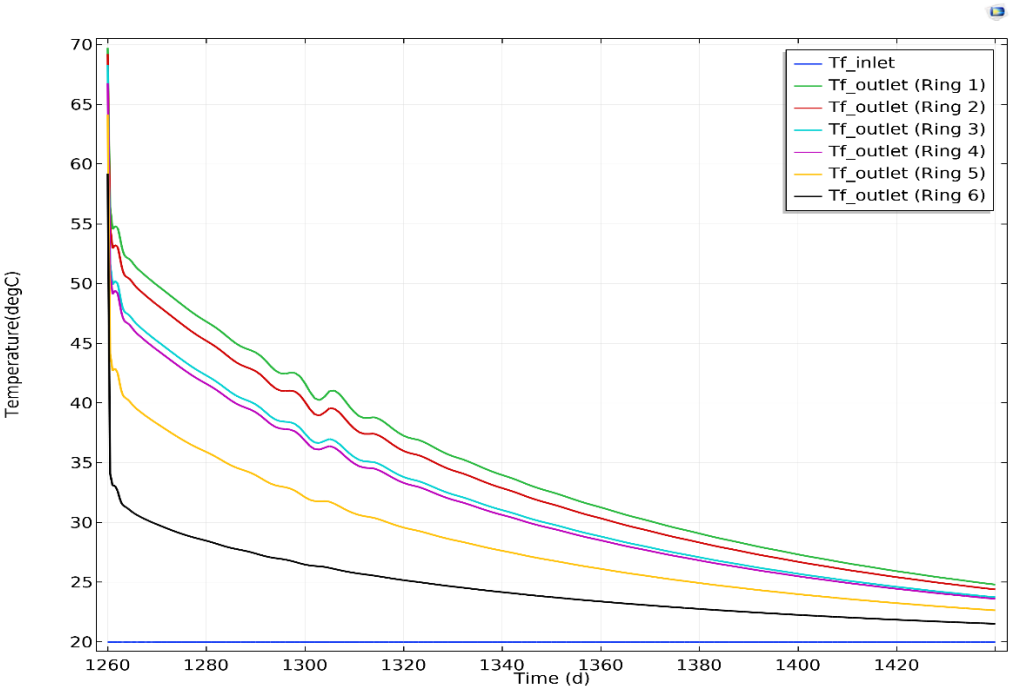

Figure 57. Extraction temperatures(discharging) in the last six months for the fourth year